

**Safety Regulation Group**

**Paper 2013/03**

# **Reliability of Damage Detection in Advanced Composite Aircraft Structures**



**Safety Regulation Group**

**Paper 2013/03**

# **Reliability of Damage Detection in Advanced Composite Aircraft Structures**

**Prepared for CAA by:** L Cook  
A Boulic  
D Harris  
P Bellamy  
P E Irving  
**Cranfield University**

**Research conducted 2005-2008, report updated in 2012**

---

© Civil Aviation Authority 2013

All rights reserved. Copies of this publication may be reproduced for personal use, or for use within a company or organisation, but may not otherwise be reproduced for publication.

To use or reference CAA publications for any other purpose, for example within training material for students, please contact the CAA at the address below for formal agreement.

ISBN 978 0 11792 728 5

Published January 2013

Enquiries regarding the content of this publication should be addressed to:  
Safety Performance, Safety Regulation Group, Civil Aviation Authority, Aviation House, Gatwick Airport  
South, West Sussex, RH6 0YR.

The latest version of this document is available in electronic format at [www.caa.co.uk/publications](http://www.caa.co.uk/publications), where you may also register for e-mail notification of amendments.

Published by TSO (The Stationery Office) on behalf of the UK Civil Aviation Authority.

Printed copy available from:

TSO, PO Box 29, Norwich NR3 1GN  
Telephone orders/General enquiries: 0844 477 7300  
Fax orders: 0870 600 5533

[www.tsoshop.co.uk](http://www.tsoshop.co.uk)  
E-mail: [caa@tso.co.uk](mailto:caa@tso.co.uk)  
Textphone: 0870 240 3701

---

## List of Effective Pages

Part	Page	Date	Part	Page	Date
	iii	January 2013	Report	44	January 2013
Contents	1	January 2013	Report	45	January 2013
Executive Summary	1	January 2013	Report	46	January 2013
Executive Summary	2	January 2013	Report	47	January 2013
Report	1	January 2013	Report	48	January 2013
Report	2	January 2013	Report	49	January 2013
Report	3	January 2013	Report	50	January 2013
Report	4	January 2013	Report	51	January 2013
Report	5	January 2013	Report	52	January 2013
Report	6	January 2013	Report	53	January 2013
Report	7	January 2013	Report	54	January 2013
Report	8	January 2013	Report	55	January 2013
Report	9	January 2013	Report	56	January 2013
Report	10	January 2013	Report	57	January 2013
Report	11	January 2013	Report	58	January 2013
Report	12	January 2013	Report	59	January 2013
Report	13	January 2013	Report	60	January 2013
Report	14	January 2013	Report	61	January 2013
Report	15	January 2013	Report	62	January 2013
Report	16	January 2013	Report	63	January 2013
Report	17	January 2013	Report	64	January 2013
Report	18	January 2013	Report	65	January 2013
Report	19	January 2013	Report	66	January 2013
Report	20	January 2013	Report	67	January 2013
Report	21	January 2013	References	1	January 2013
Report	22	January 2013	References	2	January 2013
Report	23	January 2013	References	3	January 2013
Report	24	January 2013	Acknowledgements	1	January 2013
Report	25	January 2013	Appendix A1	1	January 2013
Report	26	January 2013	Appendix A1	2	January 2013
Report	27	January 2013	Appendix A1	3	January 2013
Report	28	January 2013	Appendix A1	4	January 2013
Report	29	January 2013	Appendix A2	1	January 2013
Report	30	January 2013	Appendix A2	2	January 2013
Report	31	January 2013	Appendix A2	3	January 2013
Report	32	January 2013	Appendix A2	4	January 2013
Report	33	January 2013	Appendix A2	5	January 2013
Report	34	January 2013	Appendix A2	6	January 2013
Report	35	January 2013	Appendix A2	7	January 2013
Report	36	January 2013	Appendix A2	8	January 2013
Report	37	January 2013	Appendix A3	1	January 2013
Report	38	January 2013	Appendix A3	2	January 2013
Report	39	January 2013	Appendix A3	3	January 2013
Report	40	January 2013	Appendix A3	4	January 2013
Report	41	January 2013	Appendix A3	5	January 2013
Report	42	January 2013	Appendix A3	6	January 2013
Report	43	January 2013			

INTENTIONALLY LEFT BLANK

## Contents

	<b>Executive Summary</b>	1
<b>Report</b>	<b>Reliability of Damage Detection in Advanced Composite Aircraft Structures</b>	
	Background information	2
	Investigation Plan	7
	Manufacture of CFRP Laminates	8
	Impact Testing Procedures	9
	Examples of Surface Flaws Produced by Impact	11
	Characterisation of Impact Damage	13
	Derivation of Flaw Shapes for Inspection Trials	22
	Relationships Between Surface Flaw Geometry Variables	24
	Design and Manufacture of Facsimile Specimens	28
	Visual Inspection Trials Method	38
	Results of Inspection Trials	42
	Link Between Delamination Size and Surface Flaw Detectability	53
	Relevance of Results to Actual Damage on CFRP Structures	53
	Implications of Results	55
	Introduction	56
	Findings of the analysis	58
	Surface Flaw Geometry Effects	65
	Surface Colour Effects	65
	Surface Finish Effects	66
	Statistical Analysis	66
	<b>References</b>	1
	<b>Acknowledgements</b>	1
	<b>Appendix A1</b>	1
	<b>Appendix A2</b>	1
	<b>Appendix A3</b>	1

INTENTIONALLY LEFT BLANK



## Executive Summary

Carbon fibre reinforced composite structures are being used for up to 50% of the airframe weight in modern airliner designs, including pressurised fuselage barrels and main wings. Composite materials are susceptible to damage from inadvertent impacts. The damage takes the form of surface dents often associated with subsurface delaminations of a significantly greater area than the visible dent. While staff in the aviation industry are familiar with metallic structures and how they respond to accidental impacts, pilots, maintenance staff and ground crew may be less familiar with the way in which composite materials respond to impacts, making them less able to recognise and thus detect, a damaged composite structure.

Impact events on an aircraft structure are common occurrences; accidental impacts from birds, foreign object debris or catering trucks on composite aircraft structures can result in surface dents together with associated sub surface delaminations. If sufficiently severe, delaminations can reduce compression strength of the composite from the original design ultimate strength. Failure to detect by visual inspection, a surface dent of greater size than the Barely Visible Impact Damage (BVID) value could result in aircraft flying with undetected delaminations and strength reduced from original values. Aircraft structures must withstand service loads whilst containing damage that is too small to be detected during inspection. To support composite aircraft damage tolerant inspection plans it is necessary to know the influence of dent size and shape on probability of detection. This is information analogous to the well-established measurements of probability of detection (POD) of surface breaking cracks in metallic aircraft structures.

Visual inspection is the first line of detection for damage on aircraft structures. The maximum permissible surface dent sizes in composite structures are usually specified in terms of surface flaw depth, and flaws deeper than this must be repaired within a time or cycles limit. However, the surface flaw from impact damage can be quantitatively described by flaw width, depth and sectional profile geometry, and each of these variables depends on the impact conditions.

In this research the reliability of visual inspection of composite aircraft structures has been measured by asking participants to search for, and identify surface flaws on 600 mm x 600 mm specimen panels, presented in a randomised order. The surface flaws on the specimens represented ones produced by impact on carbon fibre composites at energies from 5-70 J using impactors of 20 mm and 87 mm diameter impacting 17 ply and 33 ply mesh-incorporated, painted composite laminates. These impact energies are typical of those achieved by dropping tools of mass 0.5-1 kg a distance of 2-3 metres. Gloss grey, gloss white, gloss blue, matt grey, matt white and matt blue specimen sets were used in individual visual inspection trials. In a single trial, the participants viewed a single specimen set. Each specimen set contained 64 panels, of which 16 panels contained surface flaws. There were 32 flaws in total in each specimen set, placed in random locations on the flawed panels. The participants viewed each specimen panel for 5 seconds, with a 20-second interval between viewing each panel, and the total inspection task lasted around 27 minutes.

For fixed colour, surface finish and dent geometry (width/depth ratio), increasing size of flaw increased the probability of detection. However, for fixed flaw depths, increasing the width beyond a certain value decreased the probability of detection. A flaw representing a 20 mm/15 J impact to a 17 ply laminate was detectable by all participants on all surface colours and finishes. An 87 mm/ 60 J impact flaw on a 33 ply material was detected by less than 50% of participants on gloss white, matt white, gloss blue and matt blue surfaces. However, the sub-surface delamination from the 87 mm impact would be greater than that of the 20 mm impact, thus implying that flaws with more severe subsurface damage are not always easier to detect. This is inconsistent with current assumptions on visual detection of defects.

Colour and surface finish interacted with flaw geometry to influence detectability in complex ways. In broad terms, gloss grey was the best colour for detection and matt blue the worst. There was little difference between flaw detection results on gloss and matt grey panels, slight differences with gloss and matt white panels, and a significant reduction in detection rates on matt blue panels compared to gloss blue. This may have implications for recommended paint colour and finish on composite parts. It may also suggest that aircraft with composite structure should be washed before inspection, since even a light covering of dust will reduce gloss levels.

Throughout this study, it was observed that lighting conditions can affect flaw detection and that gridlines, networks of regularly spaced lines, in lighting systems are very advantageous. This may indicate that lighting in maintenance areas can be optimised for flaw detection on composite structures.

The usual method for presenting reliability of inspection results is a probability of detection (POD) curve. Conventional POD curves represent POD as a function of one variable, as used to represent crack length in metallic structures. A single POD curve cannot be used to represent detection reliability of a 3D surface flaw, with many variables to define geometry.

The surface flaw produced by a larger object, striking at a higher energy and causing larger subsurface damage, may be wider and deeper, yet less visible than a smaller object impacted at a lower energy, which would cause less subsurface damage. However, if flaw depth is used as the only metric on which damage tolerance is based, the larger flaw could be over the damage tolerance limit, yet not be reliably detected by visual inspection. When specifying damage limits based on visual inspection reliability, designers must also consider that the width and geometry of flaws may affect how reliably they are detected.

Aviation personnel, perhaps most importantly those working in the immediate vicinity of aircraft, must also be made aware that whilst a shallow 30 mm or 40 mm dent, or depression on a metallic structure may have previously been of little concern, similarly sized flaws on a composite structure could be an indicator of subsurface damage. This depends on their depth; they should not be ignored.

In summary:

- Wide, shallow dents (typical of slow vehicle impact) can be difficult to detect although they could be associated with significant hidden delaminations.
- Detection rates are affected by flaw depth and flaw width, surface colour and finish, and environment lighting.
- Single variable POD curves are not suitable for representing visual detection probability of dents in composite structures.
- These issues are not recognised by current inspection and Structural Repair Manual data. The potential exists for visual inspection to be less reliable than has been assumed.
- Structural Repair Manuals should specify allowable limits for surface flaws in terms of both depth and width.
- Flaw size limits should be based on visual tests for worst case (matt blue) samples.
- Inspection manuals should warn inspectors of the difficulties of detection of flaws on dark matt surfaces.
- Future work should consider not only whether flaws can be detected, but also the likely interpretation of flaw significance by personnel whose experience has been with metallic structures.
- It is possible to improve the effectiveness of inspection using specific lighting arrangements (e.g. grids) and surface paint colours/finishes.

# Report      **Reliability of Damage Detection in Advanced Composite Aircraft Structures**

## **1 Introduction**

The aviation industry is familiar with inspection of metallic aircraft structures, and there is a wealth of knowledge and experience amongst trained personnel regarding how damage will manifest itself in a metallic structure. Maintenance crew and pilots perform regular checks in order to ensure that aircraft are undamaged. Airport ground staff are given training that alerts them to the fact that aircraft are easily damaged, and are made aware that any suspected damage, such as a bag dropped onto an aircraft skin, or a bump from a vehicle must be reported. Ramp rash, i.e. the day-to-day damage that an aircraft suffers whilst on the ground is a common occurrence [e.g. 1], and much of the damage is caused by impacts from objects.

Most people working around aircraft would be able to identify a dent or tear in a metallic structure, and distinguish between significant and insignificant damage in reports. However, after an impact on a composite aircraft structure, the significance of the resulting surface defect may not be appreciated because of the very different relationship in composites between surface defect appearance and degradation in performance of the structure. Maintenance technicians, pilots, and ground crew may be less experienced at recognising impact damage on a polymer composite aircraft structure than in a metal one. This could lead to a situation where detected damage to composite aircraft structures is not reported due to staff not recognising significant damage. Surface defects appearing after impact on composite structures may have significant associated subsurface damage which could degrade residual strength and durability of the structure.

In a further complication, in metallic aircraft structures, the relation between probability of detection of cracks and their surface length is well established for many NDT techniques, including visual inspection. In contrast, the reliability of detection of surface flaws in composite structures is not well established, and the relation between probability of detection and surface defect size for visual inspection is unquantified. In metallic aircraft structures the crack length at 90% probability of detection (POD), 95% confidence for the NDT technique under consideration generally is taken as the detectable crack size to be used in design calculations of aircraft structure strength and durability. The corresponding surface defect size detectable at this level of probability and confidence in composite aircraft structures is not well established. The factors influencing it are largely unknown. Consequently the reliability of detection of surface defects and their associated subsurface damage which are of sufficient size to be significant in a structural sense is similarly poorly defined.

This study was performed in order to establish the appearance of surface flaws arising from impact to a polymer composite aircraft structure, and then to determine the relation between detection reliability using visual inspection procedures and the size and shape of surface flaws. Other factors with potential influence on visual detection reliability such as surface colour and texture have also been investigated.

1.1 **Background information**

1.1.1 **Use of Composite Materials in Aircraft Structures**

The current trend in modern airliner design is for increased use of composite materials on structures that until now have been constructed from metals. Composite structures can be either of sandwich or monolithic construction. Sandwich structures consist of a thin fibre laminate skin on top and bottom surfaces bonded to a foam or cellular core. Monolithic structures have a thicker skin with reinforcing stiffeners to provide additional stiffness. The current trend favours the use of monolithic structures as sandwich laminates have proved susceptible to water ingress through disbonds and mechanical damage promoting in turn further damage as well as additional weight.

The Boeing 787 aircraft and the planned Airbus A350 make greater use of composite materials than previous aircraft such as the Boeing 767 and 777 and Airbus A330, A340 and A380. The 787 is currently unique in using CFRP for the entire pressurised fuselage. The CFRP skin of the horizontal stabiliser of the Airbus A340-200/300 aircraft is a typical example of CFRP composite use on a current production aircraft (Figures 1 and 2).

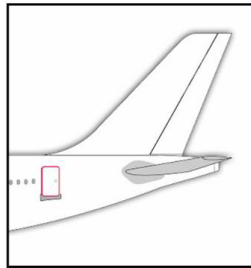


**Figure 1** Location of Horizontal Stabiliser\*

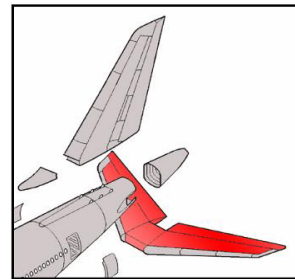


**Figure 2** Detail of Horizontal Stabiliser\*

\*Courtesy of Airbus

CFRP aircraft structures include metal mesh lightning strike protection and are normally externally painted [2-4]. A typical section through a horizontal stabiliser skin material is shown in Figure 3 [2]. CFRP plies are the innermost layer.

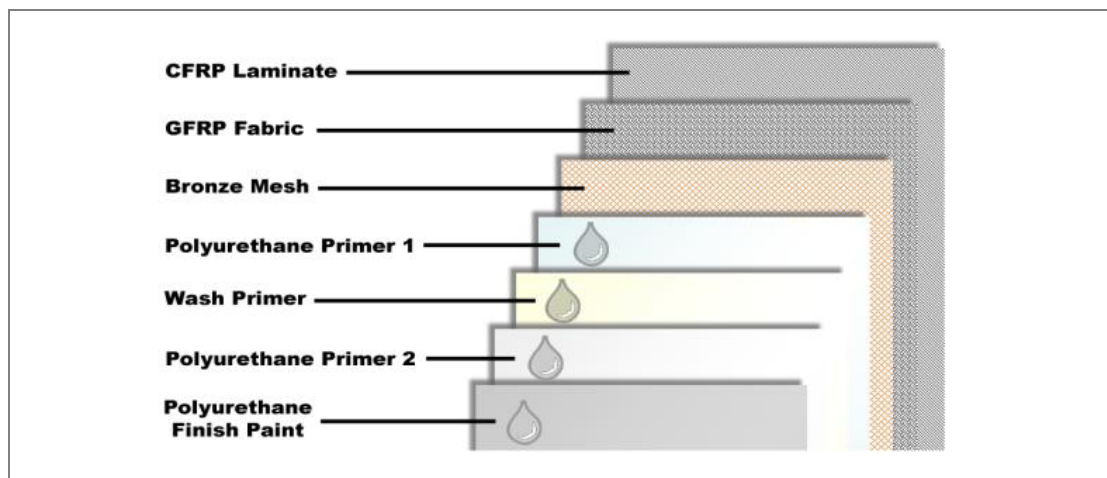


**Figure 3** Material Lay-Up and Paint Coats applied to Horizontal Stabiliser Skin

A thin layer of GFRP fabric separates the bronze mesh and the CFRP to avoid galvanic corrosion between the carbon fibres and the metal mesh.

### 1.1.2 Damage to composite aircraft structures

Around 80% of in service damage to composite aircraft structures is caused by impact strikes [5]. It is well documented that composite structures are particularly sensitive to impacts [6], causing sub-surface damage in the form of delaminations and cracks with little visual evidence on the surface as to the extent of the delaminated area other than a small dent [7,8]. Figure 4 shows a section through an impact damaged laminate showing the extent of delamination and also a surface dent which may be regarded as a three-dimensional (3D) surface flaw with both depth and width.

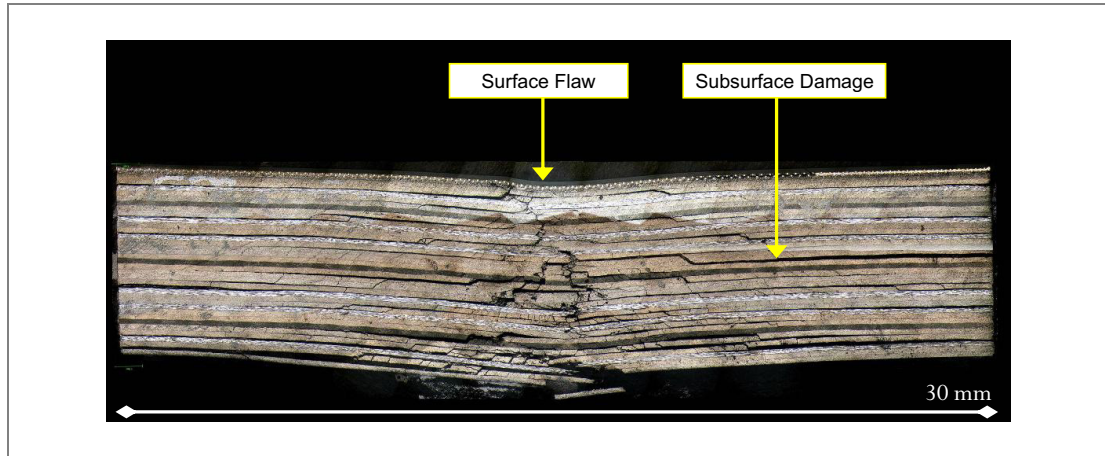


**Figure 4** Cross section through impact damage to a 33 ply, bronze mesh incorporated, painted, CFRP laminate [9]

The subsurface delamination and cracking will be invisible on visual inspection, only the surface flaw being visible. As seen in figure 4, the visible surface flaw due to impact damage can often be significantly smaller in width than the subsurface delamination.

Delamination in CFRP laminates reduces the strength particularly the compression strength of the structure; if undetected and unrepaired it may result in reduction of ultimate load capability or even inability to withstand design limit load [10]. Where impact damage occurs to an aircraft structure, the structure must "*withstand reasonable loads without failure or excessive structural deformation*" for the "*operational life of the aircraft*" or "*until the damage is detected*" [11].

### 1.1.3 Inspection of composite aircraft structures

Psymouli et al [12] studied the inspection process for composite aircraft structures, and observed that the first inspection for damage on composite aircraft structures is visual inspection. If inspectors suspect damage after visual detection, they investigate further or perform non-destructive testing or inspection (NDT/ NDI) to assess the damage [12]. Successful detection of damage is known as a 'hit' in signal detection theory. Where damage exists but the inspector does not detect it, or misinterprets the damage as something insignificant, this becomes a 'miss'. Where an inspector misinterprets something insignificant as a flaw, and chooses to investigate further only to find nothing, this is referred to as a 'false alarm'.

There are two levels of visual inspection: a General Visual Inspection (GVI): performed within 1.52 m (5 ft) of the inspection site, and a Detailed Visual Inspection (DVI): performed within 0.2 m to 0.3 m (8-12 ins) [5]. Psymouli et al [12] observed that most of the time, an aircraft's exterior surface will be inspected at GVI level. Lock [13] points out that inspectors '*need to be able to make a fast, but comprehensive scan of several feet of surface*'.

If a visual inspection reveals damage to a structure, inspectors will request NDT/ NDI to determine the extent of the associated subsurface damage [12]. If the damage exceeds the threshold levels, as specified by the aircraft maintenance or structural repair manual, the inspector will request corrective action [13]. A small dent on the surface could in fact be associated with a large subsurface delamination. Therefore, inspectors could be looking for small visible surface flaws that indicate large subsurface damage. Furthermore, their task may be further impeded by the fact that the aircraft may be dirty, and that the lighting or viewing conditions may be far from perfect for visual inspection tasks.

Regardless of material, there will always be damage on a structure, be it from fatigue or accidental damage, which is too small for an inspector to find using visual inspection, i.e. Non-visible damage (NVD) [5]. Some damage will only be visible in certain conditions, i.e. barely visible damage (BVD) [5]. To determine the NVD and BVD size for a structure, one must know the characteristics of the damage that could occur, and the size of such damage that an inspector is capable of finding with specified levels of reliability, i.e. how reliable the inspectors are at finding damage of a certain type using the visual inspection process.

#### 1.1.4 **Visibility of 3D surface flaws to the inspector**

Depth information about an object is reconstructed from a 2D retinal image [14]. When observing an object, we are in fact seeing nothing more than patterns of light [16]. In fact, *'subtle changes in light reflection can be the determining factor'* [6] in a surface flaw being visible to an inspector. Patterns of light can be created by areas of shadow, reflections of a light source (highlights), or reflections of the surrounding environment.

The intensity of shadows (darker areas) and highlights (lighter areas) can vary as a surface changes shape, such variations being referred to as gradients. Humans are able to derive 3D information from 2D gradient (shadow and highlight) cues. These are termed monocular depth cues. Figure 5 provides an example of a 2D image containing shadow and highlight gradients, which the observer can translate into an image of a 3D surface flaw.

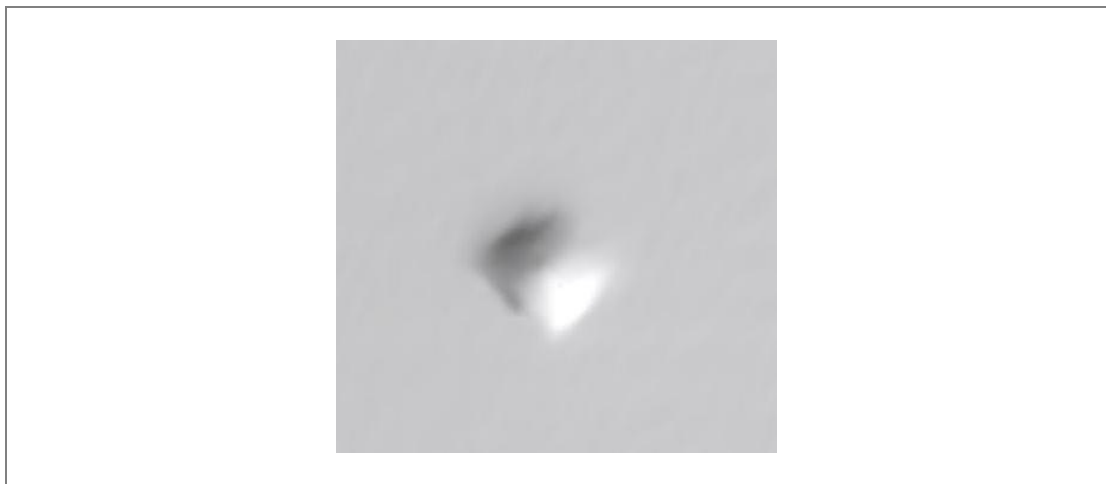


**Figure 5** 2D image of a 3D surface flaw

The amount of shine and shadow information produced by a surface flaw will be dependent on the shape of the flaw, the lighting angle, and the surface colour. A dark shadow on a white surface will be more apparent than a dark shadow on a dark blue or black surface. Conversely, a white shine, or highlight on a white surface may be less apparent to the observer than it would be on a blue or black surface.

Humans are able to identify distortions in reflections of light, which also provide depth cues to the eye. Figure 6 illustrates the patterns of light reflected by a glossy surface containing several circular, hemi-spherically shaped surface flaws. The flaws are identifiable because they distort the reflection of grid pattern of the lighting luminaire (light fitting reflection housing).



**Figure 6** Surface flaws producing distorted reflections

The reflections seen in Figure 6, and those of people seen on the aircraft in Figure 8, are specular reflections, i.e. they are reflected by the surface of the material. The shape of the surface flaw determines how it distorts these specular reflections – a deep, sharply contoured flaw will produce different distortions to a much wider, less deep, softer contoured flaw. Glossy materials will produce clear, mirror-like undistorted reflections of a light source or object, semi-matt materials will distort the reflections, and matt materials will not reflect a discernable image of the original object.

Perception of depth is also aided by the disparity in each eye's view of the object (binocular vision) and '*the optical deformations that occur from viewing an object in motion*' (as occurs when moving one's head to view a stationary object) [15, 16]. Head movement is an aid to visual inspection, as it allows the eye to gather greater amounts of information than would be possible from a single view of an object. An observer will not see or identify a surface flaw, if it does not return enough information to their eyes, i.e. it is too small or too shallow.

The majority of published literature [e.g. 7,8] on impact damaged composites refers to impact testing of unpainted laminates without a metal mesh. The appearance of the damage created would be seen on an aircraft only if it were to leave the factory without lightning strike mesh or paint, as seen in Figure 7. An aircraft inspector is more likely to be performing visual inspection of a fully finished aircraft, as seen in Figure 8.



**Figure 7** Unfinished structure of Boeing 787 aircraft\*

\*Courtesy of the Boeing Company



**Figure 8** Fully finished, painted Boeing 787 aircraft\*

A surface flaw produced by impact may have a different shape and appearance on a fully finished aircraft compared with that on an unpainted laminate without a mesh. Furthermore, as seen in Figure 8, in-service aircraft may be painted in a range of different colours. The flaw shape and size, the surface colour, and the surface finish may all affect the visual appearance of a surface flaw. Depth cues provided by a surface flaw on an unpainted laminate without a mesh may have little relevance to those provided by a painted laminate with mesh incorporated,

#### 1.1.5 **Visual inspection reliability**

Much work has been published on the subject of human factors that may affect aircraft inspection [for example see 13,17,18-21], and there are published works on the reliability of visual inspection [22-24]. The effects of lighting, inspection time, inspector fatigue, inspector experience/ training, and environmental conditions on inspection tasks be it visual or other inspection methods, are all well documented [13,18,24-29].

There are several publications describing data from inspection reliability experiments, but all are limited to the inspection of metallic aircraft structures [18,22], which contain cracks, not 3D surface flaws. The results of these experiments thus apply only to inspection of metallic structures. The published data cover visual inspection, eddy current inspection, and ultrasonic inspection using both actual aircraft and facsimiles of aircraft structures. Most of the studies follow similar published protocols and recommendations on how to design and perform reliability assessments of NDI techniques [31-33]. The result of a reliability assessment of NDI/NDT procedures is invariably a set of probability of detection (POD) curves, which give POD as a function of one dimensional flaw size, [17,20,21,31-34]. Thus existing POD statistical analyses use only one variable such as crack length [35, 36]. This is appropriate for 1D cracks described by their length; it will not be appropriate for 3 dimensional surface flaws having width, breadth and depth.

The specimens for a reliability assessment experiment must contain flaws that are representative of those seen in the field [31-34]. For a reliability assessment of visual inspection of composite aircraft, specimens containing 3D surface flaws with width, length and depth are required. This posed issues for experimental design of this study: Which flaw characteristics should be used to describe a surface flaw produced by impact damage to a composite material?

Current literature generally describes impact damage to composite materials only in terms of surface flaw depth. However, two flaws of the same depth could have different surface dimensions, depending on the size and shape of the striking object.



It was decided for experimental simplicity in the main inspection reliability study that surface flaws studied would have circular symmetry about an axis perpendicular to the laminate surface. Flaws thus had a distorted hemispherical shape and could be described by 2 rather than 3 major variables: depth and width, although their 3 D surface was not an exact hemisphere and required further parameters to define the geometry exactly. Sections normal to the surface across the maximum diameter of the flaws thus had a constant width and depth, independent of orientation of the section. Some flaws without circular symmetry were produced using irregular impactors and their morphology studied, but were not part of the inspection reliability study.

Surface flaws in the study would therefore have two major independent variables describing their shape and size: depth and width. These were systematically changed by choosing a range of impact energies, laminate thicknesses and impactor dimensions.

In previous research, Erhart and Gant [23,24] investigated the reliability of visual inspection for impact damage to composite aircraft structures. However, the first study [24], although using a real aircraft structure, allowed the participants to touch the specimens during inspection, thus providing the participants with tactile feedback, which takes the inspection beyond being purely "visual". The second study [24] used sandwich type composite structures, which behaves differently to a monolithic structure under impact conditions and hence were of limited relevance to this study.

The size and shape of the flaw, and the colour and finish of the surface may affect the visibility, and thus reliability of visual inspection of impact damage surface flaws. There are no published works that quantify the effect of surface finish and surface colour on visual inspection of impact damage to composite aircraft structures, yet there is agreement by both Erhart [23] and Gant [24] that the investigation of these factors is of valuable interest to the aviation industry. These factors were therefore incorporated into the study.

## 1.2 Investigation Plan

The objectives for this project were to investigate and understand the effects of flaw size and geometry, surface colour and surface finish have on the reliability of visual inspection. This was to be accomplished by performing a reliability assessment on the visual inspection process, using a set of specimens containing examples of impact damage. The specimens for a reliability assessment must accurately represent both the flaws and the structure that is the subject of inspection [31-33]. Furthermore, for reliability assessments, it is recommended that for every flawed specimen, there are 3 unflawed specimens within the specimen set [31]. The reliability assessment thus required a large set of specimens, some of which contained surface flaws that faithfully represented an aircraft structure with different sizes of impact damage. A number of sets of specimens with different surface colours and surface finishes were required.

The project plan was as follows:

- 1 Manufacture mesh incorporated, painted CFRP impact test coupons.
- 2 Subject these to a range of impacts objects and energies.
- 3 Characterise surface flaws produced by impact events.
- 4 Describe surface flaw topography using geometric variables.

- 5 Design methodology for assessment of reliability of visual inspection of impact damage.
- 6 Design facsimile specimens for visual inspection reliability assessment, using geometry relationships from impact testing examples to design flaw sizes and characteristics.
- 7 Produce specimens and equipment for reliability assessment.
- 8 Recruit participants for reliability assessment experiment.
- 9 Conduct reliability trials.
- 10 Analyse data and produce reports.

## 2 Experimental Work

### 2.1 Manufacture of CFRP Laminates

A specification for the laminate materials used in a typical composite horizontal stabiliser skin was derived from an aircraft Structural Repair Manual (SRM) [2]:

- Hexcel AS4/8552 pre-preg Carbon Fibre Epoxy Pre-Preg Carbon Tape (UD).
- Hexcel P0108 - 8552/42%/120 (Pre-Preg Glass Fibre 120 Style, 120g/m<sup>2</sup>, 4H Satin).
- Aeroconsultants Bronze Mesh, 166 threads/in.

Samples of mesh incorporated, CFRP laminate were made at Cranfield University using these materials. GKN Aerospace Engineering Services provided the GFRP pre-preg fabric material.

Four 750 mm x 1000 mm panels, two 17 ply and two 33 ply, were produced by laying up 300 mm wide Hexcel AS4/8552 pre-preg tape as follows:

17 ply - [+45,-45,0,-45,+45,90,-45,+45,0,+45,-45,90,+45,-45,0,-45,+45]

33 ply - [+45,-45,0,-45,+45,90,-45,+45,0,+45,-45,0,-45,+45,+45,-45,90,-45,+45,+45,-45,0,-45,+45,0,+45,-45,90,+45,-45,0,-45,+45]

The lay-up was de-bulked every 5 plies. The lay-up for one of the 17 ply and one of the 33 ply panels included a single layer of glass fabric and a single layer of bronze mesh on one side of the panel before curing. After co-curing the carbon layup, glass fabric and bronze mesh at 180°C according to the manufacturers recommended cure cycle [37], the mesh incorporating side of the panels were painted by GKN Aerospace with primer and paint according to Airbus specifications [38]. Samples of undamaged laminate were sectioned and polished and examined using optical microscopy to confirm that the ply layup sequence was correct. Figure 9 shows a section through the laminate, illustrating that the laminate produced was of good quality, i.e. free of voids or resin rich areas, correct fibre directions for each ply, The completed painted and unpainted panels were cut into 100 mm x 150 mm coupons for impact testing.

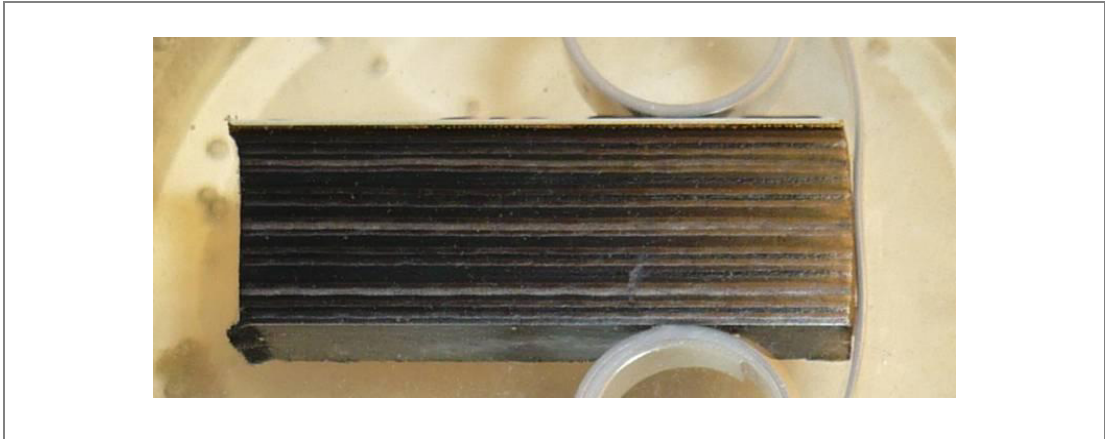




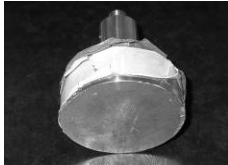

**Figure 9** Section through 17 ply laminate with bronze mesh, glass fabric and paint layers

## 2.2 Impact Testing Procedures

A Rosand falling weight impact tester with interchangeable tups was used to create impact damage on the coupons. For impact testing, the coupons were placed into a support fixture conforming to Boeing BSS7260 [39].

Ideally, a reliability assessment of visual inspection of composite aircraft structures would contain several shapes of surface flaw, across a range of flaw depths and widths. In this project a more limited selection of impacting objects were used. Four different impact tups were used as shown in Table 1. There were 2 hemispherical impactors with 20 mm and 87 mm diameter tups, a wedge (or tool) shaped tip with rounded edges, and a flat faced 70 mm diameter cylindrical impactor. The 17 ply coupons were impacted at energies between 5 J and 50 J, and the 33 ply coupons were impacted with energies ranging from 5 J to 70 J. Published research has shown that impacts below 5 J are unlikely to produce subsurface damage on the 17 ply and 33 ply AS4/8552 material [6, 7]. The impact energies and tup type to which each coupon was subjected are given in Table 1.

**Table 1** Test Matrix for impact testing of CFRP coupons

Impactor Type							
							
20 mm Hemispherical		87 mm Hemispherical		70 mm Flat Cylinder		13 mm x 4 mm Wedge/ Chisel	
Carriage Mass – 2.030 kg		Carriage Mass – 2.030 kg		Carriage Mass – 2.030 kg		Carriage Mass – 2.030 kg	
Total Mass – 2.172 kg		Total Mass - 2.431 kg		Total Mass - 2.960 kg		Total Mass - 2.054 kg	
<b>17 ply with lightening strike protection painted</b>							
Coupon #	Impact Energy	Coupon #	Impact Energy	Coupon #	Impact Energy	Coupon #	Impact Energy
27	5 J	95	5 J	36	10 J	34	5 J
26	10 J	94	10 J	37	15 J	33	10 J
25	15 J	93	15 J	38	20 J	32	15 J
24	20 J	29	20 J	40	30 J	35	17.5 J
23	30 J	92	30 J	39	40 J	31	20 J
		30	40 J				
		90	50 J				
<b>17 ply Unpainted no lightening strike protection</b>							
Coupon #	Impact Energy	Coupon #	Impact Energy	Coupon #	Impact Energy	Coupon #	Impact Energy
U13	5 J	U18	5 J	U25	10 J	U30	5 J
U14	10 J	U19	10 J	U26	15 J	U31	10 J
U15	15 J	U20	15 J	U27	20 J	U32	15 J
U16	20 J	U21	20 J	U28	30 J	U34	17.5 J
U17	30 J	U22	30 J	U29	40 J	U35	20 J
		U23	40 J				
		U24	50 J				
<b>33 ply with lightening strike protection painted</b>							
Coupon #	Impact Energy	Coupon #	Impact Energy	Coupon #	Impact Energy	Coupon #	Impact Energy
2	5 J	9	20 J	18	10 J	14	20 J
3	10 J	8	30 J	19	20 J	15	30 J
4	15 J	10	40 J	20	30 J	16	40 J
5	20 J	11	50 J	21	40 J	17	50 J
6	30 J	12	60 J	1	50 J		
7	50 J	13	70 J	70	60 J		
<b>33 ply Unpainted no lightening strike protection</b>							
Coupon #	Impact Energy	Coupon #	Impact Energy	Coupon #	Impact Energy	Coupon #	Impact Energy
U38	5 J	U44	20 J	U50	10 J	U56	20 J
U39	10 J	U45	30 J	U51	20 J	U57	30 J
U40	15 J	U46	40 J	U52	30 J	U58	40 J
U41	20 J	U47	50 J	U53	40 J	U59	50 J
U42	30 J	U48	60 J	U54	50 J		
U43	50 J	U49	70 J	U55	60 J		

### 2.3 Examples of Surface Flaws Produced by Impact

Figures 10 – 19 show photographs of surface flaws created on painted and unpainted laminates. Comparisons between surface flaw appearance on the protected and unprotected laminates are also given.

#### 20 mm Impactor

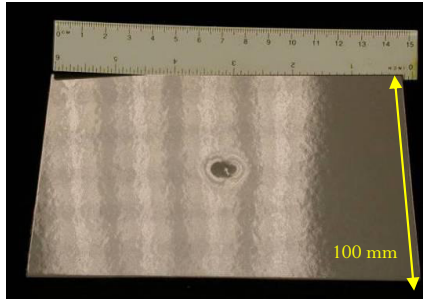


**Figure 10** 20 mm impact at 20 J on 17 ply painted laminate produced a smooth circular surface flaw

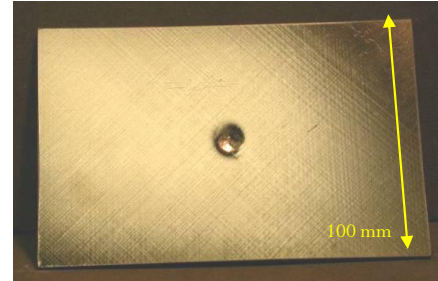


**Figure 11** 20 mm impact at 20 J on 17 ply unpainted produced a deeper, jagged edged surface flaw

The shape of surface flaws produced by impact with a 20 mm hemispherical tup was similar on painted and unpainted laminates. However, on unpainted laminates the impact caused the upper plies to split, with small surface cracks evident, as seen in Figure 13. Cracks were not visible on the painted laminate, shown in Figure 12.



**Figure 12** 15 J, 20 mm impact on 17 ply painted laminate

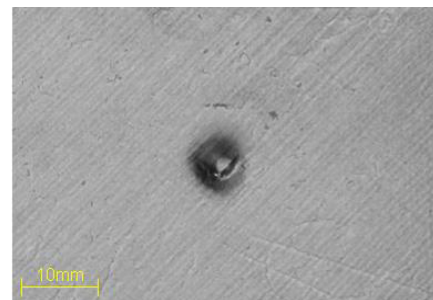


**Figure 13** 15 J, 20 mm impact on 17 ply unpainted laminate produced a less jagged flaw than in Figure 12 that also exhibited surface cracking

### 87 mm Impactor

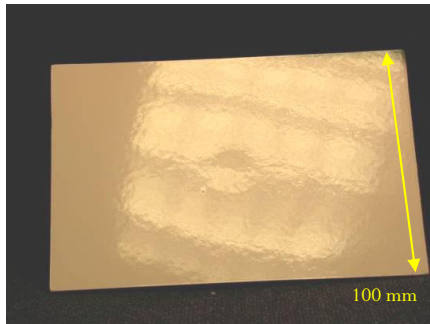


**Figure 14** 30 J, 87 mm impact on 17 ply painted laminate produced a wide, very shallow surface flaw

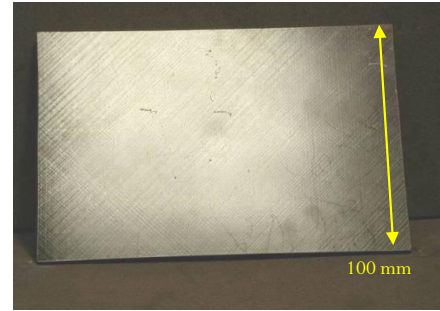


**Figure 15** 30 J, 87 mm impact on 17 ply unpainted laminate produced a more acute, dimple like flaw

The appearance of surface flaws produced by impact with the 87 mm hemispherical tup on painted laminates (Figure 14), and unpainted ones (Figure 15), was very similar. The visual appearance was a rounded, very shallow, circular dent.

### 70 mm Flat Cylindrical Impactor

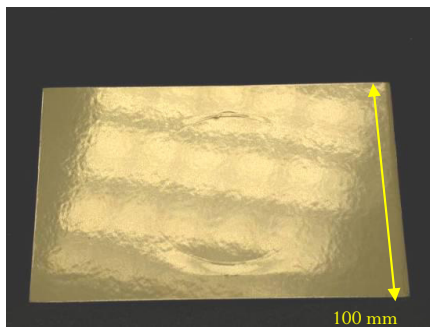


**Figure 16** 30 J, 70 mm flat cylinder impact on 17 ply painted laminate produced two distinct surface flaw areas with circular shaped depressions

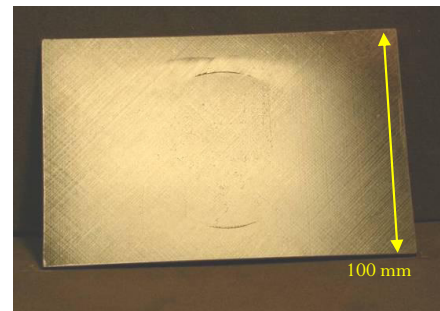


**Figure 17** 30 J, 70 mm flat cylinder impact on 17 ply unpainted laminate again produced two surface flaw areas with deeper, but less complete circular shaped depressions

On painted laminates (Figure 16), the impact from the cylinder left a shallower depression in the surface, but of greater area, giving the appearance of a more extensive surface flaw than was actually present. The depressions generally formed more of a complete circle on the painted coupons than on the unpainted coupons.

Typical visual appearance of these surface flaws is a circular impression on the surface, which became more pronounced as impact energy increased. Due to natural curvature of the coupon surface, and coupon flexing during the impact strike, some impacts from this impactor resulted in two flaw sites that were opposing sections of a circular depression (Figure 17).

### Wedge Shaped Impactor

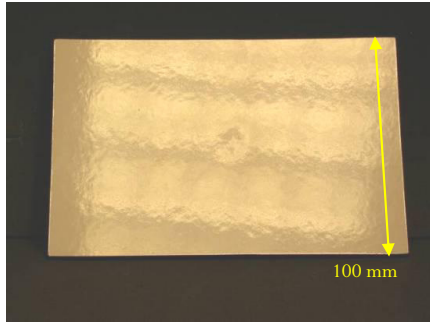


**Figure 18** 15 J, wedge shaped impactor on 17 ply painted laminate produced a small depression in surface

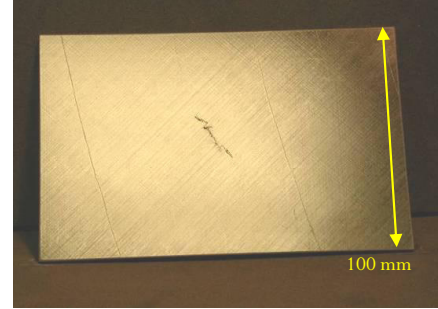


**Figure 19** 15 J, wedge shaped impactor on 17 ply unpainted laminate produced a small depression and surface cracking

The appearance of surface flaws produced by the wedge shaped impactor on painted laminates (Figure 18), and unpainted laminates (Figure 19), was similar in shape. However, on unpainted laminates, the impact caused the upper plies to split, with small surface cracks becoming evident as seen in Figure 19. Typical visual appearance of surface flaws is of a small, rectangular impression, which at higher impact energies became surrounded by a shallow depression.

## 2.4 Characterisation of Impact Damage

To limit the number of variables in the inspection reliability tests it was decided to include only the surface flaws from impact of 20 and 87 mm hemispheres. Hemispherical objects are commonly used in impact testing of composite materials, thus it would be possible to compare reliability of visual inspection findings and impact testing work by other researchers, should it be required. The surface flaws considered in this report are smooth circularly symmetric dents of a range of size and geometries without surface breaking cracks. Impacts by the flat cylinder and the wedge producing irregular dents with surface cracking were not analysed further and were not included in the inspection reliability study. Such events form an important class of service damage types and it is essential that they be investigated in future extensions of this research.

### 2.4.1 Characterisation Methods

#### C-Scanning

Each coupon was C-Scanned before impact testing to check laminate quality. A second C-Scan was made of each coupon after impact to measure the sub-surface delamination area and width. Figure 20 illustrates a typical C-Scan image of an impacted coupon. Further details of the techniques used are found in [40].

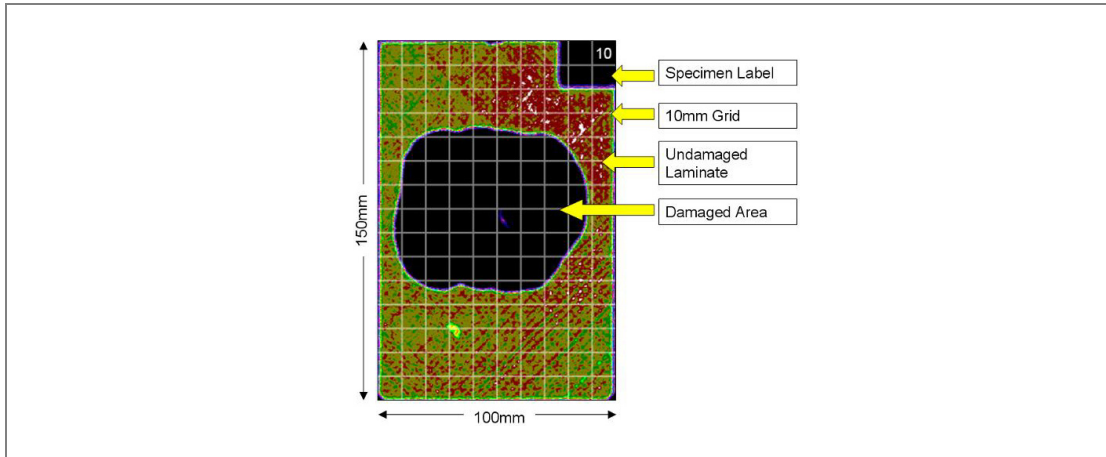


**Figure 20** C-Scan of 40 J impact damage from 87 mm on 33 ply painted, laminate with bronze mesh

### **CMM (Coordinate Measuring Machine)**

A Renishaw Cyclone Series 2 touch-trigger probe CMM machine was used to produce a set of three dimensional data points with X, Y and Z coordinates (3D points cloud) from each of the coupons. The machine was set to scan with a pitch of 1 mm by 1 mm in the X and Y axes, and is accurate to  $\pm 1 \mu\text{m}$  in the vertical Z-axis. The machine scanned an area of 80 mm x 80 mm, centred approximately on the surface flaw on each coupon. The point cloud data was saved as IGES data, and imported into a computer aided design (CAD) file using CATIA. The CATIA system is able to produce section lines through the points cloud in any chosen plane. This method was used to make section lines in a Z/Y plane through the transverse (100 mm) section of each coupon.

For each of the surface flaws, the series of points representing the profile through the surface flaw centre, and a series of points on the coupon surface close to the flaw area were identified within the CMM point cloud data (see Figure 21) by producing section lines through the points cloud. Once these two sections were isolated within the CMM points cloud, the other section lines were removed leaving only two section lines as seen in Figure 22.

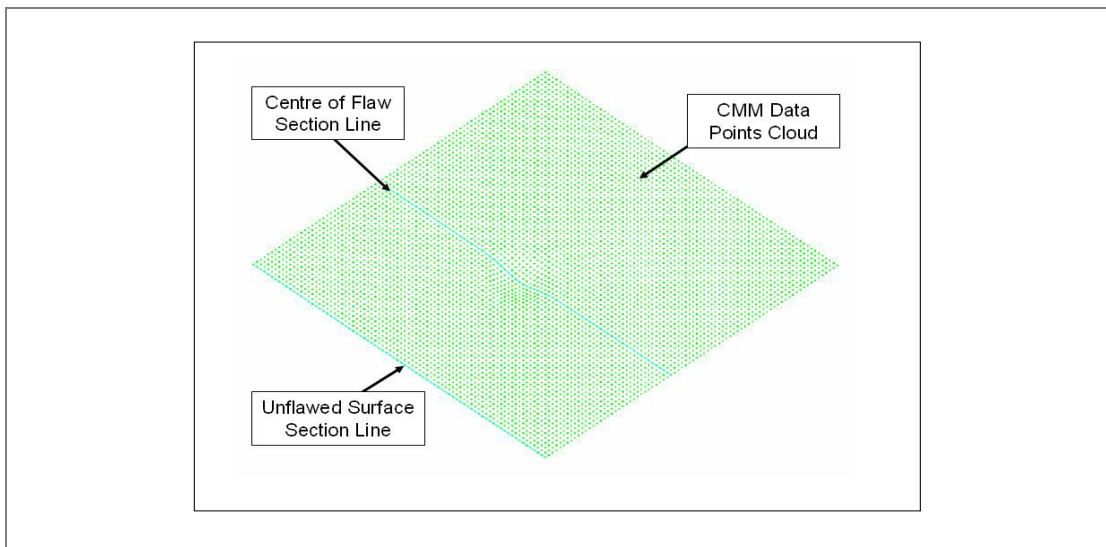


**Figure 21** Section line positions on CMM data points cloud



Vertical Z depth measurements were made every 1 mm along the line (Figure 22). The Z depth measurements were taken along a second flat section made through the coupon surface outside of the flaw area. The Z depth measurements were placed into a spreadsheet, as with the depth gauge measurements. This allowed comparisons to be made between the data obtained by the two measurement methods.

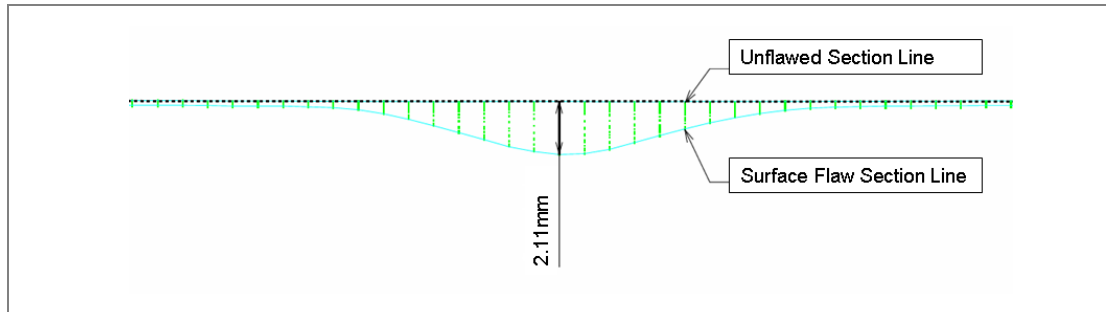


**Figure 22** CAD drawing of data obtained from 2.11 mm deep surface flaw using CMM machine, vertical data lines are 1 mm spacing

### Depth Gauge measurements

Depth measurements were made across the 100 mm width of the surface of each impact damaged coupon, through the centre of the surface flaw, at 5 mm intervals in undamaged areas and at 1 mm intervals within the flawed area, using a dial gauge (0.01 mm accuracy) and a sliding track (see Figure 23).

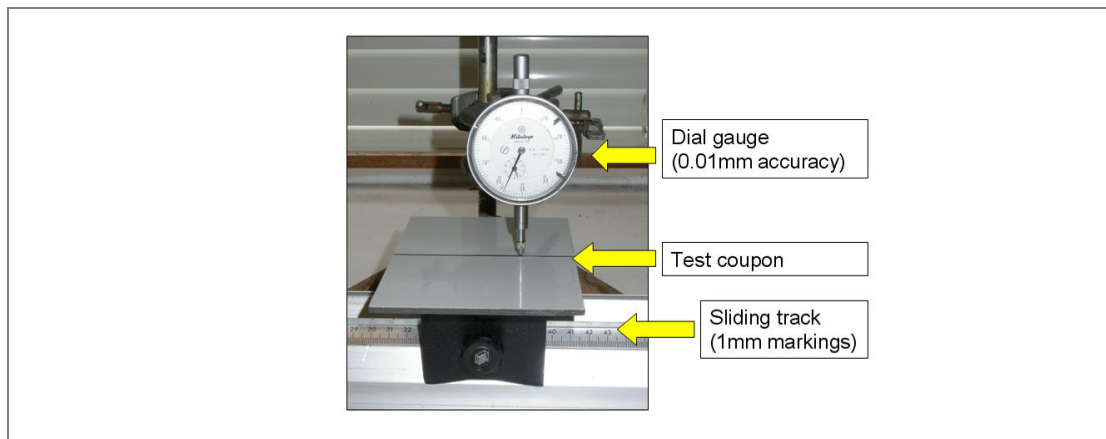


**Figure 23** Dial gauge depth measuring setup

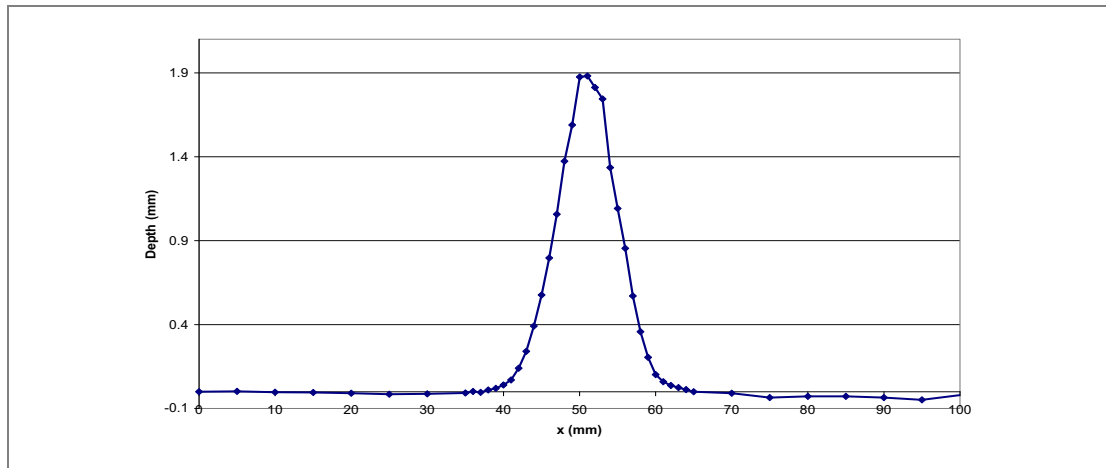


**Figure 24** Example profile of section through surface flaw produced from depth gauge measurements.

Figure 24 illustrates an example of the flaw profile resulting from a 30 J impact with a 20 mm impactor on a 17 ply painted laminate. The maximum flaw depth could be obtained directly from the maximum deflection of the dial gauge. Flaw width was more difficult to measure as the depth profiles exhibited some small change in surface position even at several mm from the approximate edge of the defect. To define the width of the flaw as the point where zero surface deflection occurred would result in a width occupying a much larger portion of the test sample than was evident in the visual appearance of the defect. To obtain a flaw width relevant to the visual appearance the following procedure was followed.

Firstly an approximate measurement of flaw width was made with vernier callipers, and the estimated flaw endpoint regions were marked on the deflection–distance plot. An extension of the unflawed surface was drawn by extending a line of best fit through data points known to represent an unflawed region. Using the vernier measurement of width as a guide, the first point of three points, running towards the flaw centre in the marked region, that were consecutively lower than the unflawed surface line were identified. The flaw endpoints were defined at each set of points on each side of the flaw centre. Flaw width was obtained by taking the distance between the two endpoints. Although this method is subject to a degree of human judgment, and is not ideal there was not considered to be a practical alternative.

### Metallographic Sectioning

A 30 mm square was cut from selected coupons with the centre of the square placed at the centre of each surface flaw. The squares were set into resin, ground back and polished so that the section ran through the centre of the surface flaw.



**Figure 25** Section through 50 J, 20 mm impact on 33 ply painted, mesh covered laminate

A microscope fitted with a digital camera was used to take multiple small photograph images of the finished sections. The 3 mm x 3 mm images were then combined into a composite image (example shown in Figure 25) giving a view through the 30 mm section of damaged laminate. From these composite images, it is possible to see the sectional profile of the surface flaw, and the extent of the subsurface damage. Furthermore, it is easy to visualise the severity of the subsurface damage compared to the relatively small size of the surface flaw.

### 2.4.2 Flaw geometry and delamination data

A study by Boulic [9] characterised damage on 12 painted coupons; six 17 ply and six 33 ply, containing impact damage introduced by 20 mm and 87 mm impactors. The surface flaw geometry was characterised using a depth gauge and a coordinate measuring machine (CMM). Subsurface delamination damage was measured using water immersion C-Scan together with metallographic sectioning.

Shape profiles produced by both CMM and depth gauge together with measurements of delamination area and maximum width are given in Appendix A1.

The 12 flaws used in Boulic's study [9], and a further 14 surface flaws were measured using CMM equipment in order to provide more information on surface flaw topography. By using a CATIA CAD system to produce sections through the CMM data, it was possible to reconstruct the full set of 26 surface flaws by overlaying geometric lines and arcs onto the original CMM data. The quantitative values for the lines and arcs became the "geometric variables" used to describe surface flaw topography. Relationships between the geometric variables within the surface flaw shape were identified. These relationships made it possible to develop geometric variable values for surface flaws produced by arbitrary impact energies on 17 ply and 33 ply CFRP laminate from 20 mm and 87 mm impactors,

The results of the C-scan, depth gauge and CMM work for the set of 12 surface flaws [9], were combined into graphs, to show the surface flaw sectional profile and subsurface damage width for each flaw. Examples are given in Figures 26–29. Where a surface flaw was too small for width measurement, no value is given.

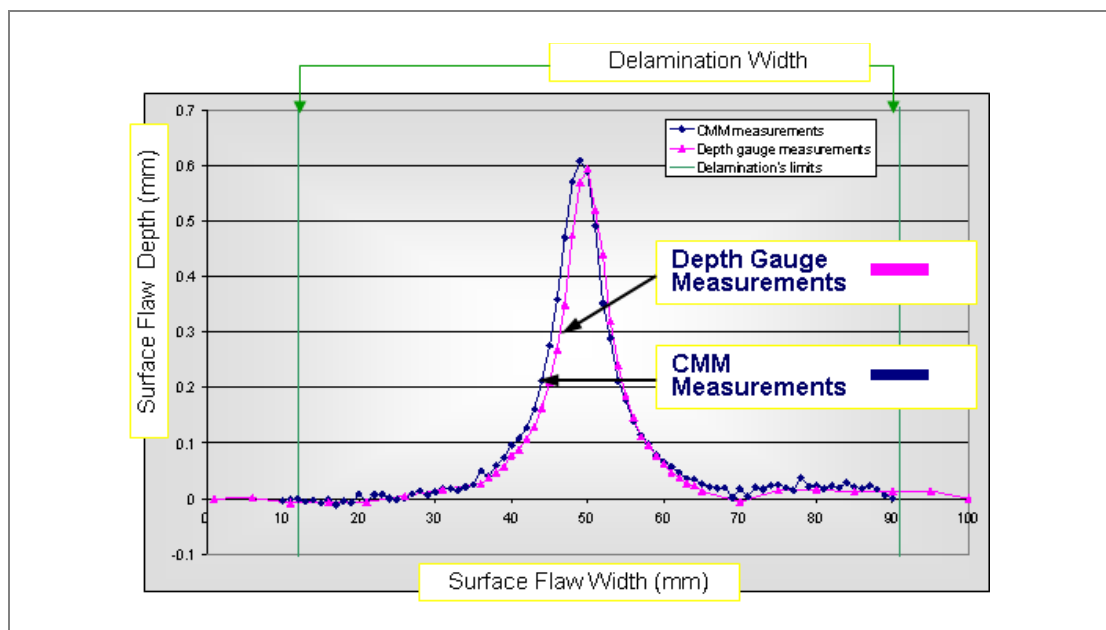


**Figure 26** Graphical representation of depth gauge, CMM and C-Scan measurements of impact damage and surface flaw on a coupon

These geometric variables and relationships were then used to specify flaws to be reproduced on specimens for the visual inspection reliability assessment.

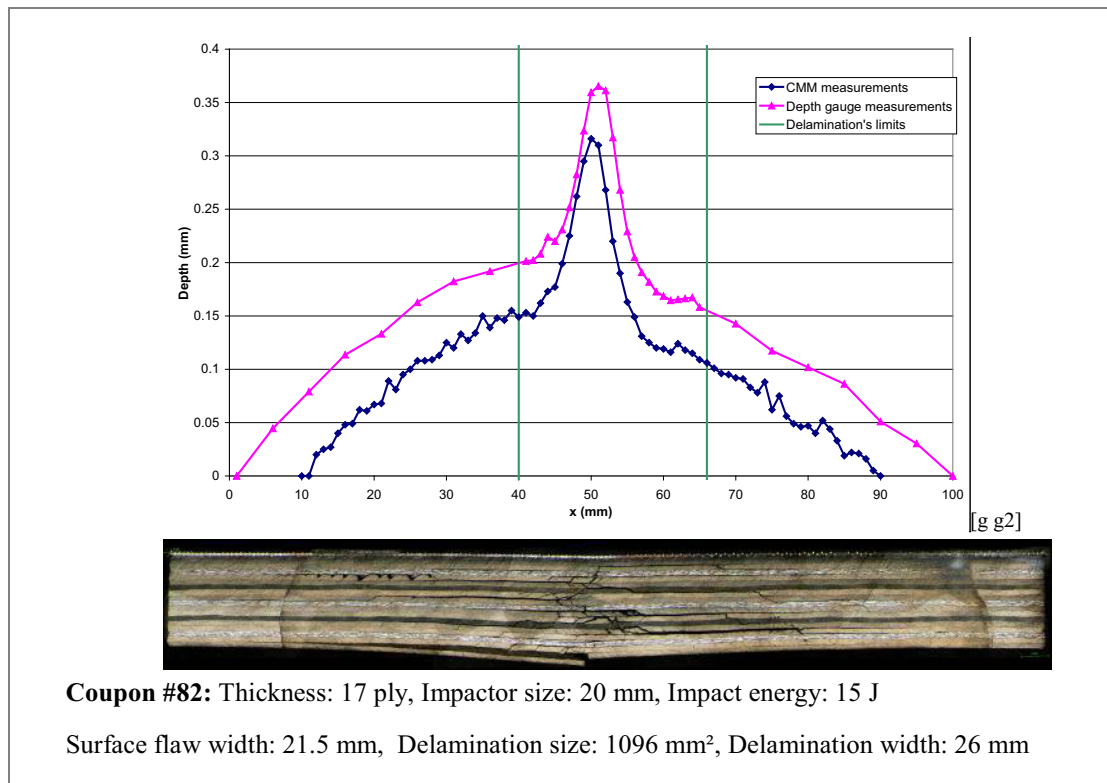


**Figure 27** Section graph, section photograph and measurement data for surface flaw on Coupon #82

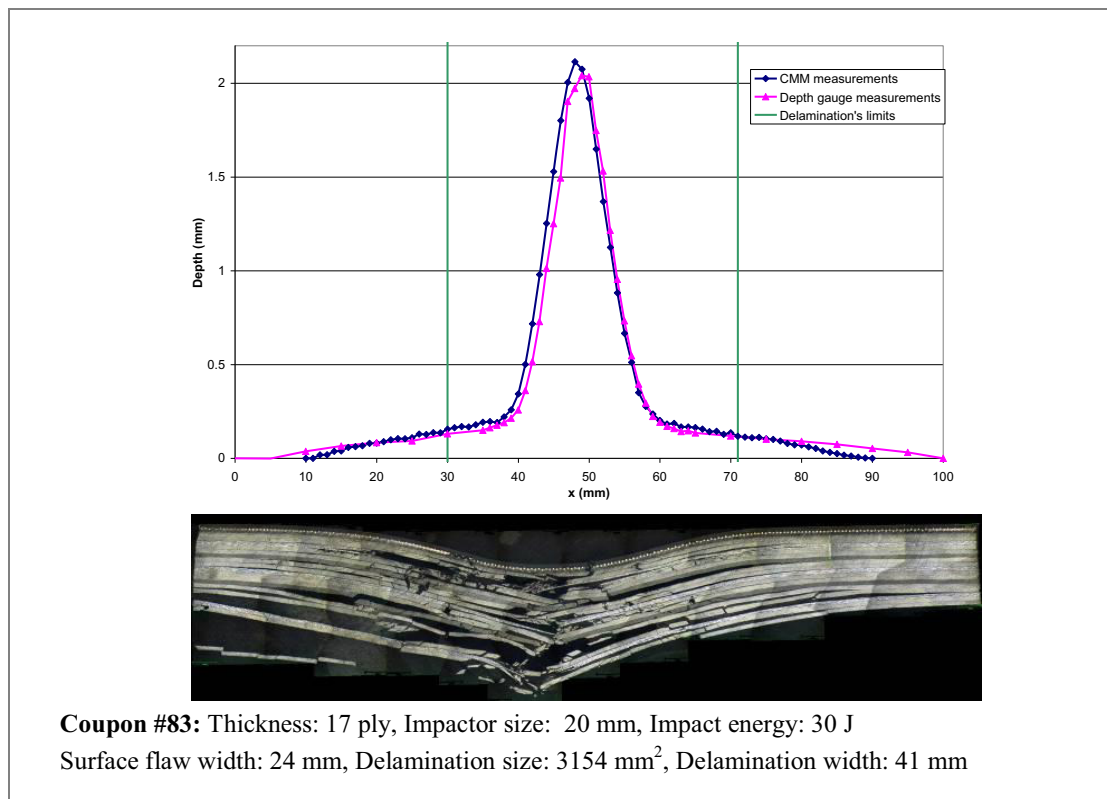


**Figure 28** Section graph, section photograph and measurement data for surface flaw on Coupon #83

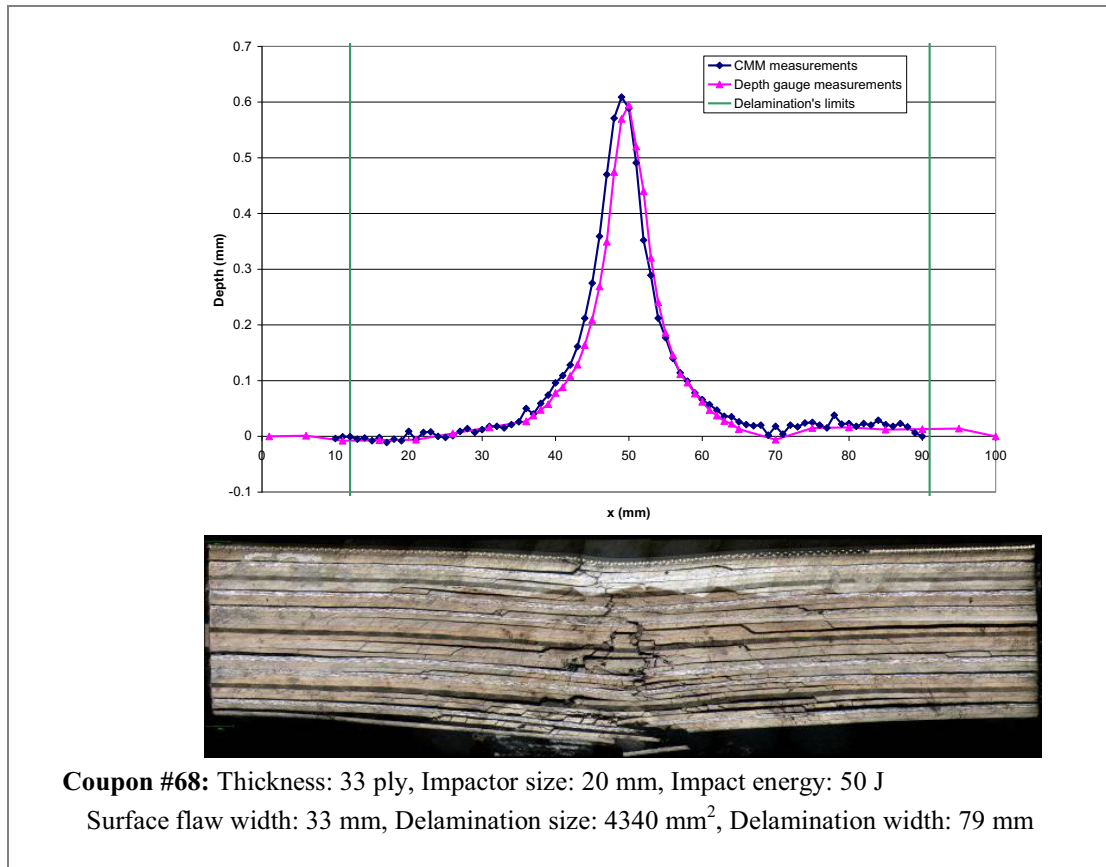


**Figure 29** Section graph, section photograph and measurement data for surface flaw on Coupon #68

The defect geometry characterisation from [9] together with the additional 14 impact flaws are summarised in Table 2, which gives the measurements of the subsurface damage and surface flaw widths on all 4 combinations of impactor diameter (20 mm or 87 mm) and sample ply thickness (17 ply or 33 ply).

**Table 2** Impact damage width, depth and associated delamination area for 26 samples used to develop inspections reliability flaws

Sample No	Top diam mm	Ply No	Impact energy J	Depth mm	Width mm	Flaw area mm <sup>2</sup>	Delam Area mm <sup>2</sup>
27	20	17	5	0.09	4.5	16	400
26	20	17	10	0.09	6	28	500
82	20	17	15	0.32	21.5	363	1050
24	20	17	20	0.7	16.5	214	1900
83	20	17	30	2.11	24	452	2400
84	87	17	10	0.12	44.5	1548	700
93	87	17	15	0.07	28	615	900
29	87	17	20	0.06	29.9	700	2000
85	87	17	20	0.18	36.4	1041	3083
88	87	17	30	0.03	25	491	3400

**Table 2** Impact damage width, depth and associated delamination area for 26 samples used to develop inspections reliability flaws (Continued)

Sample No	Top diam mm	Ply No	Impact energy J	Depth mm	Width mm	Flaw area mm <sup>2</sup>	Delam Area mm <sup>2</sup>
30	87	17	40	0.11	37.4	1100	4900
86	87	17	40	0.45	22.5	394	9114
4	20	33	15	0.14	12	79	1300
5	20	33	20	0.22	10	113	1550
69	20	33	20	0.19	16	201	1673
6	20	33	30	0.27	15	177	2800
7	20	33	50	0.86	18	255	4890
68	20	33	50	0.6	33	855	4340
9	87	33	20	0.12	20	314	2700
8	87	33	30	0.19	22	380	3500
10	87	33	40	0.21	26	531	5100
66	87	33	40	0.26	60	2827	4224
11	87	33	50	0.21	30	707	6400
65	87	33	60	0.29	52.5	2157	5944
12	87	33	60	0.22	34	908	7000
13	87	33	70	0.23	35	962	8900

From the data in Table 2, it is possible to observe that for higher energy levels (>20J) the delamination area measured on the C scan can be significantly larger than the flaw area calculated from  $(width/2)^2$ . The results for coupon 69 and 86 both illustrate this to good effect. The delamination width for coupon 69 is almost 3 times greater than the flaw width, and over 4 times greater for coupon 86. The data illustrate that lower energy impact damage can produce a 21.5 mm wide flaw (#82) that has less subsurface damage beneath than a 22.5 mm wide flaw (#86), due to the use of a differently shaped impact object. Furthermore, the flaw on coupon 68 is less wide than the flaw on coupon 66 (33 mm vs. 60 mm), yet coupon 68 received a lower energy impact and has similar delamination size to coupon 66. This illustrates that flaw width can depend on the shape and size of the impacting object. The relation between impact energy, defect depth and defect width for the four variants of impactor diameter (20 mm /87 mm) and two thicknesses of laminate (17 ply/ 33 ply) are shown in Figures 30 and 31.

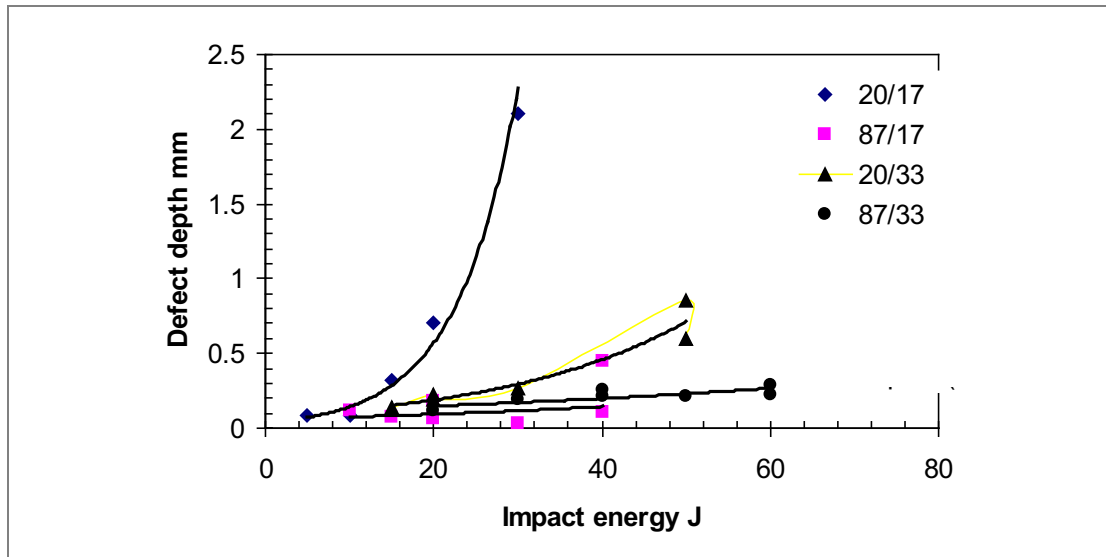


**Figure 30** Plot of impact energy vs. flaw depth for the 4 laminate and impactor diameter combinations

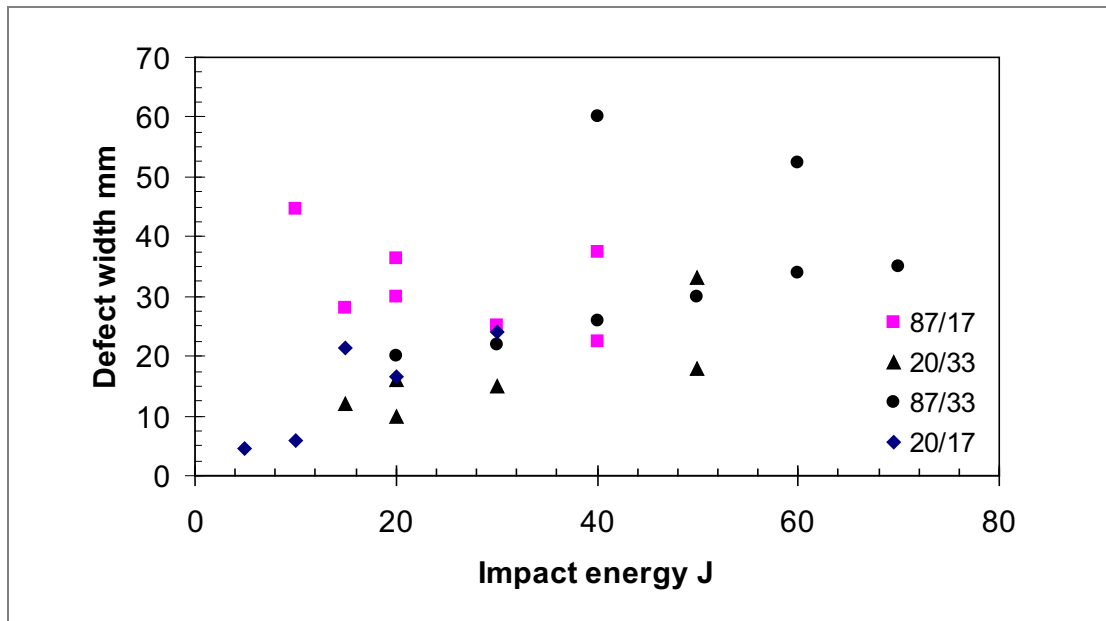


**Figure 31** Plot of impact energy vs. flaw width for the 4 laminate / impactor combinations

It can be seen that the relation between impact energy and flaw depth can be represented as 4 families of points, each representing one of the 4 variants. Each curve characterises the relation between impact energy and flaw depth for the particular combination of laminate thickness (17 or 33 ply) and impactor diameter (20 or 87 mm). There are similar relations between impact energy and flaw width, but as can be seen in Figure 31 the relation is much more approximate with considerable scatter in data points. This increased scatter in width is almost certainly a consequence of the difficulties in measuring and defining defect width. There is no definite boundary to the edge of the defect and the defect surface gradually merges with the undamaged part of the laminate.

Because of the difficulties of creating a selection of defects of reproducible geometry via impacts on composite laminates, it was decided to machine into facsimile samples a series of defects representative of size and geometry of the 4 families in Figures 30 and 31 above. The advantages of doing this are firstly that specific shapes and sizes can be accurately reproduced many times if necessary in samples of different colour and surface finish. Secondly noting that the defects in Figures 30 and 31 fall into 4 families, if the relation between impact energy and defect depth is known for each family, defects of size intermediate between impact data points can be created, independently of having performed an impact test under those conditions. This facility allows the visual inspection trials to be performed with selections of defect size optimised for each trial.

In fact defect geometry is specified by a number of parameters additional to width and depth. To convert the defect geometry produced by impacts into instructions for a numerically controlled milling machine to cut specified defects into facsimile samples, the following procedure was adopted. The defect profiles measured by the CMM machine were converted into parameters representing the defect geometry, recognisable by the CAD software. The way in which these changed with impact energy, impactor geometry and laminate thickness was approximated by equations. Arrays of defect sizes and shapes to be used in the inspection trials were specified, and the parameters describing them determined. These were then used in the NC machine to cut the defects. The details of this process will now be described.

## 2.5 Derivation of Flaw Shapes for Inspection Trials

### 2.5.1 Geometric Reconstruction of Surface Flaw Topography

The flaw shapes in Figures 32 and 33 show a section through the surface flaw on an impact damaged coupon. Above the section photograph, a line is shown, which is a direct trace of the surface flaw. It was possible to draw the traced flaw shape using geometric, or parametric lines Figure 34 illustrates the way in which section lines through a surface flaw were constructed using geometric variables to define the section shape. These parameters were used to characterise the sectional profile of each surface flaw.

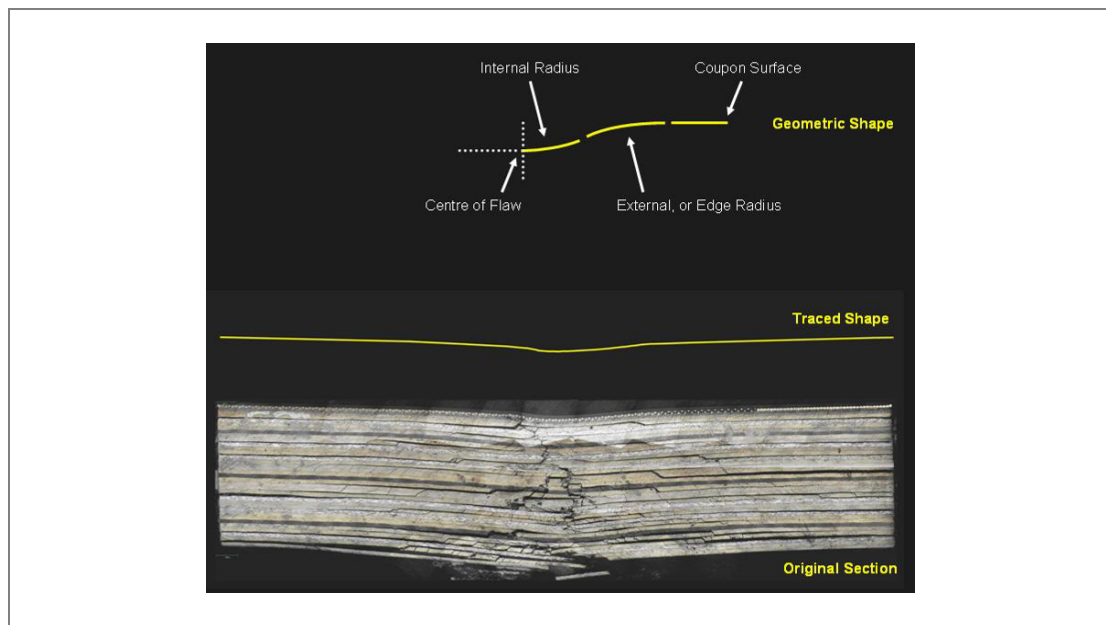


**Figure 32** 20 mm/50 J Surface flaw on a 33 ply coupon



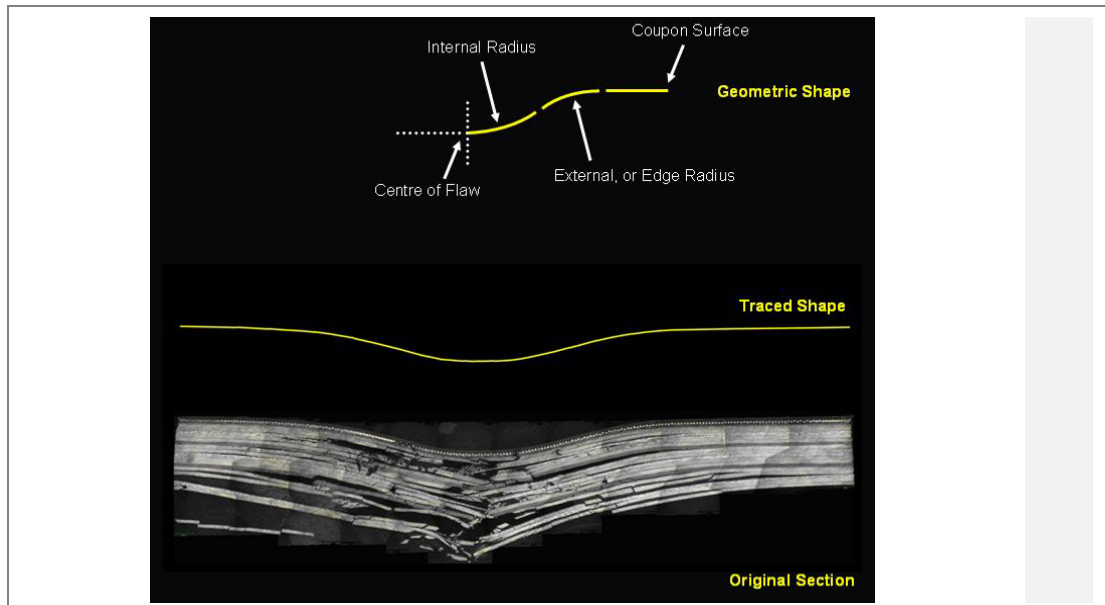


**Figure 33** 20 mm/ 30 J Surface flaw on a 17 ply Coupon

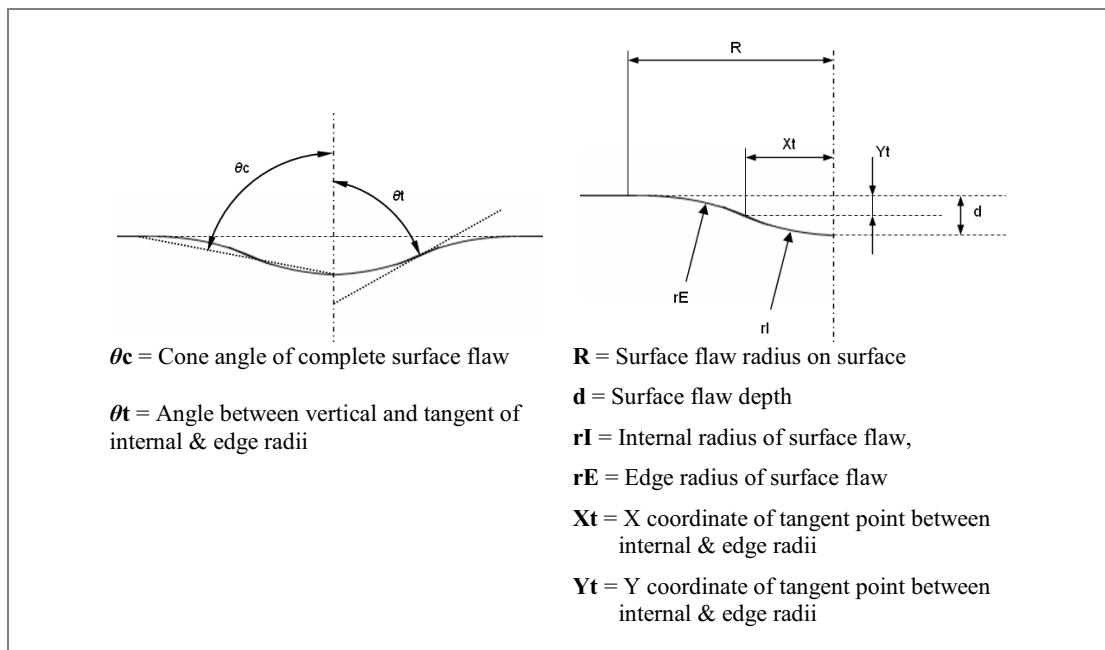


**Figure 34** Geometric variables used to reconstruct a surface flaw section

The sectional profile of surface flaws was recreated in a CATIA CAD system, by overlaying geometric lines, constructed using the variables in Figure 34, onto the CMM points data of the surface flaws.

The section lines through the CMM points data were created as splines, and were non-parametric, i.e. they have no geometric features such as radii within them. New geometric lines, as described in Figures 32 and 33 were overlaid to match the shape of the non-parametric surface flaw section lines. The geometric variables of the lines were adjusted until the geometric line fitted as best as possible to the original CMM points data (see Figure 35). From these fitted lines, it was possible to derive geometric variable values describing the original shape.

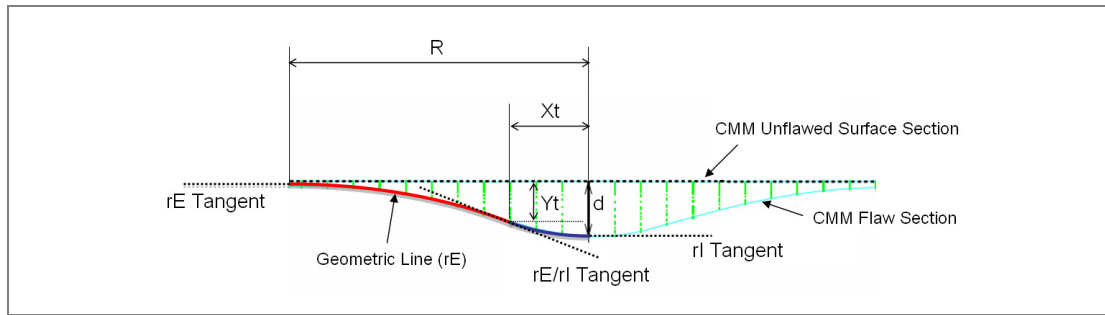


**Figure 35** Construction of geometric lines to match CMM data section lines

In order to ensure a smooth transition between the surface flaw lines and the original flat surface, without a visible join line, the tangent at the end of curve  $rE$  where it meets the planar surface was set to be horizontal (i.e. the same as the surface). To ensure symmetry, and not create a V shape at the centre of the flaw, the end of curve tangent of  $rl$  at the flaw centre line was constrained to be horizontal. A final tangent constraint was placed between the join of curves  $rE$  and  $rl$ , in order to ensure a smooth, step-less transition between the curves. These tangents can be seen in Figure 35.

### 2.5.2 Reconstruction of Surface Flaw Topography

The set of 26 surface flaws in Table 2 were reconstructed using the aforementioned method. The values of each geometric variable within the overlaid lines were recorded for each surface flaw, and are presented in Table 3.

### 2.6 Relationships Between Surface Flaw Geometry Variables

The data in Table 3 were plotted so as to identify relationships between the geometric variables for each combination of ply thickness and impact diameter. Best-fit lines were constructed to the data points. Graphs describing flaw width vs. impact energy, depth vs. energy, width vs.  $Xt$  value, and depth vs.  $Yt$  value are shown in Figures 36 to 39.

**Table 3** Geometric variable data obtained from surface flaws on painted, mesh incorporated CFRP laminate coupons

Impactor Size	Sample thick	Sample No	Energy J	R = w/2 (mm)	d (mm)	rl (mm)	rE (mm)	Xt (mm)	Yt (mm)	$\theta_t$ (°)	$\theta_c$ (°)	
20 mm	17 ply	27	5	2.5	0.11	11.78	16.68	1.03	0.06	84.96	87.48	
		26	10	6	0.07	85.73	171.45	2	0.05	88.66	89.33	
		82	15	10.75	0.32	58.84	121.89	3.5	0.22	86.59	88.29	
	33 ply	24	20	20	11	0.67	8.22	82.15	1	0.61	83.01	86.5
		83	30	30	15	2.11	5.44	48.94	1.5	1.9	73.99	81.99
		4	15	6	0.17	6.9	96.63	0.4	0.16	86.68	88.34	
		5	20	7.5	0.2	9.57	134.02	0.5	0.18	87.01	88.5	
		69	20	8	0.19	12.64	155.88	0.6	0.18	87.28	88.64	
		6	30	11.5	0.19	24.09	322.21	0.8	0.18	88.1	89.05	
		7	50	15	0.86	8.75	122.49	1	0.8	83.44	86.72	
	68	50	16.5	0.61	13.54	209.92	1	0.57	85.77	87.88		
	87 mm	17 ply	84	10	2.5	0.12	10.42	84.5	1	0.12	84.5	87.25
			93	15	6	0.11	41.68	125.04	1.5	0.08	87.94	88.97
29			20	5	0.08	46.89	109.4	1.5	0.06	88.17	89.08	
33 ply		85	20	6.5	0.18	36.14	81.31	2	0.12	86.83	88.41	
		88	30	8	0.02	666.67	1466.67	2.5	0.01	89.79	89.89	
		30	40	11	0.21	91.7	196.5	3.5	0.14	87.81	88.91	
		86	40	11.25	0.45	43.82	97.03	3.5	0.31	85.42	87.71	
		9	20	6.5	0.14	78.69	204.6	2.5	0.1	88.18	89.09	
		8	30	10.5	0.18	101.55	203.1	3.5	0.12	88.02	89.01	
		10	40	14	0.3	104.01	219.57	4.5	0.21	87.52	88.76	
66		40	30	0.26	286.48	1442.42	5	0.26	89.01	89.5		
11		50	23	0.37	203.73	517.16	6.5	0.26	88.17	89.09		
65		60	20	0.28	286.79	430.19	8	0.17	88.4	89.2		
12	60	35	0.29	521	1893.82	13	0.13	88.57	89.53			
13	70	31	0.34	659.17	750.09	14.5	0.18	88.74	89.37			

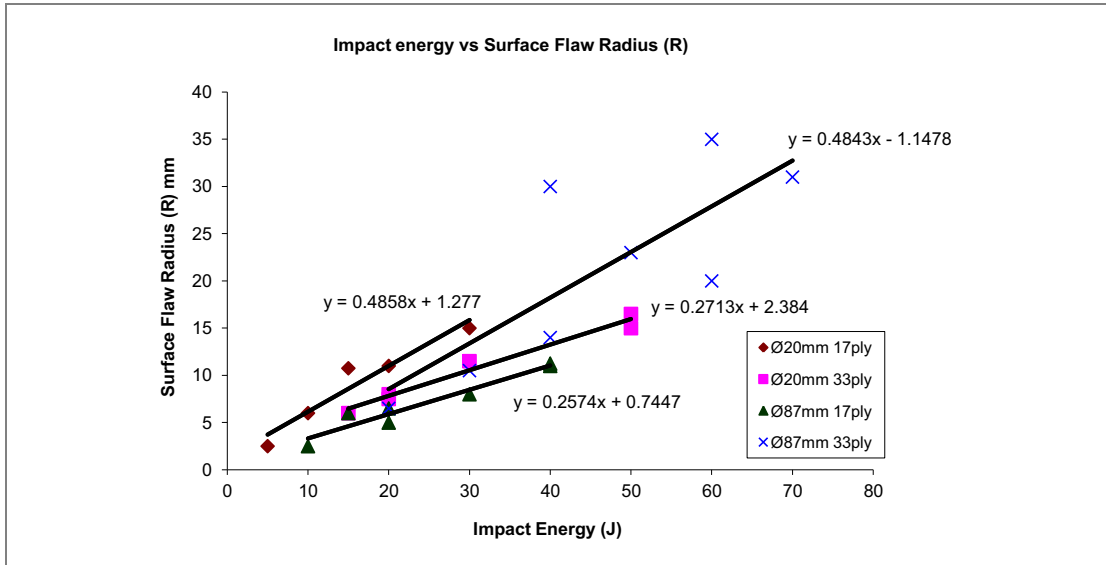


**Figure 36** Plot of impact energy vs. surface flaw radius with lines of best fit

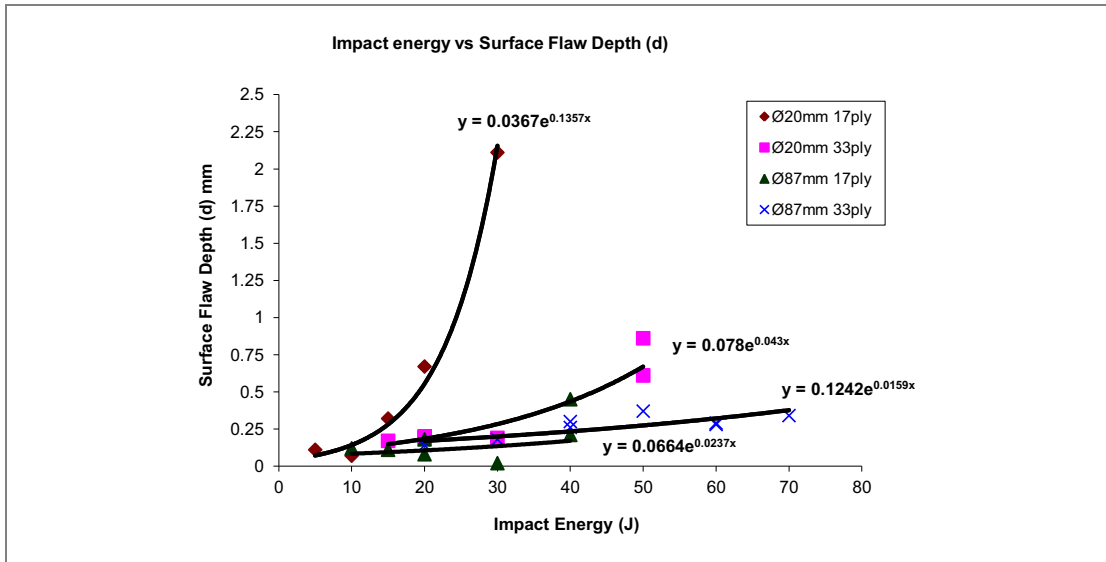


**Figure 37** Plot of impact energy vs. surface flaw depth with exponential curves of best fit

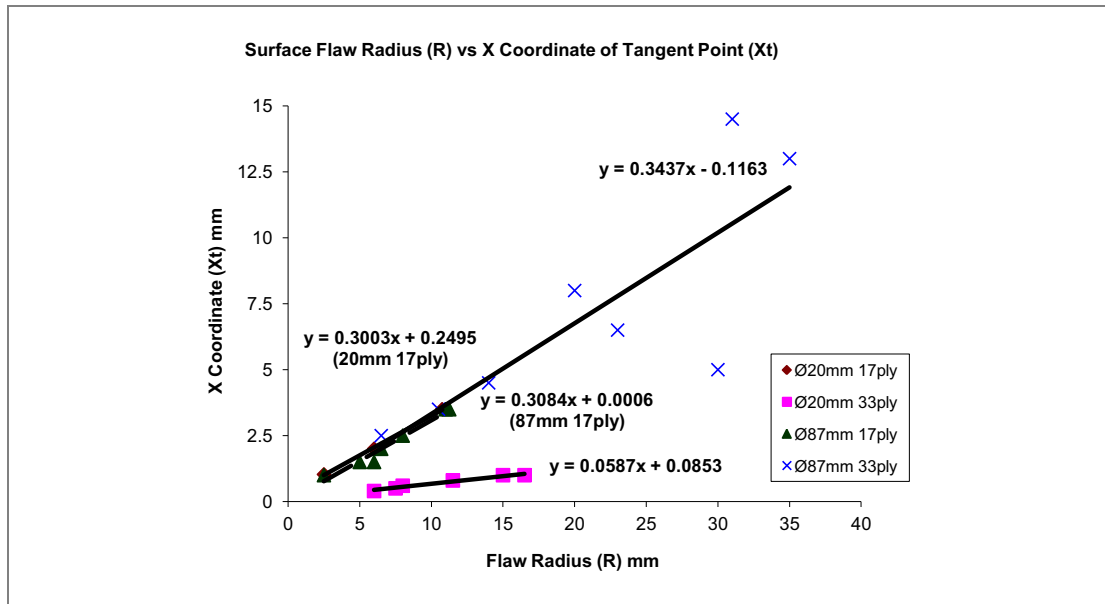


**Figure 38** Plot of surface flaw radius vs. Xt with lines of best fit

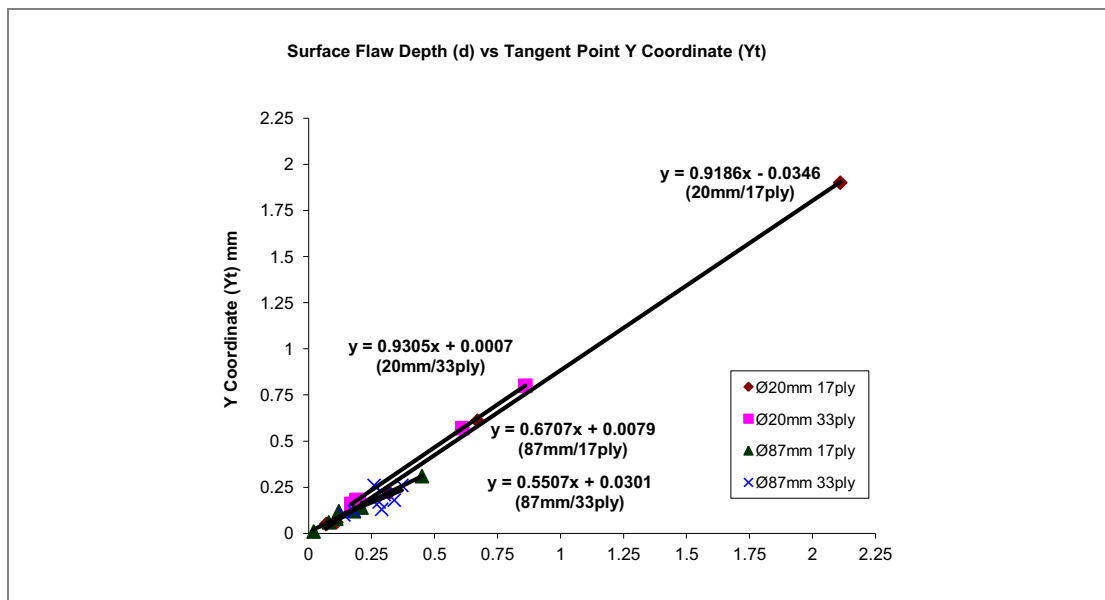


**Figure 39** Plot of surface flaw depth vs. Yt with lines of best fit

Figures 36 and 37 can be compared with Figures 30 and 31; both showing the relation between impact energy and flaw depth and width (radius = width/2 for Figure 36). The difference between them is that Figures 30 and 31 use directly measured width and depth data, whereas 36 and 37 show depth and radius derived from geometric variables fitted to the original flaw profile measurements. There are close similarities in the two sets for the depth measurements. In the case of the width (radius) measurements, there is significantly less scatter in the case of derived radius values than for the direct width measurements. This difference can be explained by the curve fitting process giving a more consistent representation of flaw width than was the case for direct measurement which as already noted was subject to significant measurement errors.

Table 4 gives the equations of the lines obtained by the best fit-line method from Figures 36–39. Also given is the energy range for which the relationship remains valid. All the relationships are only valid for impacts greater than 4J; impacts below this

energy level will not produce subsurface damage. Impacts above the given limit will penetrate the laminate, or cause a significant shape change to the laminate, in which the case the surface flaw characteristics are outside the scope of this study.

**Table 4** Geometry variable relationships for impact damage surface flaws

<b>17 ply/ 20 mm</b>	<b>17 ply/ 87 mm</b>
Radius R = 1.277 + 0.4858E	Radius R = 0.7447 + 0.2574E
Depth <b>d</b> = 0.0367( <i>exp</i> (0.1357 <b>E</b> ))	Depth <b>d</b> = 0.0664( <i>exp</i> (0.0237 <b>E</b> ))
X Point <b>Xt</b> = (0.247 <b>E</b> )-0.2933	X Point <b>Xt</b> = (0.0824 <b>E</b> )+0.1555
Y Point <b>Yt</b> = 0.0199( <i>exp</i> (0.1553 <b>E</b> ))	Y Point <b>Yt</b> = 0.0598( <i>exp</i> (0.0137 <b>E</b> ))
Applicable energy range: 4J -30J	Applicable energy range: 4J – 50J
<b>33 ply/ 20 mm</b>	
<b>33 ply/ 87 mm</b>	
Radius R = 2.374 + 0.2713E	Radius R = 1.1478 + 0.4843E
Depth <b>d</b> = 0.078( <i>exp</i> (0.043 <b>E</b> ))	Depth <b>d</b> = 0.1242( <i>exp</i> (0.0159 <b>E</b> ))
X Point <b>Xt</b> = (0.0159 <b>E</b> )+0.2263	X Point <b>Xt</b> = (0.2393 <b>E</b> )-3.8805
Y Point <b>Yt</b> = 0.0727( <i>exp</i> (0.043 <b>E</b> ))	Y Point <b>Yt</b> = 0.1198( <i>exp</i> (0.0075 <b>E</b> ))
Applicable energy range: 4J – 80J	Applicable energy range: 4J – 80J

By using the relationships listed in Table 04, and specifying impact energy or flaw radius, it is possible to determine all the variables required for constructing a surface flaw 2D section. Once determined, these variables can be used to construct 2D or 3D (via rotation about a normal to the sample plane) CAD instructions which can then be reproduced in facsimile samples by numerically controlled (NC) machining.

**2.7 Design and Manufacture of Facsimile Specimens**

Facsimile specimens, of 3 mm thick Plexiglas (PMMA) [41] material, were designed as 3D CAD objects, reproducing the surface flaws by NC machining into Plexiglas material. The specimens for inspection reliability assessments should be of a size representing the original structure [32]. To satisfy this requirement, a sample 600 mm x 600 mm was chosen, in order to provide the best compromise between providing a large search area and production equipment capability.

The surface finish (paint, coatings) of the specimen must be typical of what would be on an actual aircraft [31,32]. The use of Plexiglas material satisfied this recommendation, as it has a smooth glossy surface finish, and is available in various colours, thus providing a surface similar to a clean, painted aircraft structure.

**2.7.1 Facsimile Flaw Size Definition and Distributions**

Published guidelines on reliability assessment experiment design, state that *"specimens containing flaws so large that they are always found, and flaws so small that they are always missed"*, are not useful to the experiment [31]. With regard to flaw size *"there is a tendency to include too many "large" flaws"* in reliability assessments [31].

In order to set the flaw size range, upper values of impact energy for each flaw type were set as the maximum energy observed in coupon testing before the impact flaw

exhibited surface cracking or severe distortion of the entire coupon surface occurs. The lower value of the impact energy range was set at that, which using the relationships listed in Table 4, gave a flaw depth of 0.1 mm, or a positive value for the X-tangent. Using these impact energy limits, a series of 8 flaw widths evenly spaced between the largest and smallest energy values for each of the 4 impactor/thickness combinations was derived. These are shown in Table 5.

**Table 5** Calculated surface flaw widths

20 mm/17 ply		20 mm/33 ply		87 mm/17 ply		87 mm/33 ply	
Energy (J)	Width (mm)	Energy (J)	Width (mm)	Energy (J)	Width (mm)	Energy (J)	Width (mm)
11.9	9.03	4.8	7.39	18.5	11.02	11.7	14.15
14.3	10.49	7.8	9.03	23.3	13.46	13.2	16.44
17.0	12.18	11.5	11.02	29.1	16.44	14.9	19.11
20.2	14.15	16.0	13.46	36.1	20.09	17.0	22.20
23.9	16.44	21.5	16.44	44.8	24.53	19.3	25.79
28.2	19.11	28.2	20.09	55.3	29.96	22.1	29.96
33.2	22.20	36.4	24.53	68.2	36.60	25.3	34.81
39.0	25.79	46.4	29.96	83.9	44.70	29.0	40.45

Using the widths in Table 5 and the relationships in Table 4 to calculate flaw depth, a graph of flaw width vs. flaw depth can be produced, as seen in Figure 40. When using an even width interval, there are 9 flaws greater than 30 mm wide, and 6 flaws that are deeper than 0.6 mm.

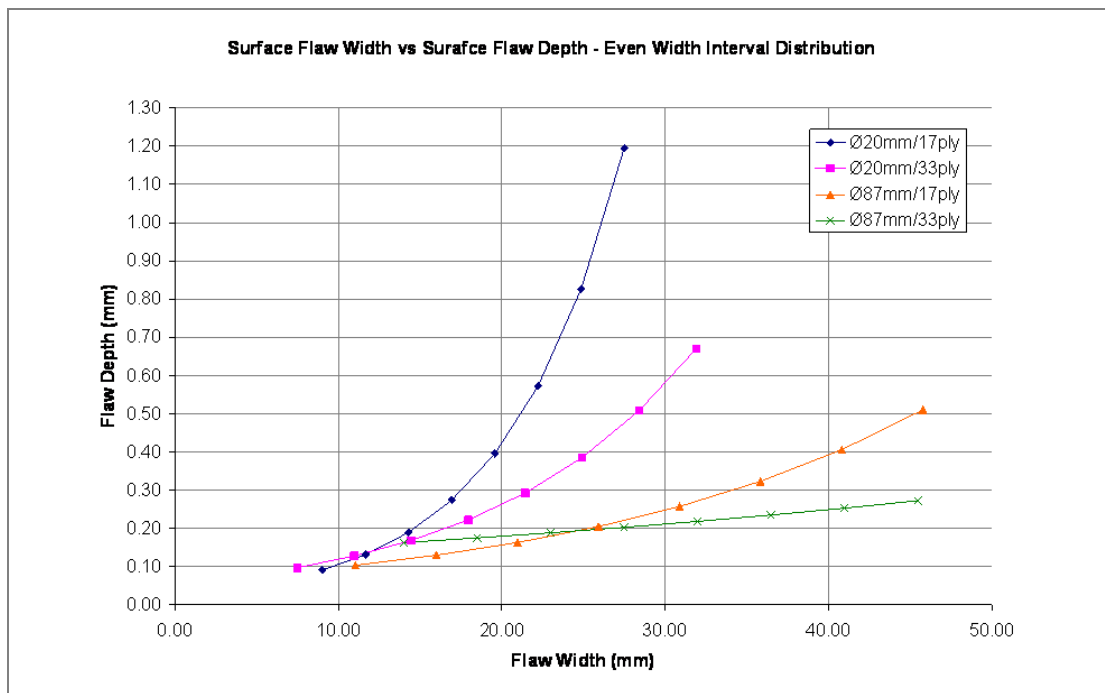


**Figure 40** Graph of flaw widths vs. flaw depths with even spacing between flaw widths

In view of earlier comments regarding too many large flaws being included in experiments, this flaw geometry distribution was modified to include a greater proportion of small to mid size flaws in the specimen set. The lognormal of each of the flaw widths in Table 5 was found, shown in Table 6. A flaw size interval that would space the lognormal values across a similar range to the original lognormal values was chosen, i.e. if the original range was 2.235 to 3.326, an interval of 0.15 was used to space new lognormal values across a range of 2.200 to 3.250. Using the exponential of the evenly spaced lognormal intervals, a new value was obtained for each flaw width. This resulted in a modified set of flaw widths, which are given in Table 6.

**Table 6** Values for flaw widths with even intervals between lognormal width values

<b>20 mm/ 17 ply flaws</b>				<b>20 mm/ 33 ply flaws</b>			
Original Width (mm)	ln(width)	New Value	New Width (mm)	Original Width (mm)	ln(width)	New Value	New Width (mm)
9.350	2.235	2.200	9.025	7.480	2.012	2.000	7.389
11.988	2.484	2.350	10.486	10.969	2.395	2.200	9.025
14.626	2.683	2.500	12.182	14.457	2.671	2.400	11.023
17.264	2.849	2.650	14.154	17.946	2.887	2.600	13.464
19.902	2.991	2.800	16.445	21.434	3.065	2.800	16.445
22.540	3.115	2.950	19.106	24.923	3.216	3.000	20.086
25.178	3.226	3.100	22.198	28.411	3.347	3.200	24.533
27.816	3.326	3.250	25.790	31.900	3.463	3.400	29.964
<b>87 mm/ 17 ply flaws</b>				<b>87 mm/ 33 ply flaws</b>			
Original Width (mm)	ln(width)	New Value	New Width (mm)	Original Width (mm)	ln(width)	New Value	New Width (mm)
10.499	2.351	2.400	11.023	13.995	2.639	2.650	14.154
15.463	2.738	2.600	13.464	18.492	2.917	2.800	16.445
20.427	3.017	2.800	16.445	22.989	3.135	2.950	19.106
25.391	3.234	3.000	20.086	27.486	3.314	3.100	22.198
30.356	3.413	3.200	24.533	31.983	3.465	3.250	25.790
35.320	3.564	3.400	29.964	36.480	3.597	3.400	29.964
40.284	3.696	3.600	36.598	40.977	3.713	3.550	34.813
45.248	3.812	3.800	44.701	45.474	3.817	3.700	40.447

Using the same method as for the graph in Figure 40, the plot of flaw width vs. flaw depth seen in Figure 41 was produced using the flaw widths from Table 6. On this graph, it can be seen that with the new distribution, there are now only 4 flaws wider than 30 mm and there is only one flaw greater than 0.6 mm deep.



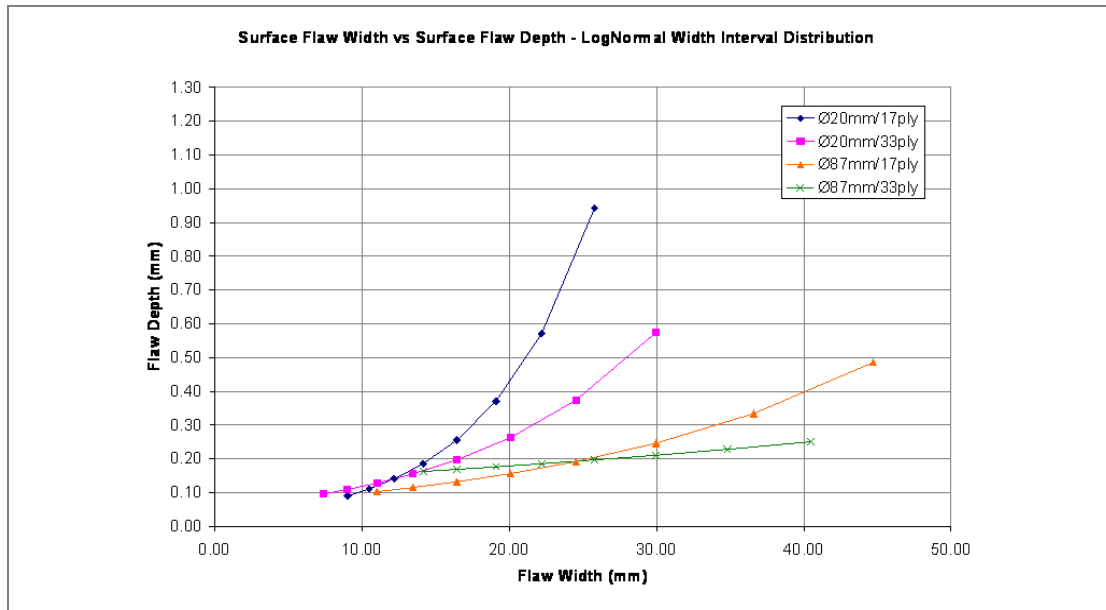


**Figure 41** Graph of flaw widths vs. flaw depths with even spacing between lognormal of flaw widths

**Table 7** Flaw variables used to define size of specimen flaws

<b>20 mm/17 ply</b>					<b>20 mm/33 ply</b>				
Energy (E) (J)	Width (2R) (mm)	Depth (d) (mm)	Xt (mm)	Yt (mm)	Energy (E) (J)	Width (2R) (mm)	Depth (d) (mm)	Xt (mm)	Yt (mm)
6.7	9.03	0.09	1.352	0.056	4.8	7.39	0.10	0.303	0.089
8.2	10.49	0.11	1.723	0.071	7.8	9.03	0.11	0.351	0.102
9.9	12.18	0.14	2.154	0.093	11.5	11.02	0.13	0.410	0.119
11.9	14.15	0.19	2.656	0.127	16.0	13.46	0.16	0.481	0.145
14.3	16.44	0.26	3.238	0.183	21.5	16.44	0.20	0.568	0.183
17.0	19.11	0.37	3.915	0.280	28.2	20.09	0.26	0.675	0.245
20.2	22.20	0.57	4.701	0.460	36.4	24.53	0.37	0.805	0.348
23.9	25.79	0.94	5.614	0.816	46.4	29.96	0.57	0.965	0.535
<b>87 mm/17 ply</b>					<b>87 mm/33 ply</b>				
Energy (E) (J)	Width (2R) (mm)	Depth (d) (mm)	Xt (mm)	Yt (mm)	Energy (E) (J)	Width (2R) (mm)	Depth (d) (mm)	Xt (mm)	Yt (mm)
18.5	11.02	0.10	1.681	0.077	17.0	14.15	0.16	0.184	0.136
23.3	13.46	0.12	2.072	0.082	19.3	16.44	0.17	0.749	0.139
29.1	16.44	0.13	2.549	0.089	22.1	19.11	0.18	1.407	0.141
36.1	20.09	0.16	3.132	0.098	25.3	22.20	0.19	2.171	0.145
44.8	24.53	0.19	3.844	0.110	29.0	25.79	0.20	3.058	0.149
55.3	29.96	0.25	4.713	0.128	33.3	29.96	0.21	4.090	0.154
68.2	36.60	0.33	5.775	0.152	38.3	34.81	0.23	5.288	0.160
83.9	44.70	0.49	7.072	0.189	44.1	40.45	0.25	6.679	0.167

The flaw widths in Table 06 and the relationships given in Table 4, were used to calculate the complete set of flaw geometry variables for each of the 32 surface flaws. Table 7 lists these variables. It should be noted that the values of rE and rI are driven by the position of Xt and Yt due to tangency constraints between the curves and the planar surface. Their calculation is not required if Xt and Yt are to be specified.

**2.7.2 Number of Specimens**

Following recommendations [30-32] on the number of specimens for a reliability assessment experiment, 64 specimen panels were used for each specimen set, of which 16 contained surface flaws. This resulted in a ratio of 3 unflawed specimen panels for every 1 flawed specimen panel, which also conformed to published recommendations [30-32].

**2.7.3 Flawed Specimen Specifications**

The specimen design placed 32 flaws onto 16 specimen panels using random X and Y coordinates with a 50 mm margin within the edge of the 600 mm x 600 mm panels. The placement order of the flaws onto the specimen panels was also randomised, such that a specimen panel contained up to 3 flaws of different sizes and types. Table 8 gives the details of each of the flawed specimen panels.

**Table 8** Specimen panel flaw location and size details

Panel Number	Number of Defects	Defect Number	X Coordinate	Y Coordinate	Defect Type	Defect Energy	Defect Width (R)	Defect Depth (d)	Defect X Point (Xt)	Defect Y Point (Yt)	Internal Radius (rI)	External Radius (rE)
1	1	1	290	490	Ø20mm/17ply	7	4.51	0.09	1.352	0.063	33.930	79.370
2	1	19	480	160	Ø87mm/17ply	29	8.22	0.13	2.549	0.090	80.608	179.336
3	1	12	490	80	Ø20mm/33ply	16	6.73	0.16	0.481	0.149	10.122	131.499
4	1	10	290	90	Ø20mm/33ply	8	4.51	0.11	0.351	0.101	7.208	85.507
5	1	6	190	310	Ø20mm/17ply	17	9.55	0.37	3.915	0.218	50.627	72.934
6	2	24	50	350	Ø87mm/17ply	84	22.35	0.49	7.072	0.335	161.362	348.599
		22	270	400	Ø87mm/17ply	55	14.98	0.25	4.713	0.171	141.241	307.685
7	2	20	160	440	Ø87mm/17ply	36	10.04	0.16	3.132	0.110	98.340	217.058
		7	490	60	Ø20mm/17ply	20	11.10	0.57	4.701	0.329	45.894	62.470
8	2	25	170	200	Ø87mm/33ply	17	7.08	0.16	0.184	0.156	4.070	152.434
		31	500	340	Ø87mm/33ply	38	17.41	0.23	5.288	0.160	200.117	152.434
9	2	8	330	260	Ø20mm/17ply	24	12.90	0.94	5.614	0.531	38.711	50.206
		13	470	470	Ø20mm/33ply	22	8.22	0.20	0.568	0.186	11.679	157.342
10	2	27	260	80	Ø87mm/33ply	22	9.55	0.18	1.407	0.153	37.357	216.338
		26	330	310	Ø87mm/33ply	19	8.22	0.17	0.749	0.155	18.116	180.700
11	2	16	110	60	Ø20mm/33ply	46	14.98	0.57	0.965	0.533	12.699	184.429
		4	180	490	Ø20mm/17ply	12	7.08	0.19	2.656	0.119	49.486	82.334
12	3	18	180	80	Ø87mm/17ply	23	6.73	0.12	2.072	0.083	58.121	130.660
		15	230	290	Ø20mm/33ply	36	12.27	0.37	0.805	0.346	13.354	190.115
		30	460	250	Ø87mm/33ply	33	14.98	0.21	4.090	0.153	145.905	388.486
13	3	14	200	370	Ø20mm/33ply	28	10.04	0.26	0.675	0.243	13.048	181.124
		28	340	120	Ø87mm/33ply	25	11.10	0.19	2.171	0.153	63.435	260.897
		9	420	490	Ø20mm/33ply	5	3.69	0.10	0.303	0.092	5.602	62.713
14	3	3	110	530	Ø20mm/17ply	10	6.09	0.14	2.154	0.090	46.874	85.653
		21	250	210	Ø87mm/17ply	45	12.27	0.19	3.844	0.130	124.100	271.864
		29	280	540	Ø87mm/33ply	29	12.90	0.20	3.058	0.153	98.606	317.197
15	3	11	190	340	Ø20mm/33ply	12	5.51	0.13	0.410	0.120	8.694	108.141
		5	480	200	Ø20mm/17ply	14	8.22	0.26	3.238	0.158	51.237	78.833
		17	290	290	Ø87mm/17ply	19	5.51	0.10	1.681	0.069	46.327	105.524
16	3	23	60	440	Ø87mm/17ply	68	18.30	0.33	5.775	0.226	160.177	347.397
		32	370	340	Ø87mm/33ply	44	20.22	0.25	6.679	0.167	270.207	548.019
		2	450	430	Ø20mm/17ply	8	5.24	0.11	1.723	0.074	41.096	84.005

### 2.7.4 Inspection panel Manufacture

3D CAD data of the specimen panels containing surface flaws, conforming to the specifications of Table 8 were produced using the Solid Works CAD program. The surface flaws were created by revolving the 2D geometric surface-flaw section line around the vertical centre line of the flaw, as illustrated in Figure 42.

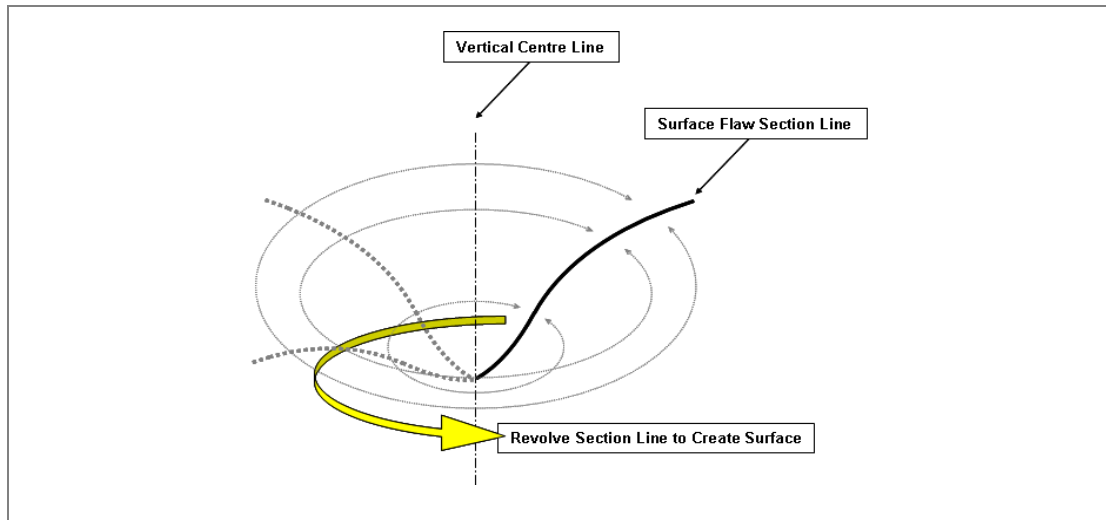


**Figure 42** Revolution of surface flaw section line to produce 3D flaw surface

The X and Y coordinates in Table 8 specify the location on the inspection face of the panel of the vertical centre line of the defect. The co ordinate origin is at the top left corner of the panel. Figure 43 illustrates the X/Y coordinates specified on a specimen panel with 3 surface flaws.

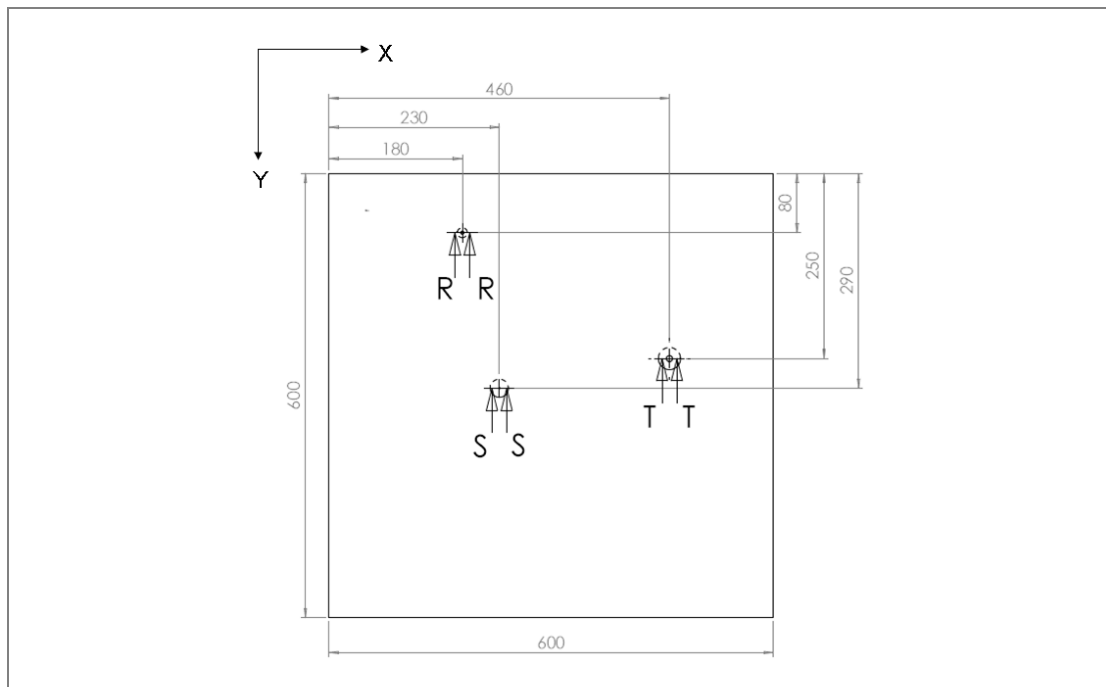


**Figure 43** X/Y coordinates used for placement of flaws on to specimen panels

The 3D revolved geometry was cut away from the 3 mm thick panel, leaving a circular surface flaw on the panel surface. Reference drawings of each 3D CAD model were produced for each specimen panel, and can be found in Appendix A2.

After NC machining the surface flaw into 3 mm thick Plexiglas panels, the flaw area was polished to return the flaw site to its original surface finish. Figure 44 illustrates a test piece that contains 12 surface flaws produced in this way, and can be compared with Figure 45 which shows a photograph of an actual impact damage surface flaw on a painted/mesh laminate.

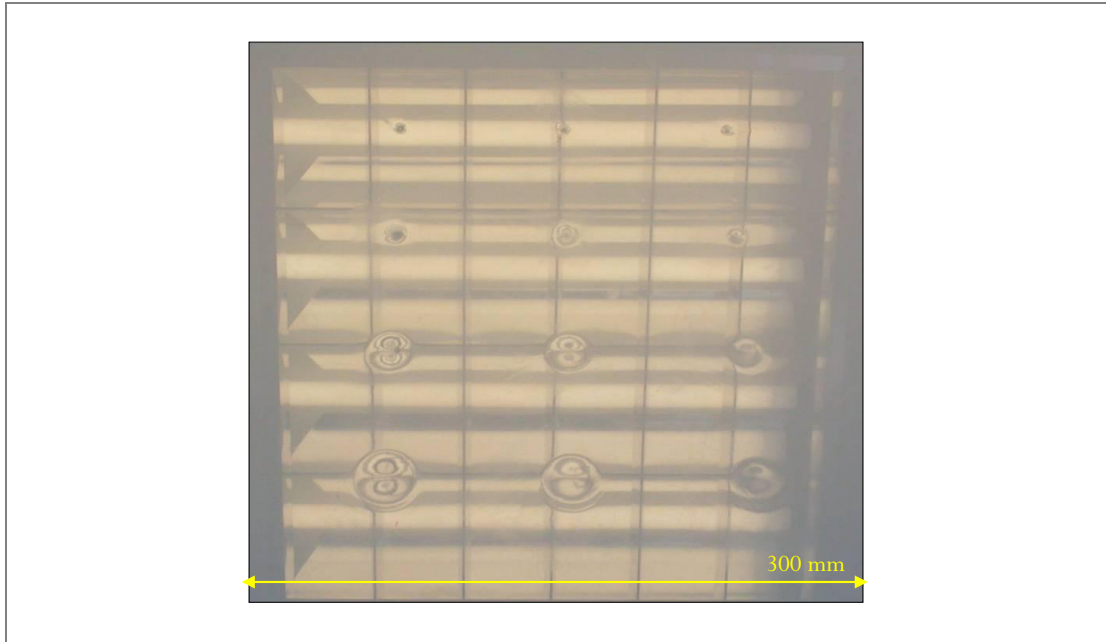


**Figure 44** Test piece containing Surface flaws

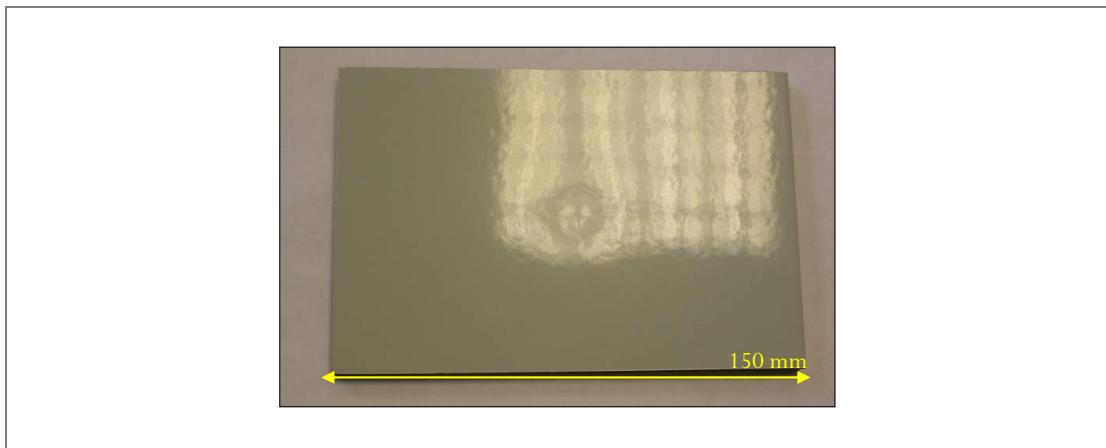


**Figure 45** Impact damage surface flaw on a painted/ bronze mesh CFRP laminate

Complete specimen sets, with surface flaws as given in Table 8, were machined in grey, white and blue Plexiglas panels making 3 sets in all, thus providing different coloured sets of panels without the need for painting.

### **Matt Finish Specimens**

Upon completion of visual inspection trials with the gloss grey, white and blue panels, the flawed specimens received a thin coat of matt finish paint of the same colour. This allowed their use in reliability assessments of the effect of surface finish on visual inspection, without the need for new machining work. 16 unflawed matt panels of each colour were also prepared in the same way, and were recycled into the specimen set during visual inspection trials in order to provide the required number of 48 unflawed specimens.

## 2.7.5 Characterisation of Specimens after Manufacture

### CMM Checking

Five selected flaws on each colour of specimen underwent CMM measurement to check for conformity to the original specification. An example of a comparison between the CMM data, and the original flaw specification can be seen in Figure 46. The CMM data taken from the machined flaw run are barely distinguishable from the specified geometry.

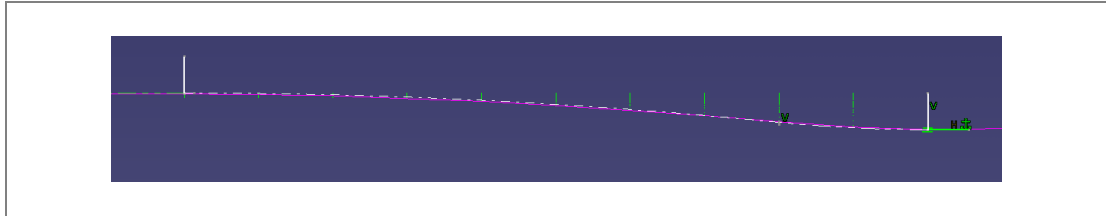


**Figure 46** CMM data (pink solid line) and specified geometry (white dashed line) of 22.2 mm/ 0.57 mm deep NC machined surface flaw

Three Y-Axis measurements of the CMM data were made using CATIA at the endpoint, the Xt point, and the centre point of the flaw, as shown in Figure 47. Table 9 details the findings. One can see in Table 9 that there was maximum average discrepancy across the different coloured panels of 15% on flaw #9 between the specified flaw depth, and the actual flaw depth (as obtained by subtracting the endpoint measurement from the total specified depth). However, the other flaws measured had an average depth discrepancy of less than 5%. The average discrepancy between the actual and specified depth at the Xt point was less than 10% for all surface flaws measured. The surface flaws were deemed to be within an acceptable tolerance of the original size specifications, and the overall shapes conformed to the design specification.

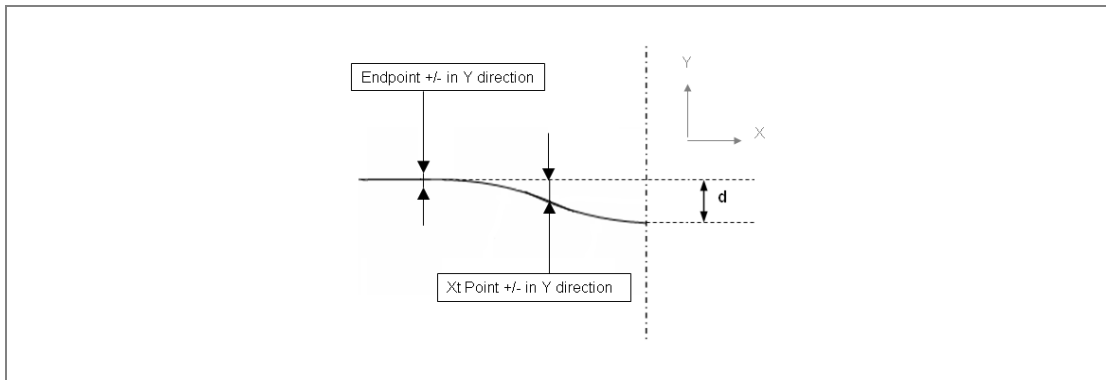


**Figure 47** Checking points for CMM data vs. original specification

**Table 9** +/- Y-Axis measurements from CMM data of specimen surface flaws

Flaw Number	Check Point	Original Specification	Grey Specimen	White Specimen	Blue Specimen	Average Discrepancy
7	Endpoint	0 mm	0.044 mm	-0.010 mm	-0.023 mm	0.0037 mm (0.64% of depth)
	Xt Point	-0.329 mm	0.018 mm	-0.050 mm	-0.005 mm	-0.0123 mm (3.75%)
	Centre (d)	-0.57 mm	0 mm	0 mm	0 mm	0 mm
9	Endpoint	0 mm	-0.019 mm	-0.013 mm	-0.013 mm	-0.0150 mm (15% of depth)
	Xt Point	-0.092 mm	-0.007 mm	-0.008 mm	-0.004 mm	-0.0063 mm (6.88%)
	Centre (d)	-0.1 mm	0 mm	0 mm	0 mm	0 mm
14	Endpoint	0 mm	-0.011 mm	-0.017 mm	-0.011 mm	-0.0130 mm (5% of depth)
	Xt Point	-0.243 mm	0.000 mm	0.007 mm	0.007 mm	0.0047 mm (1.92%)
	Centre (d)	-0.26 mm	0 mm	0 mm	0 mm	0 mm
20	Endpoint	0 mm	0.019 mm	-0.007 mm	0.010 mm	0.0073 mm (4.58% of depth)
	Xt Point	-0.11 mm	-0.011 mm	-0.004 mm	-0.013 mm	-0.0093 mm (8.48%)
	Centre (d)	-0.16 mm	0 mm	0 mm	0 mm	0 mm
28	Endpoint	0 mm	0.027 mm	-0.011 mm	0.012 mm	0.0093 mm (4.91% of depth)
	Xt Point	-0.153 mm	-0.014 mm	-0.002 mm	-0.010 mm	-0.0087 mm (5.66%)
	Centre (d)	-0.19 mm	0 mm	0 mm	0 mm	0 mm

**Gloss Measurements**

Gloss meter measurements of the gloss level of each specimen colour provided quantitative values for surface glossiness, and allowed comparisons with an actual aircraft surface finish. A gloss meter measures the intensity of light reflected by a surface from a light source of known intensity, and quantifies the amount of reflected light in terms of gloss units. Gloss measurements range from 0 to 100, with 100 being very glossy, i.e. the surface reflects light with 100% of original intensity. A matt finish surface will diffuse the light reflection, causing less light intensity to be detected, resulting in a lower gloss reading.

Table 10 gives the measurements made from the panels using a Novo Gloss dual-angle (20°, 60°) gloss meter.

**Table 10** Gloss measurements of specimens

Panel/ Specimen Colour	Gloss units (measurement angle)
Gloss Grey	84.666 (60°)
Gloss White	88.033 (60°)
Gloss Blue	79.833 (60°)
Matt Grey	1.733 (60°)
Matt White	7.766 (60°)
Matt Blue	0.533 (60°)

Aircraft paint specifications state that for gloss paints, the minimum gloss is 90 gloss units [42,43]; however, this is likely to reduce to between 80 and 90 gloss units after 3 years of aircraft service [44]. For matt finish paints, the manufacturers specify that the maximum gloss will be 5 gloss units [42,43]. The gloss-finish Plexiglas specimens are no glossier than one would expect a painted aircraft structure to be [43-44], and the matt finish grey and blue specimens are below the maximum gloss level that one would expect from a matt finish aircraft structure [42,43]. For the matt white finish specimens, the gloss reading of 7.766 gloss units is low enough to still be considered as a matt finish, despite being slightly higher than that specified by aircraft paint manufactures for a matt finish aircraft paint [42,43].

**Paint Thickness Measurement**

For the matt specimens, the thickness of the paint was measured. This was accomplished by metallographic sectioning of samples of a painted Plexiglas test piece. Figure 48 details the image obtained using a microscope. The measurement of the paint thickness was made using the microscope image processing software. The thickness was measured in several different places, and was found to be consistently within 12µm to 20µm, and therefore the defect geometry was not significantly influenced by the matt coating.

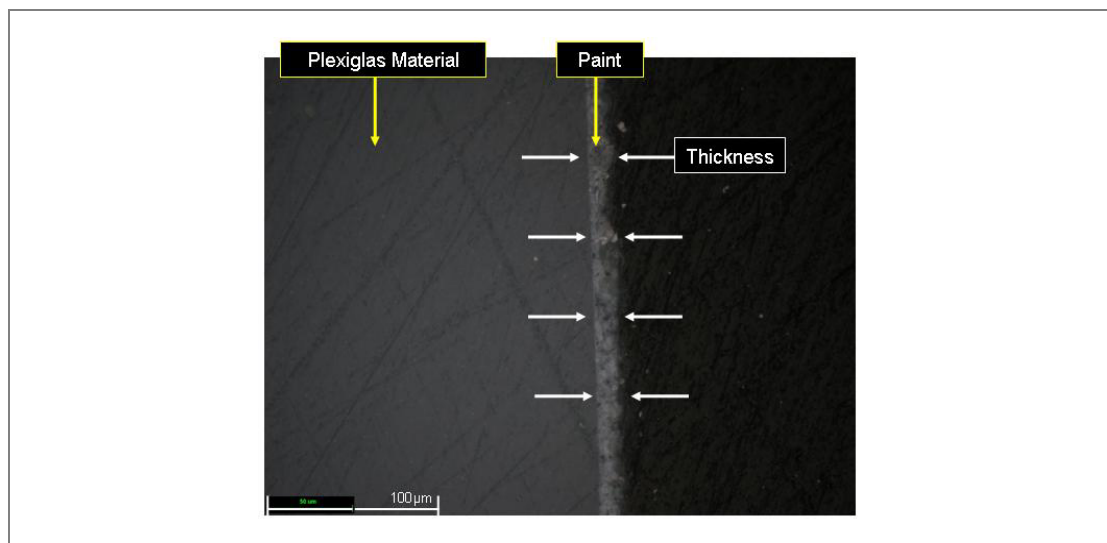


**Figure 48** Section of painted Plexiglas material used for thickness measurements

## 2.8 **Visual Inspection Trials Method**

The reliability assessment was performed as a series of visual inspection trials, using volunteer participants. A single trial constituted visual inspections of a set of specimens by an individual participant. Six sets of trials were performed:

- 1 Visual Inspection Trials with gloss grey specimens – 15 participants.
- 2 Visual Inspection Trials with gloss white specimens – 16 participants.
- 3 Visual Inspection Trials with gloss blue specimens – 16 participants.
- 4 Visual Inspection Trials with matt grey specimens – 17 participants.
- 5 Visual Inspection Trials with matt white specimens – 18 participants.
- 6 Visual Inspection Trials with matt blue specimens – 20 participants.

### 2.8.1 **Participants**

The participants for the visual inspection trials were volunteers from Cranfield University. Each was paid £5 for participating in a visual inspection trial. The participants were of mixed ages, most were between 25 and 35 years of age. Actual aircraft inspectors were not required for the visual inspection trials, as the trials constitute a reliability assessment that simulates the inspection task [45]. As the participants are not currently working as aircraft inspectors, they are less likely to use judgement during the trial. They are more likely to mark down every surface flaw that they see, instead of perhaps not marking flaws that they do not consider needing further NDT or repair. This gives a better representation of what the participants' eyes are actually capable of detecting during the trial.

### 2.8.2 **Equipment**

Six sets of specimen panels containing NC machined surface flaws were used in the visual inspection trials:

- Gloss grey specimens (Plexiglas Grey 812).
- Gloss white specimens (Plexiglas White 003).
- Gloss blue specimens (Plexiglas Blue 601).
- Matt painted grey specimens (grey primer).
- Matt painted white specimens (white primer).
- Matt painted blue specimens (RAL 5002 Ultramarine Blue).

Each specimen panel was labelled on the reverse (non-inspection) side.

A pivoted display stand was used to display the specimens to the participants (see Figures 49 and 51). The design of the stand allowed the participants to inspect the panel, after which the operators swung the panel round and replaced it with the next specimen, without the participants seeing the changeover.



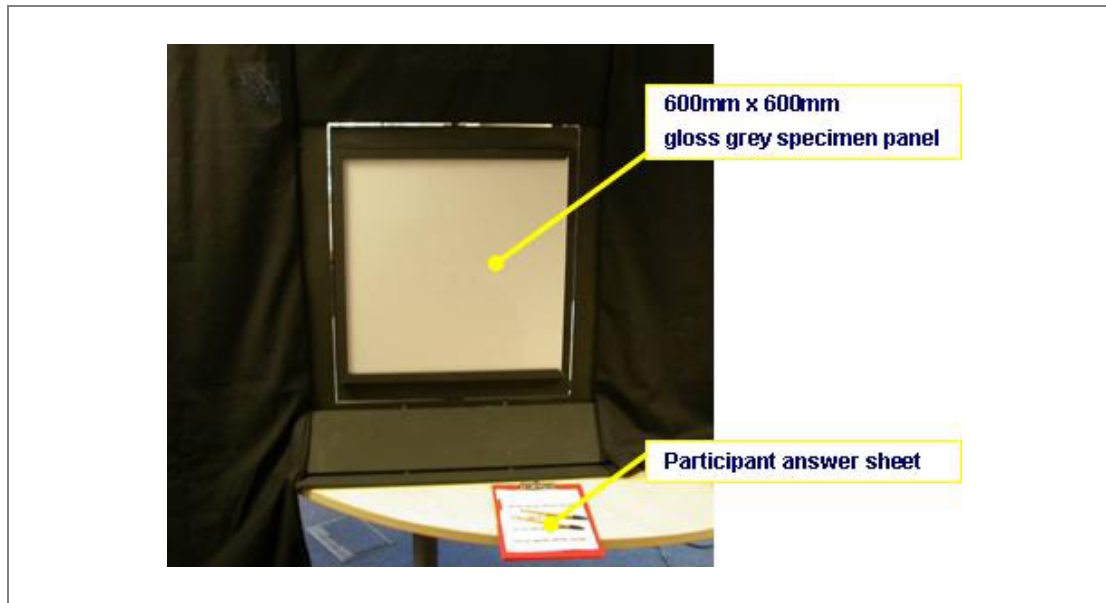


**Figure 49** Specimen display stand for visual inspection trials

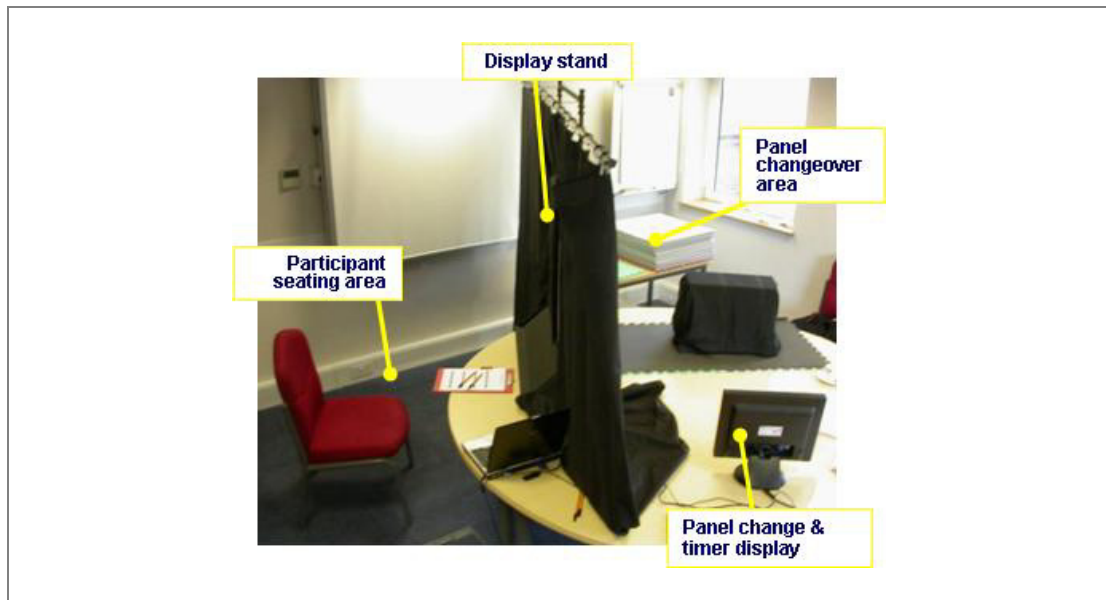


**Figure 50** Specimen display stand setup in meeting room

Figures 49 and 50 show the inspection trials experiment as it was set up in the meeting room. The display stand was table mounted, and curtains attached to it in order to provide a screen behind which the personnel performed the panel changeover. A small, detachable display curtain hid the panels from view whilst they were swung into the inspection position.

The lighting of the inspection task was provided by downwards reflecting fluorescent ceiling luminaires of the type commonly found in office buildings. The lights were located above, and in line with the front of the inspection side of the display stand. A computer with a display screen and speakers was used to run a Microsoft PowerPoint presentation, which provided the audible and visual timing signals for the display curtain operations, and changeover of the panels. The display screen was hidden from the participants view in order to avoid alerting them as to whether a flawed or unflawed specimen would be shown next. The participants were given a clipboard and paper answer sheet, on which they marked their answers with a pen.

### 2.8.3 Inspection Task

For each individual trial, the participants were asked to inspect a set of 64 specimen panels, containing 16 flawed specimen panels. The visual inspection task was to search the surface of the specimen panel for damage, and mark any detected damage sites on the answer sheet. The participants were seated in a chair, viewing the panels normal to the inspection surface plane, in a position where the participant's eyes were 1.2m from the specimen panels. The specimen panels were displayed individually, in a pre-determined, random order, for 5 seconds each. A regular interval of 20 seconds between each panel display was allowed for panel changeover. The complete task duration was approximately 27 minutes.

### 2.8.4 Experimental Procedures

#### Participant Briefing

The participants were given a 10-minute briefing before undertaking a visual inspection trial. The briefing explained the experimental task, provided examples of the surface flaws that the participants would be asked to find, and gave instructions on how to complete the answer sheet.

The answer sheet contained a diagram of each of the 64 specimen panels. The diagrams, as seen in Figures 51 and 52 illustrated the edge of the specimen panels, and a nine square guide grid to help the participants place their answers in the correct location. The participants were asked to mark the location of surface flaws with a cross (Figure 51), and to put a line through the entire panel for any specimens that the participant deemed free of surface flaws (Figure 52).

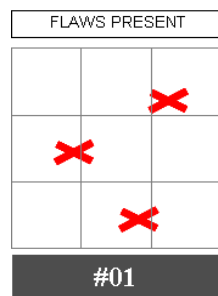


**Figure 51** Surface flaws detected

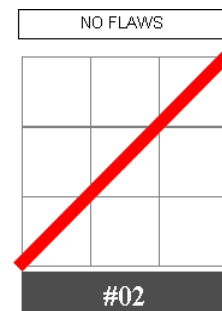


**Figure 52** No surface flaws detected

The participants were advised of how long the trial would be and how many panels they would view. The participants were told that some panels could contain more than one flaw and that some panels would be unflawed. The participants were advised that the panel display order had been randomised, and were told not to be anxious if they experienced a succession of panels on which they did not see flaws. The participants were not told how many flaws were in the specimen set, or how many flawed and unflawed specimen panels there were in the experiment. The participants were advised that their payment would not be affected by the results of the trials.

Participants were asked if they would normally wear corrective eyewear for medium to long-range vision, (i.e. to see presentation screens during lectures or for driving), and if so, that they wear them during the trial. The participants were told that they could move their heads to a reasonable extent during the visual inspection trials, but persons moving excessively would be asked to reduce the amount by which they moved their viewing position. The participants were instructed not to touch the

panels during the visual inspection trial. After being briefed, participants were given a clipboard, pen, and answer sheet. The answer sheet was marked with a serial number that identified the colour of the panels, the finish of the panels, the date of the trial, and the participant number.

### **Implementation of Visual Inspection Trial**

Two operators were required to run the visual inspection trials, operator 1 to perform the panel changeover, and operator 2 to remove and replace the small display curtain and act as moderator. After starting the timing presentation created in PowerPoint, operator 2 removed the display curtain on hearing a single beep from the computer, moved and held it clear of the display stand for a 5 seconds, and replaced it as instructed by a second beep from the computer. The display stand was swung round, and operator 1 removed the specimen panel, and replaced it with the next panel in the specimen display sequence. The computer display behind the display screen gave information on which panel to place into the display stand. An audible signal of three consecutive beeps sounded after 17 seconds, alerting the operators that the display stand and new specimen should now be ready in display position. After 20 seconds, a single beep sounded, thus repeating the process until the 64<sup>th</sup> panel was displayed.

For trials with gloss finish specimens, 48 unflawed specimen panels were available. This made it possible to stack the complete set of 64 (16 flawed/ 48 unflawed) specimens in the correct display sequence prior to beginning the first trial, ready for display to participants as instructed by the PowerPoint timing presentation. During the trial, the changeover operator re-stacked the specimens in reverse order, when removing them from the display stand. For the next trial, the specimens were displayed in reverse sequence. A record was kept of which sequence the participants saw the specimens in by adding FO (forwards order) or RO (reverse order) into the serial number on each participant's answer sheet.

For the inspection trials with matt finish specimens, only 16 unflawed specimens were available. In order to display the 48 required unflawed specimens, the set of 16 unflawed specimens were displayed cyclically. The specimen sequence was displayed on the panel change screen (see Figure 50) for these trials, and the flawed and unflawed specimens were kept in separate piles. The changeover operator chose the correct flawed specimen, or an unflawed specimen, as instructed by the panel change screen. Prior to the first trial with a matt finish specimen set, the flawed specimens were stacked in the correct order in which the display screen would request their display for inspection. Upon removing a flawed specimen from the display stand, operator 2 restacked the flawed panels in the reverse order ready for the next trial, in which the display sequence reversed, as described for the gloss specimens. Two different timing presentations were used, one for forwards order trials and one for reverse order trials.

In any situation where a pause in the trial was required, the moderator stopped the inspection trial timer at the end of the display time for the current specimen, and re-started when convenient in order to avoid the possibility of distractions affecting participant performance during the trial.

#### **2.8.5 Data Collection**

Hit/miss data, and false call data were extracted from the answer sheets by comparing the answer sheets with a marking sheet that contained the actual locations of the 32 surface flaws within the specimen set. A hit was when the participant viewed a specimen panel detects the surface flaw, and marked down the presence of a surface flaw in the correct position on the diagram. A miss occurred when the participant did not detect and mark a flaw despite having viewed it. A false

call occurred when the participant marked the presence of a flaw on a specimen panel, or an area of a panel, that was known to be unflawed.

The criteria for a successful detections, or hits, were as follows:

- For multiple surface flaws, the participant answer marks should be in similar positions, or follow the same pattern as that shown on the marking sheet.
- For the remaining flaw answer marks on a multiple flaw specimen, where the participant missed one or more flaws, the participant answer mark should be within a distance equal to the size of one grid square of the position shown on the marking sheet
- For single flaws, or for judging a borderline hit/miss for individual flaws on a multiple flaw specimen, the participant answer should be within a distance equal to the size of one grid square of the position shown on the marking sheet.

Any answer mark made by the participant that did not correspond to a surface flaw on a specimen was a false call. The number of false calls made by each participant was recorded.

Some participants believed they saw a surface flaw and marked it down, but then decided that what they saw may not have been a surface flaw, and crossed out their answer. Where a participant correctly detected, and marked down a surface flaw, but subsequently crossed the answer out, the mark was recorded as a hit, as the participant must have had some cause to make the original mark. The marking ignored crossed out marks that did not correspond to a surface flaw, as such marks are the result of the participants realising that they have made a false call.

The hit/ miss data for each of the visual inspection trials were recorded as a set of six data tables, one for each set of specimens used. The tables list each of the flaws within the specimen set, and each of the participant's responses. A hit is recorded as 1 and a miss as 0. The total number of false calls for each participant are also listed in the tables, which can be found in appendix A3.

## 2.9 Results of Inspection Trials

In order to accommodate participant availability for 6 inspection trials, two participants performed the inspection trial sat side-by-side. The author considered the possible advantage of being seated at a slight angle to the specimen panel as negligible, especially given that other participants were free to move their heads during inspection. The operators checked, and found that the view of a panel, and surface flaw, at a slight angle was indiscernible to the view from exactly 90° to the panel. The results from these trials showed no difference to trials with a single participant.

Participant 12 experienced some degree of eye strain during an inspection trial with matt white specimens, and could not decide if they were able to inspect better with or without their glasses. The operators offered to pause, or stop the trial, but the participant expressed a wish to continue, and inspected without glasses thereafter. When checked after the trial by the moderator, the results for this trial did not appear to be significantly different to any other participants, and were thus included in the experimental results.

### 2.9.1 Presentation of results

The results of each of the visual inspection trials are originally recorded as a set of simple hit/ miss data. The percentage of participants detecting each surface flaw was calculated. allowing the results of trials with different numbers of participants to be compared.

A table of the percentage of flaws detected on each specimen set is given in Table 11. Whilst it is possible to plot simple graphs of percentage of detections vs. flaw width, or flaw depth, such graphs are unable to illustrate flaw depth at the same time. Similarly, simple graphs of detections vs. flaw depth are unable to convey the fact that two flaws of the depths may have different widths. As flaw visibility is believed to be dependent on both width and depth, it is of little use to attempt to base conclusions on graphs that only list one of the variables.

**Table 11** % of detection for each flaw on each colour and surface finish

Flaw Number	Type	Flaw Size		% Detections					
		Width (mm)	Depth (mm)	Gloss Grey	Matt Grey	Gloss White	Matt White	Gloss Blue	Matt Blue
1	20 mm/17 ply	9.03	0.09	33%	41%	6%	0%	44%	5%
2	20 mm/17 ply	10.49	0.11	7%	35%	19%	22%	44%	10%
3	20 mm/17 ply	12.18	0.14	87%	71%	75%	39%	75%	10%
4	20 mm/17 ply	14.15	0.19	93%	94%	100%	94%	69%	45%
5	20 mm/17 ply	16.44	0.26	27%	35%	75%	94%	69%	50%
6	20 mm/17 ply	19.11	0.37	100%	94%	100%	100%	69%	95%
7	20 mm/17 ply	22.2	0.57	93%	94%	81%	89%	81%	50%
8	20 mm/17 ply	25.79	0.94	100%	100%	100%	100%	100%	100%
9	20 mm/33 ply	7.39	0.1	13%	12%	6%	6%	25%	0%
10	20 mm/33 ply	9.03	0.11	27%	29%	19%	39%	6%	5%
11	20 mm/33 ply	11.02	0.13	80%	100%	75%	56%	31%	5%
12	20 mm/33 ply	13.46	0.16	20%	18%	13%	0%	50%	0%
13	20 mm/33 ply	16.44	0.2	20%	47%	50%	33%	63%	10%
14	20 mm/33 ply	20.09	0.26	93%	100%	100%	94%	69%	60%
15	20 mm/33 ply	24.53	0.37	93%	94%	88%	100%	56%	95%
16	20 mm/33 ply	29.96	0.57	100%	100%	100%	100%	81%	85%
17	87 mm/17 ply	11.02	0.1	33%	24%	13%	39%	38%	5%
18	87 mm/17 ply	13.46	0.12	33%	29%	38%	44%	6%	5%
19	87 mm/17 ply	16.44	0.13	13%	24%	13%	6%	56%	10%
20	87 mm/17 ply	20.09	0.16	67%	71%	81%	67%	75%	30%
21	87 mm/17 ply	24.53	0.19	100%	88%	81%	61%	38%	50%
22	87 mm/17 ply	29.96	0.25	93%	88%	75%	33%	81%	40%
23	87 mm/17 ply	36.6	0.33	93%	100%	100%	89%	56%	75%
24	87 mm/17 ply	44.7	0.49	100%	88%	94%	78%	69%	85%
25	87 mm/33 ply	14.15	0.16	87%	53%	81%	56%	19%	45%
26	87 mm/33 ply	16.44	0.17	53%	65%	56%	50%	19%	25%
27	87 mm/33 ply	19.11	0.18	80%	41%	50%	17%	38%	25%
28	87 mm/33 ply	22.2	0.19	60%	47%	50%	83%	56%	15%
29	87 mm/33 ply	25.79	0.2	73%	53%	38%	22%	75%	15%
30	87 mm/33 ply	29.96	0.21	40%	35%	19%	17%	50%	10%
31	87 mm/33 ply	34.81	0.23	27%	59%	13%	0%	50%	0%
32	87 mm/33 ply	40.45	0.25	67%	59%	6%	22%	44%	0%

To allow display of both the width and depth of a surface flaw at the same time as the percentage of detections, a matrix was produced. Figures 53 – 58 show the matrices of percentage detection of surface flaws on the gloss and matt grey, white and blue specimens. The flaw widths and depths are distributed into ranges. The detection percentages of flaws that fall within these width and depth ranges are averaged, thus providing a single percentage detection value for all of the flaws within a size range.

Average % Detections from Gloss Grey Specimens								
Depth Range	Width Range:							
	5.1 - 10.0mm	10.1 - 15mm	15.1 - 20mm	20.1 - 25mm	25.1 - 30mm	30.1 - 35mm	35.1 - 40mm	40.1 - 45mm
0.05 - 0.099		33%						
0.1 - 0.149	13%	45%	13%					
0.15 - 0.199		67%	67%	80%				
0.20 - 0.249			20%		57%	27%		
0.25 - 0.299			60%		93%			67%
0.30 - 0.349							93%	
0.35 - 0.399			100%	100%				
0.40 - 0.449								
0.45 - 0.499								100%
0.50 - 0.549								
0.55 - 0.599				93%	100%			
0.60 - 0.649								
0.65 - 0.699								
0.70 - 0.749								
0.75 - 0.799								
0.80 - 0.849								
0.85 - 0.899								
0.90 - 0.949					100%			

**Figure 53** Matrix of detection percentages arranged by flaw width and flaw depth, obtained using gloss grey specimens

Average % Detections from Matt Grey Specimens								
Depth Range	Width Range:							
	5.1 - 10.0mm	10.1 - 15mm	15.1 - 20mm	20.1 - 25mm	25.1 - 30mm	30.1 - 35mm	35.1 - 40mm	40.1 - 45mm
0.05 - 0.099		41%						
0.1 - 0.149	12%	48%	24%					
0.15 - 0.199		55%	59%	68%				
0.20 - 0.249			47%		44%	59%		
0.25 - 0.299			68%		88%			59%
0.30 - 0.349							100%	
0.35 - 0.399			94%	94%				
0.40 - 0.449								
0.45 - 0.499								88%
0.50 - 0.549								
0.55 - 0.599				94%	100%			
0.60 - 0.649								
0.65 - 0.699								
0.70 - 0.749								
0.75 - 0.799								
0.80 - 0.849								
0.85 - 0.899								
0.90 - 0.949					100%			

**Figure 54** Matrix of detection percentages arranged by flaw width and flaw depth, obtained using matt grey specimens

Average % Detections from Gloss White Specimens								
Depth Range	Width Range:							
	5.1 - 10.0mm	10.1 - 15mm	15.1 - 20mm	20.1 - 25mm	25.1 - 30mm	30.1 - 35mm	35.1 - 40mm	40.1 - 45mm
0.05 - 0.099		6%						
0.1 - 0.149	6%	40%	13%					
0.15 - 0.199		65%	62%	66%				
0.20 - 0.249			50%		29%	13%		
0.25 - 0.299			88%		75%			6%
0.30 - 0.349							100%	
0.35 - 0.399			100%	88%				
0.40 - 0.449								
0.45 - 0.499								94%
0.50 - 0.549								
0.55 - 0.599				81%	100%			
0.60 - 0.649								
0.65 - 0.699								
0.70 - 0.749								
0.75 - 0.799								
0.80 - 0.849								
0.85 - 0.899								
0.90 - 0.949					100%			

**Figure 55** Matrix of detection percentages arranged by flaw width and flaw depth, obtained using gloss white specimens

Average % Detections from Matt White Specimens								
Depth Range	Width Range:							
	5.1 - 10.0mm	10.1 - 15mm	15.1 - 20mm	20.1 - 25mm	25.1 - 30mm	30.1 - 35mm	35.1 - 40mm	40.1 - 45mm
0.05 - 0.099		0%						
0.1 - 0.149	6%	40%	6%					
0.15 - 0.199		50%	45%	72%				
0.20 - 0.249			33%		20%	0%		
0.25 - 0.299			94%		33%			22%
0.30 - 0.349							89%	
0.35 - 0.399			100%	100%				
0.40 - 0.449								
0.45 - 0.499								78%
0.50 - 0.549								
0.55 - 0.599				89%	100%			
0.60 - 0.649								
0.65 - 0.699								
0.70 - 0.749								
0.75 - 0.799								
0.80 - 0.849								
0.85 - 0.899								
0.90 - 0.949					100%			

**Figure 56** Matrix of detection percentages arranged by flaw width and flaw depth, obtained using matt white specimens

Average % Detections from Gloss Blue Specimens								
Depth Range	Width Range:							
	5.1 - 10.0mm	10.1 - 15mm	15.1 - 20mm	20.1 - 25mm	25.1 - 30mm	30.1 - 35mm	35.1 - 40mm	40.1 - 45mm
0.05 - 0.099		44%						
0.1 - 0.149	25%	33%	56%					
0.15 - 0.199		46%	44%	47%				
0.20 - 0.249			63%		63%	50%		
0.25 - 0.299			69%		81%			44%
0.30 - 0.349							56%	
0.35 - 0.399			69%	56%				
0.40 - 0.449								
0.45 - 0.499								69%
0.50 - 0.549								
0.55 - 0.599				81%	81%			
0.60 - 0.649								
0.65 - 0.699								
0.70 - 0.749								
0.75 - 0.799								
0.80 - 0.849								
0.85 - 0.899								
0.90 - 0.949					100%			

**Figure 57** Matrix of detection percentages arranged by flaw width and flaw depth, obtained using gloss blue specimens

Average % Detections from Matt Blue Specimens								
Depth Range	Width Range:							
	5.1 - 10.0mm	10.1 - 15mm	15.1 - 20mm	20.1 - 25mm	25.1 - 30mm	30.1 - 35mm	35.1 - 40mm	40.1 - 45mm
0.05 - 0.099		5%						
0.1 - 0.149	0%	7%	10%					
0.15 - 0.199		30%	27%	33%				
0.20 - 0.249			10%		13%	0%		
0.25 - 0.299			55%		40%			0%
0.30 - 0.349							75%	
0.35 - 0.399			95%	95%				
0.40 - 0.449								
0.45 - 0.499								85%
0.50 - 0.549								
0.55 - 0.599				50%	85%			
0.60 - 0.649								
0.65 - 0.699								
0.70 - 0.749								
0.75 - 0.799								
0.80 - 0.849								
0.85 - 0.899								
0.90 - 0.949					100%			

**Figure 58** Matrix of detection percentages arranged by flaw width and flaw depth, obtained using matt blue specimens

A second method of presenting the results was to use Statistica statistical data analysis software [46] to produce scatter graphs, with the percentage of participants detecting each flaw plotted against the corresponding flaw depth and flaw width of each flaw (see Figures 59–64). A natural log scale is used for the X and Y-axis, allowing greater separation of individual data points at smaller values of width and depth. The scatter plots allowed the detection percentage for each flaw to be compared in terms of depth and width against the other flaws in the specimen set. For example, in Figure 59 it can be seen that on the gloss grey specimens, there is no clear correlation between flaw width and detection %. However, all flaws greater than 0.3 mm deep were detected by more than 90% of participants. On gloss grey specimens, there were instances of greater than 90% detection when flaws were below 0.3 mm. On gloss blue specimens, however, there were no instances of greater than 90% detection when flaw depth was below 0.3 mm.

The scatter plots were also useful for comparing the detectability of individual flaws across the range of surface colours and finishes. For example, it can be seen that the detection of the 44.7 mm/ 0.49 mm deep flaw varied between 69% on gloss blue specimens and 100% on gloss grey specimens.

When viewing the scatter plots, it became apparent that the levels of detection percentage appeared to form bands, or contours, of constant detectability. In order to explore the possibility of detectability bands further, the wafer plot function of Statistica was used to fit the scatter plots with contours representing percentage levels of detection. The wafer plots are shown in Figures 65–70. The wafer plots also use a natural log scale on the X and Y-axis. The contours on the wafer plots are best fit lines of constant detection percentage, and allowed changes in detection rates due to colour or finish to be easily identified. Furthermore, the effects of flaw width and depth on detection rates were easily visualised on the wafer plots.



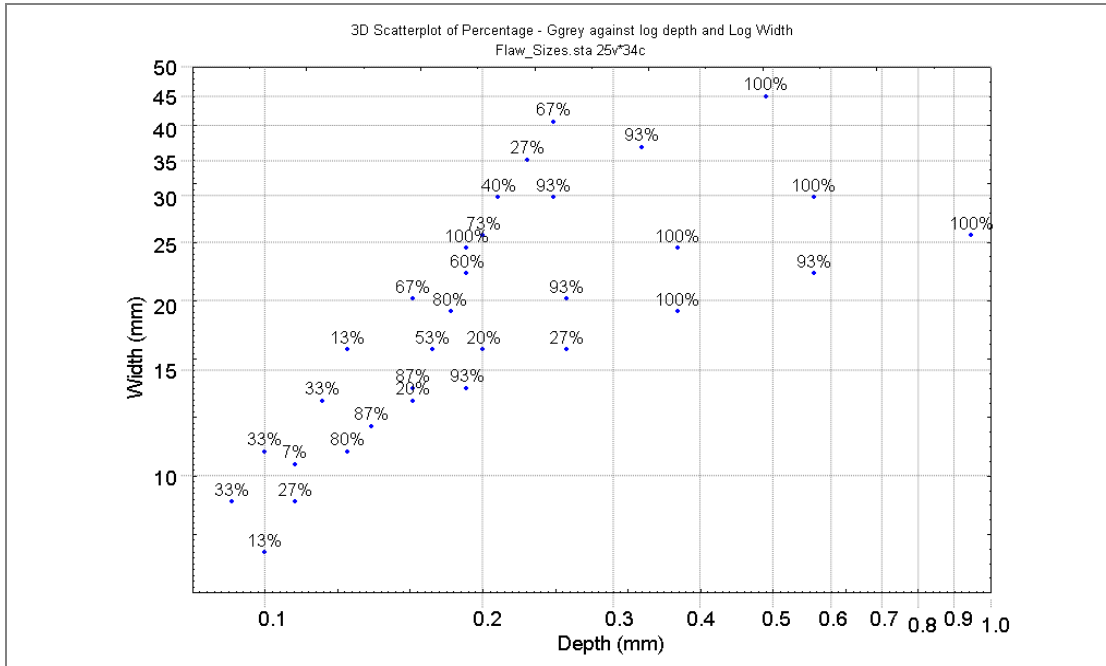


**Figure 59** Scatter plot of % of participants detecting each flaw vs. flaw depth and width for gloss grey specimens

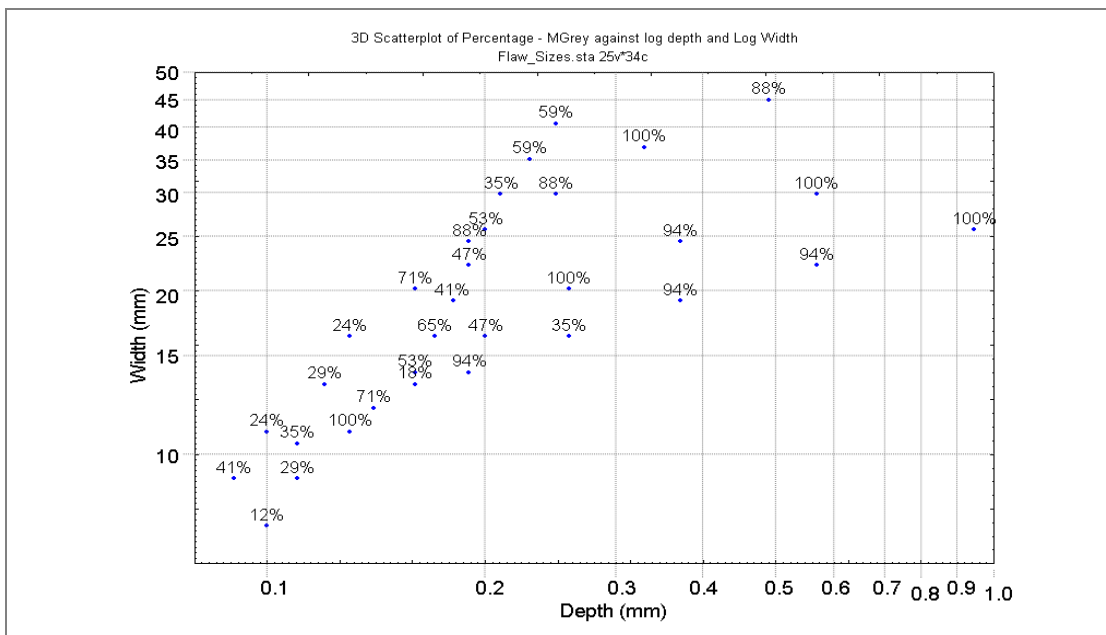


**Figure 60** Scatter plot of % of participants detecting each flaw vs. flaw depth and width for matt grey specimens

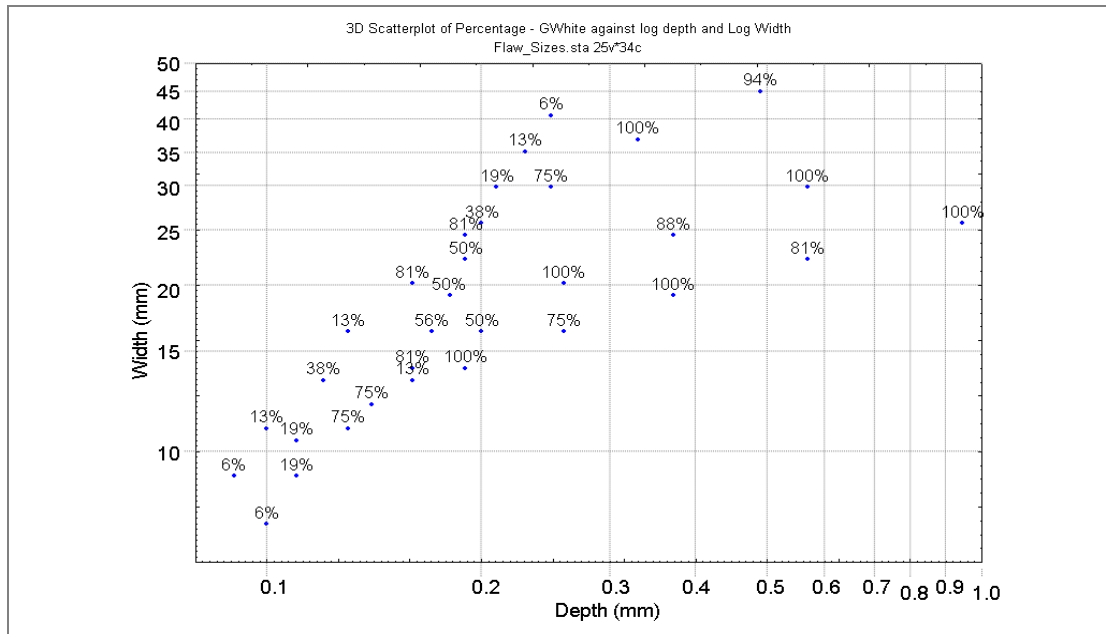


**Figure 61** Scatter plot of % of participants detecting each flaw vs. flaw depth and width for gloss white specimens

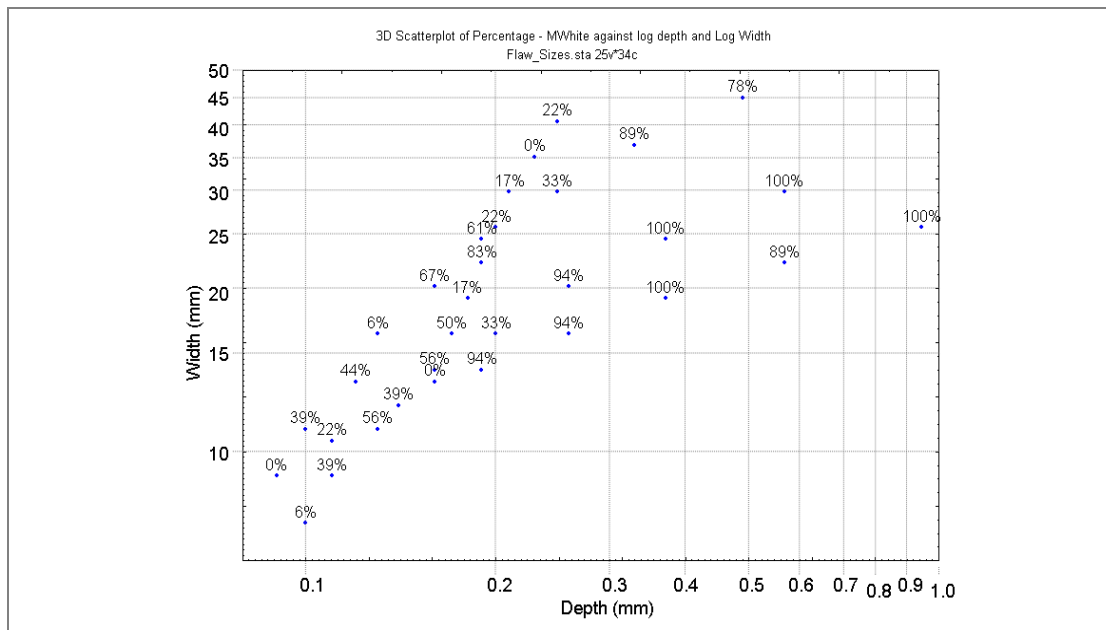


**Figure 62** Scatter plot of % of participants detecting each flaw vs. flaw depth and width for matt white specimens

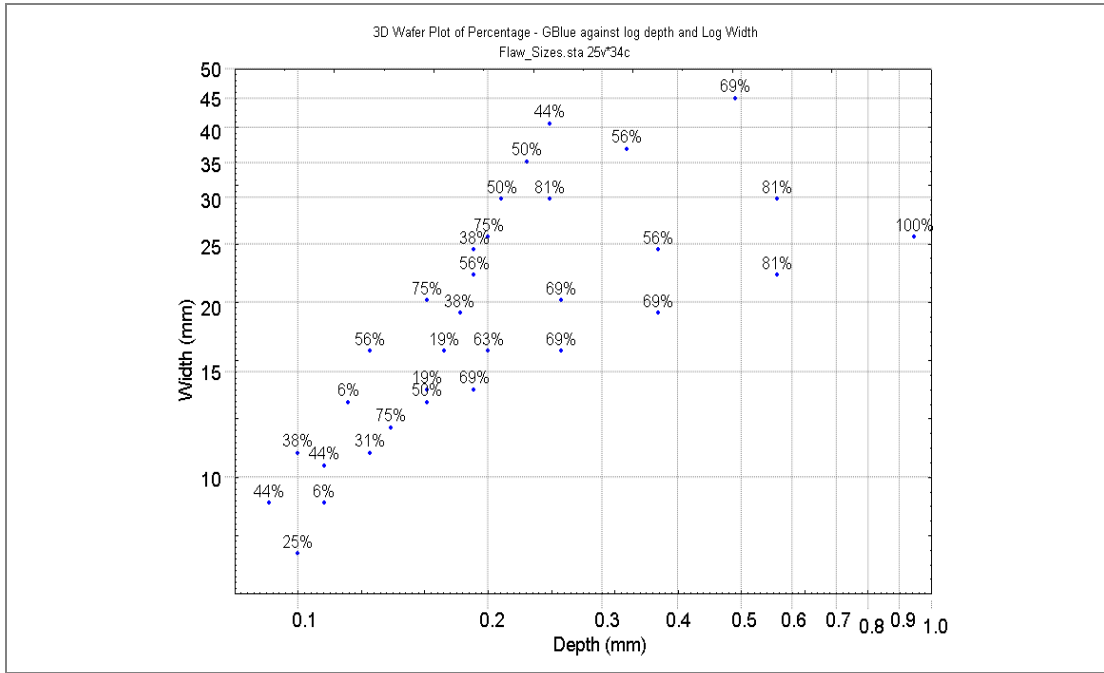


**Figure 63** Scatter plot of % of participants detecting each flaw vs. flaw depth and width for gloss blue specimens

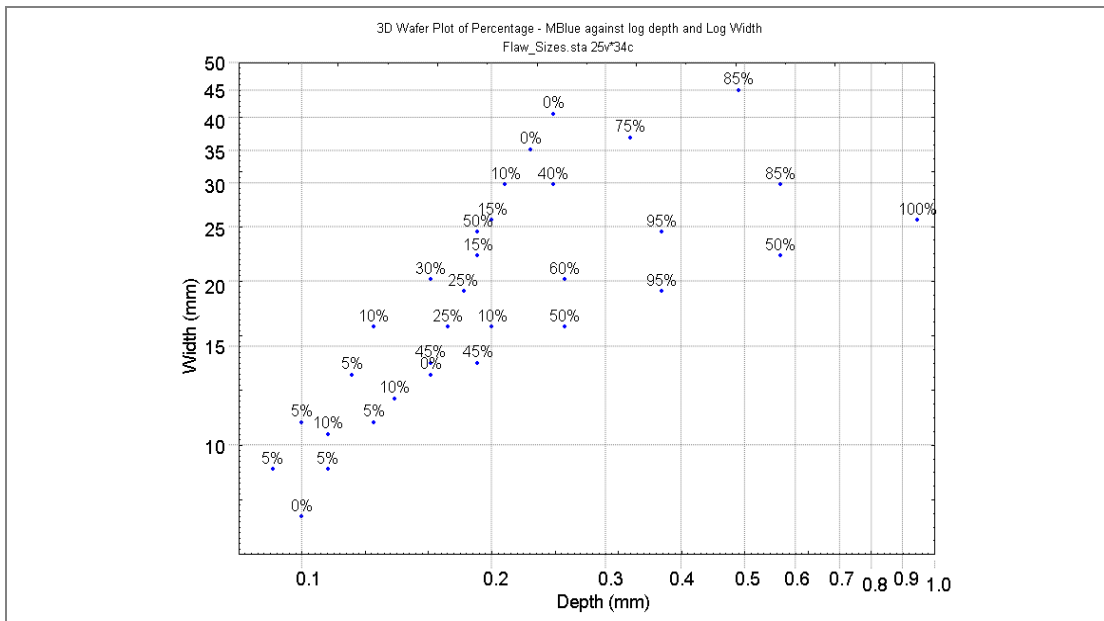


**Figure 64** Scatter plot of % of participants detecting each flaw vs. flaw depth and width for matt blue specimens

## 2.9.2 Summary of Results

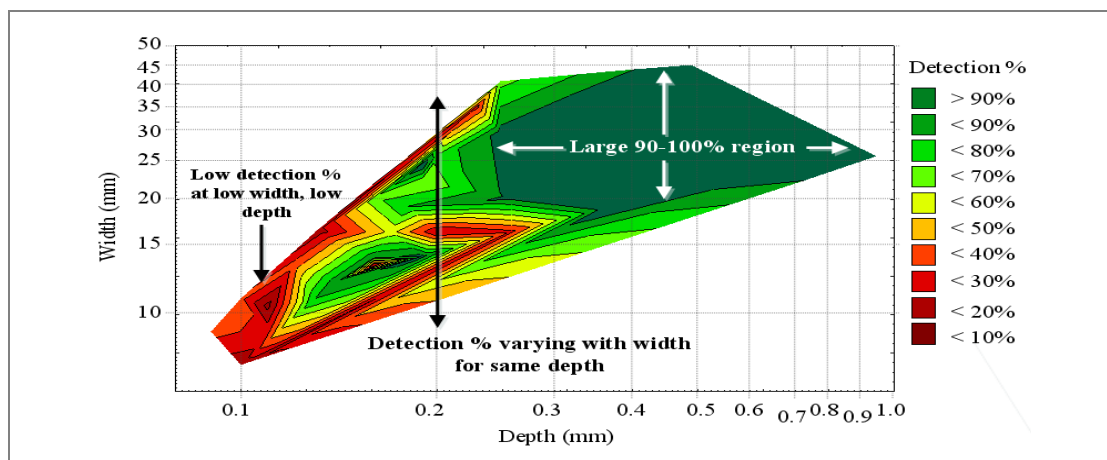
### General

All of the plots in Figures 59–64 have a number of similar features, differing in detail with changes in sample colour and surface finish. At small values of depth and width percent detections are low and approach zero. The lower limit of the data is at flaws of 0.1 mm depth and 10 mm width. The upper limit of data is at dents approaching 1 mm deep and 30-40 mm wide. Detections approached 100% for these large flaws. The extent of the region of 90-100% detections changed depending on the colour and

surface finish of the samples. The region of high % detection extended in a ridge towards smaller values of width and depth so that at constant dent depth the effect of increasing width was first to increase the detection percent, and then with further increases in width to decrease the detection probability. All the data sets show some local contour anomalies, which probably reflect participant to participant variability in the original trials.

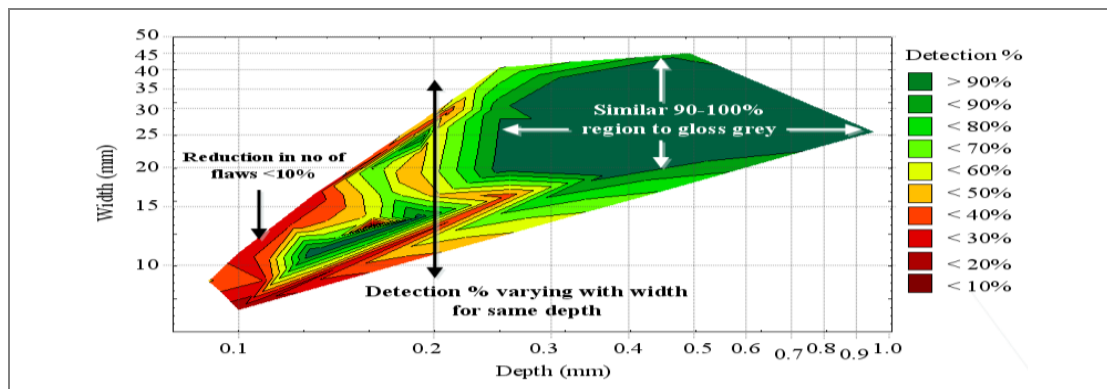
### Detailed discussion

In Figure 65, the wafer plot of gloss grey results shows a large region of width and depth greater than 20 mm and 0.3 mm respectively in which flaws were detected by over 90% of participants. The contours indicate that for flaws of small depth and width, the detection was at its lowest rate. If a nominal flaw depth of 0.2 mm is chosen, the wafer plot illustrates that flaw detection rates can vary between <10% and >90% as width varies; i.e. detection can vary for the same depth of flaw, depending on the flaw width.



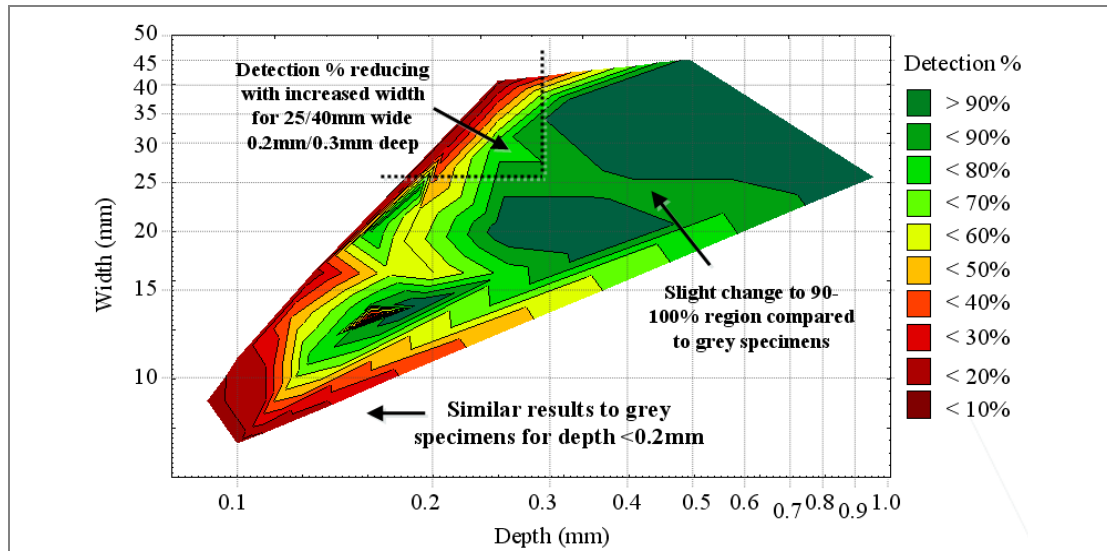
**Figure 65** Wafer plot of gloss grey results with comments

Figure 66 illustrates the wafer plot for the matt grey results. It can be seen that the matt finish has little effect on detectability of flaws greater than 0.25 mm deep; the region of 90-100% detection is similar in size and shape to the same region on the gloss grey diagram. There is a slight change to the contour shape for flaws of smaller width and depth, where the <10% detection band is no longer present. As also observed for the gloss grey specimens, the detection contours vary with width for constant depths. The overall implication is that there is little difference in detection rates on gloss and matt grey specimens.



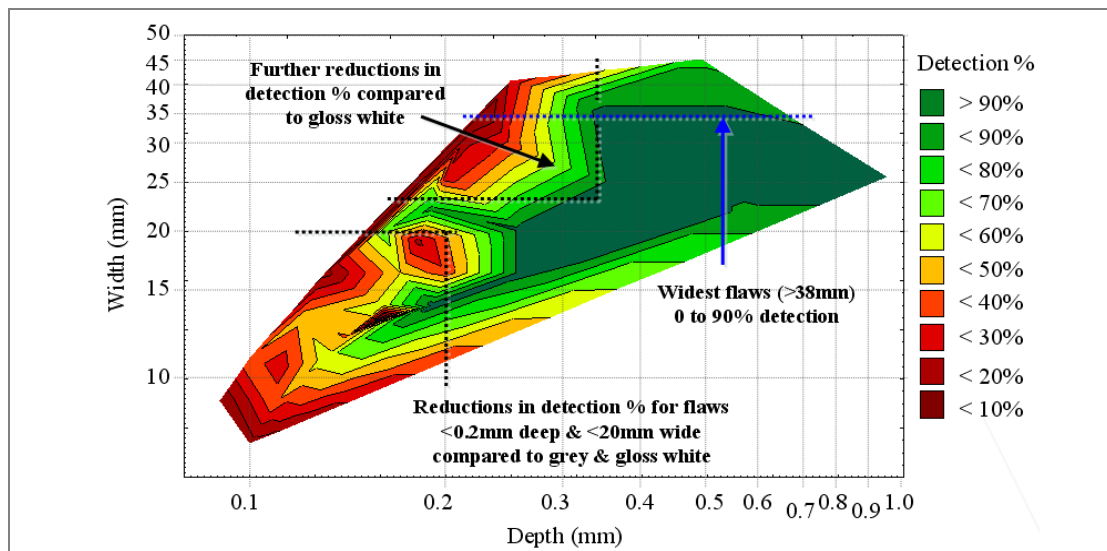
**Figure 66** Wafer plot of matt grey results with comments

In Figure 67, the wafer plot of the gloss white specimens illustrates that there are some differences compared to the results with grey specimens. The large area of 90-100% detection has changed shape slightly. For flaws between 0.2 mm - 0.3 mm deep, and >25 mm wide, the detection percentage reduces as width increases. However, for flaws below 0.2 mm deep, there is little difference to the detection contours compared to the gloss and matt grey results. This implies that there are slight differences in detection rates on gloss white specimens compared to gloss and matt grey specimens.



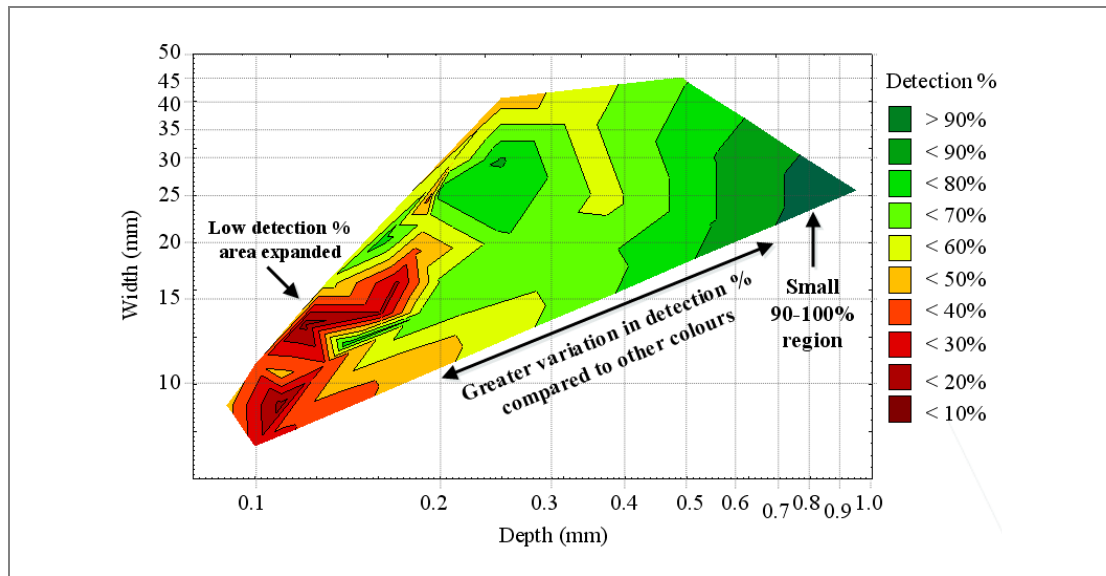
**Figure 67** Wafer plot of gloss white results with comments

In Figure 68, which shows the results from matt white specimens, there are notable differences to the contour shapes found in the gloss white results. The large area of >90% detection has changed shape, and no longer includes flaws wider than 38 mm. The detection of flaws >38 mm wide now varies from <10% to >90% depending on flaw depth. For the flaws between 0.2 mm and 0.3 mm deep and >25 mm wide, there is greater variation in detection rates compared to the same region on the gloss white results. Detection of flaws <0.2 mm deep and <20 mm wide saw reduced rates on the matt white specimens compared to the gloss grey and white, and matt grey specimens. The results seen in Figure 68 imply that the matt finish altered detection rates on the white specimens.



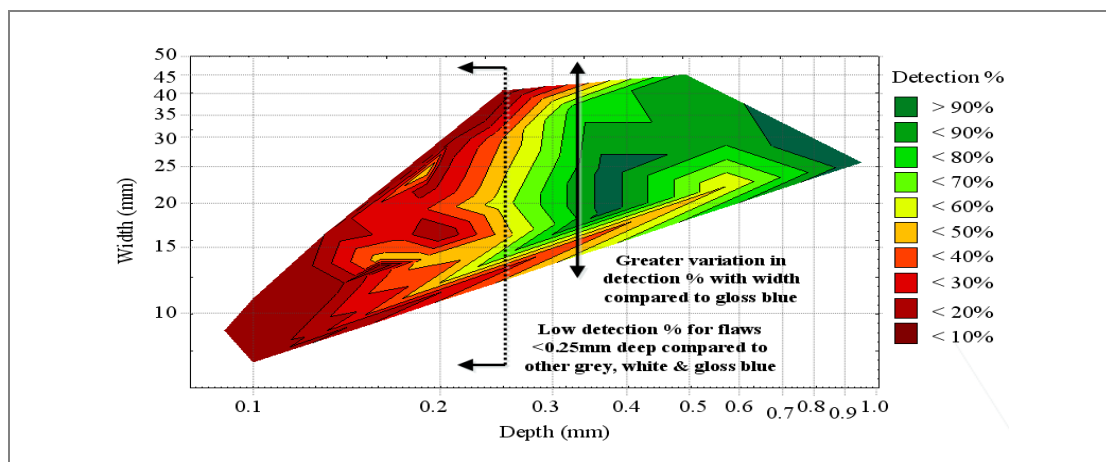
**Figure 68** Wafer plot of matt white results with comments

Figure 69 shows the results obtained from the gloss blue specimens. In this plot, it can be seen that there is a significantly different shape to the detection contours compared to the results from grey and white specimens. The lower limit of the region of >90% detection has shifted to 0.7 mm deep compared to that of the grey and white results (0.25 mm deep). The detection contours for flaws >0.2 mm vary less with flaw width than on the other plots (fig 69-72 and 73). For the gloss blue specimens, detection varies mostly with flaw depth. The area of low detection percentage (<30%) covers a larger width and depth range on the gloss blue results compared to the grey and white results. From the plot in Figure 69, it can be seen that different detection results are obtained from gloss blue specimens than from grey and white specimens.



**Figure 69** Wafer plot of gloss blue results with comments

Figure 70 illustrates the results from the matt blue specimens. It can be seen in Figure 70 that there is greater variation in detection percentage with width than on gloss blue specimens. It can also be seen that detection of flaws with <0.3 mm depth is reduced to below 50%. The results seen in Figure 70 imply that a matt blue finish gives different detection results to a gloss blue finish.



**Figure 70** Wafer plot of matt blue results with comments

### 3 Discussion

#### 3.1 Link Between Delamination Size and Surface Flaw Detectability

Table 12 gives the flaw characteristics of actual impact damage on a painted, mesh incorporated CFRP laminate coupon, produced during the flaw characterisation work described earlier in this report. Alongside, the characteristics of a similar sized flaw used in the visual inspection trials, and its detectability are given.

**Table 12** Detectability and delamination sizes for various flaw sizes

Actual Surface Flaw	Replicated Surface Flaw										
	Surface Flaw Width	Surface Flaw Depth	Delamination Width	Surface Flaw Width	Surface Flaw Depth	% Detections					
Gloss Grey						Matt Grey	Gloss White	Matt White	Gloss Blue	Matt Blue	
Impact Conditions											
Ø20mm - 17ply - 5J	5	0.11	10	9.03	0.11	33	41	6	0	44	5
Ø20mm - 17ply - 15J	21.5	0.32	26	19.11	0.37	100	94	100	100	69	95
Ø20mm - 33ply - 20J	15	0.2	47	16.44	0.2	20	47	50	33	63	10
Ø20mm - 33ply - 50J	30	0.86	79	29.96	0.57	100	100	100	100	81	85
Ø87mm - 17ply - 20J	13	0.18	67	13.46	0.12	33	29	38	44	6	5
Ø87mm - 17ply - 40J	22	0.21	100	24.53	0.19	100	88	81	61	38	40
Ø87mm - 33ply - 20J	13	0.14	12	14.15	0.16	87	53	81	56	19	45
Ø87mm - 33ply - 60J	40	0.28	83	40.45	0.25	67	59	6	22	44	0

From Table 12, it is evident that a 24.53 mm/ 0.19 mm deep surface flaw, that could have 100 mm wide impact delamination beneath, whilst being 100% detectable on a gloss grey specimen, would only be detected by 38% of participants on a gloss blue specimen. Furthermore, a 0.25 mm, 40.45 mm wide surface flaw that could have 83 mm of delamination beneath is undetectable on a matt blue surface, yet 67% detectable on a gloss grey surface. Of particular concern, is that the surface flaw that represents impact damage with 83 mm wide delamination was no more than 67% detectable.

It should be remembered that the relation between surface flaw size and associated sub surface delaminations is one established in this instance on 100 mm X 150 mm coupons manufactured from AS4/8552 prepreg. In large-scale structures, the relationship between them will be influenced by the compliance of the impacted structure as well as by the toughness and stiffness of the composite resin and fibre system used. Thus although the detection reliability of defects of various sizes, shapes, colours and surface finish will have generic applicability across all materials and structures where these surface defects occur, the level of sub surface damage associated with each of them needs to be determined by experiment for each application.

#### 3.2 Relevance of Results to Actual Damage on CFRP Structures

The flaw characteristics used in this experiment are all reproducible using falling weight impact equipment and hemi-spherical impact tips, on a painted, mesh incorporating CFRP laminate. It would be unrealistic to reproduce a 60J flaw conforming to the geometry relationships for a 20 mm impactor on a 17 ply laminate, as such an impact would undoubtedly result in the impactor penetrating through the entire laminate. Likewise, it is unrealistic to produce a 0.5 mm deep, 60 mm wide flaw, unless this size of flaw has been observed, and characterised, on an actual impact to a fully finished CFRP laminate.

The results of this experiment therefore represent the surface flaw detectability of various energies of impact damage to a 17 ply and 33 ply painted, mesh incorporating laminate, from 20 mm and 87 mm hemi-spherical objects. However, it is acknowledged that impact damage to an aircraft will not be limited to hemispherical objects. Impacts from stones, tools, vehicles, to name a few possibilities, will undoubtedly produce different shapes of surface flaw. Whilst the visual inspection trials results illustrate that flaw shape affects visual inspection reliability, numerous possible flaw shapes could occur to an actual aircraft structure. The results of the visual inspection trials represent only a small selection of these possibilities. Furthermore, the surface flaws produced by impact from some shapes of impact object will produce cracks on the surface at the impact site. It is foreseeable that a surface flaw that contains a surface crack will be easier to detect than a non-cracked flaw of the same size, as the eye will detect not only the 3D shape of the flaw but also the crack itself. However, the effect of surface cracks, or visual inspection reliability for different categories of impact damage on composite aircraft structure would require further experimental work.

The flaws used in this study represented impact damage that occurred due to impacts from a 20 mm and 87 mm hemi-spherical object on a 17 ply and 33 ply painted, mesh incorporated laminate. As seen in Figure 71, this results in a flaw size and shape range that occupies only a selection of possible flaw depths and widths. Flaw sizes outside of this range could conceivably be produced by impact objects of different sizes, or on different laminate thicknesses to those used in this study. Future work should include an extension to the range of geometries studied so that the additional areas shown in Figure 69 are included.

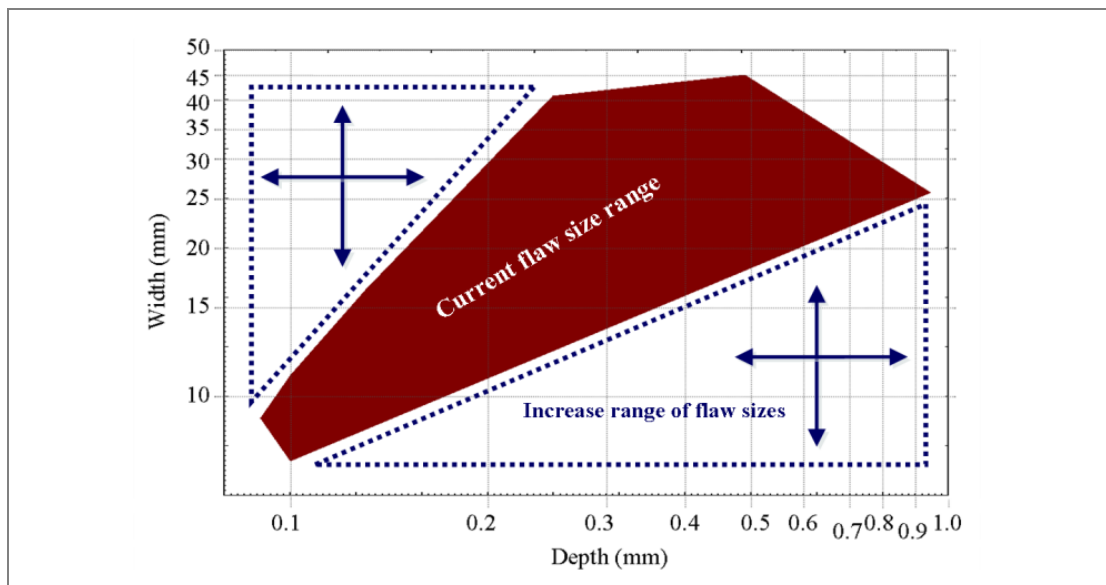


**Figure 71** Illustration of flaw size range used in study, and possible additional range of flaw geometries which could be studied

A key issue when designing flaws of these sizes will be the relationship between flaw size and internal geometric variable sizes. The flaw sizes used for this study followed four different flaw geometry relationships. Both flaw depth and flaw width were linked by a relationship to impact energy.

The flaw size range studied in future work could be populated by:

- 1 Using different sizes of hemi-spherical impact object, on the same laminate thicknesses
- 2 Using flaw sizes and shapes not related to impacts produced by actual testing



In the first case, whilst a multi-variable model of POD as a function of flaw depth and width could be obtained, the model would be unable to take account of changes in detection reliability for flaws of similar depths and widths but with different sectional profiles. Therefore, a POD model for each type of impact object would be preferable. In order for each POD model to be calculated, a large number of different flaw sizes for each impact object type would be required. This would result in a set of POD curves that would give inspection reliability as a function of width and depth, for different sizes of impact object.

In the second case, which would require width and depth to be varied independently, the relationship between width and depth must be broken. In order to avoid the other geometric flaw variables independently affecting inspection reliability, a single relationship between the other geometry variables ( $r_E$ ,  $r_l$ ,  $X_t$  and  $Y_t$ ) should be used for all the flaws. Any POD model obtained for flaw width and depth would be applicable only to the flaw geometry relationship used. A new set of flaws would need to be designed in order to develop a POD model for flaws conforming to different geometry relationships.

The two options discussed above concern the production of a multi-variable POD model, which would give visual inspection reliability as a function of surface flaw depth and width. However, each of the flaw geometry variables described in Figure 32 has the potential to affect visual inspection reliability by altering the level of shadow, shine and specular reflection distortion produced by the surface flaw. In order to develop a truly multi-variable model of visual inspection reliability, it is conceivable that a series of experiments in which a range of different flaw sizes, where only a single geometric variable is adjusted may be required.

### 3.3 Implications of Results

#### 3.3.1 Implications for designers of composite material structures

The results of the visual inspection trials show that a surface flaw occurring from an impact that causes relatively large widths of delamination may be undetectable, or difficult to detect, depending on the surface colour and finish of the structure. For example, a flaw that would represent a 44J impact from an 87 mm impactor, or 60 mm of delamination, was not detected by any participants on a matt blue specimen, but detected by 67% of participants on a gloss grey specimen. Designers cannot assume that a flaw is as detectable on one colour, or surface finish as it is on another.

Aircraft maintenance documents such as structural repair manuals (SRM) commonly give repair criteria for composite structures based on the depth of the surface flaws, and delamination size. These may well be acceptable criteria for deciding whether a structure requires repair, but aircraft and aircraft structure designers cannot simply assume that all damage over a certain depth or width will be found. The results of the visual inspection trials show that flaws of small depth and width are difficult to detect, and that for a given flaw depth, wider flaws are also more difficult to detect. When determining the damage tolerance size, i.e. what size of impact damage can be found (or missed) on composite structures, the designers should consider the limit of visual inspection reliability in terms of both the surface flaw depth and the flaw width, as both are required in order to determine a surface flaw's visibility.

Aircraft designers should not assume that visual inspection reliability of a composite aircraft structure increases for larger energy impacts, or impacts from larger objects. The visual inspection trials results show that a 0.19 mm deep, 14.15 mm wide flaw was detected by between 45% and 100% of participants across the range of colours and finishes used. However, a 0.25 mm deep, 40.45 mm flaw was detected by between 0% and 67% of participants across all colours and finishes. The 0.25 mm

deep, 40.45 mm wide, less detectable flaw would represent impact damage from a 44 J impact. The more detectable, less deep, less wide, 0.19 mm deep flaw represents impact damage from an 11.9 J impact, which would cause considerably less delamination than the 44 J impact. The results show that impact damage with smaller delamination can be more detectable than impact damage with larger delamination. Whilst one may argue that NDT techniques such as tap-test and C-Scan should easily find large areas of delaminated structure, one must remember that because the surface flaw of such damage could be undetectable, the NDT may never actually be requested by an inspector.

### 3.3.2 **Implications for aviation personnel**

Aviation personnel may drop tools or objects onto an aircraft, or may cause impact damage to aircraft with ground handling equipment. The impact testing work performed on mesh incorporated, painted composite laminate has shown that impact damage can have a similar appearance to a small dent on a metallic structure. The testing work has also shown that impact damage to a composite aircraft structure will not always produce a visible crack. Aviation personnel need to be made aware that what they may pass off as being an insignificant dent on a metallic structure could in fact be quite significant impact damage to a composite structure, and should be reported or further NDT requested.

The visual inspection trials show that a 40.45 mm wide, 0.25 mm deep surface flaw, which would represent significant impact damage to a 33 ply laminate, was less than 70% detectable on all surface colours and finishes, only 6% detectable on a gloss white surface and 0% detectable on a matt blue surface. This means that if a person were to create this damage, there is between 30% and 100% chance that they will not detect the damage, depending on whether the surface is glossy grey or matt blue. Aviation personnel must be made aware of the fact that they could produce impact damage that they cannot, or find it difficult to see, and should be encouraged to report any impact incident on a composite aircraft structure, regardless of whether or not they can see a surface flaw. If the person causing the impact is unable to see a surface flaw, the inspector performing a requested inspection or NDT may also be unable to locate the impact site. It may be beneficial to request that aviation personnel mark, or record the location of any known impact occurrence immediately, in order to avoid a requested NDT or further inspection being conducted in the wrong place. Visual inspection personnel should be encouraged to be particularly vigilant when inspecting dark coloured, matt finish surfaces.

If aviation personnel are to be encouraged to report all impact occurrences to composite aircraft, the aviation industry must be prepared for inspection or NDT by qualified personnel to be requested more frequently than with metallic aircraft structures. Aviation personnel should not be reprimanded for calling out impact occurrences that result in insignificant damage, or no damage being found, for fear of creating a non-reporting culture, which could lead to significant impact damage going unreported, undetected and unrepaired.

## **4 Statistical Analysis of Flaw Detection Data**

### 4.1 **Introduction**

In order to establish the statistical significance of the identified trends influencing reliability of inspection, a statistical analysis was performed on the flaw detection data shown in Appendix A.3. A generalised linear model with a binomial dependant variable (whether the flaw was detected or not) was used. The following flaw descriptor variables were incorporated: Flaw width and depth, panel colour (White,

Blue, Grey), panel surface finish (Gloss or Matt), impactor diameter (20 mm or 87 mm) and laminate thickness (17 ply or 33 ply). All interactions between these categorical descriptors were included. Some of the parameters will not be independent variables in that the flaw width and depth will depend on the ply thickness and the impactor diameter. Table 13 shows the significant effects identified. This is equivalent to an analysis of variance table but as a non-linear model is being fitted to the data, the same exact techniques to estimate the effects cannot be used using maximum likelihood estimation. A significant p value ( $p < 0.05$ ) indicates that there is a significant effect of the parameter in question. Figure 72 shows that the fit of the data to the model is reasonable as the residuals follow a normal distribution. This is indicated by the close adherence of the data to a straight line as shown in Figure 72.

**Table 13** Summary of P values found for significance analysis

Effect	Response - Test of all effects (response data.sta) Distribution: BINOMIAL, Link function: LOGIT Modelled probability that Response = 1		
	Degr. of Freedom	Wald Stat.	P
Intercept	1	207.0878	0.000000
Defect Width	1	10.5207	0.001180
Defect Depth	1	176.5483	0.000000
Colour	2	99.6724	0.000000
Finish	1	31.5355	0.000000
Impactor Diameter 20 /mm / 87	1	0.7036	0.401564
Ply Number 17 / 33	1	26.1627	0.000000
Colour*Finish	2	34.1721	0.000000
Colour*mm	2	6.0233	0.049210
Finish*mm	1	1.2622	0.261239
Colour*ply	2	2.5409	0.280707
Finish*ply	1	0.0120	0.912726
mm*ply	1	0.9211	0.337184
Colour*Finish*mm	2	2.8811	0.236797
Colour*Finish*ply	2	0.2116	0.899605
Colour*mm*ply	2	0.6758	0.713266
Finish*mm*ply	1	2.0073	0.156545
Colour*Finish*mm*ply	2	3.3158	0.190534

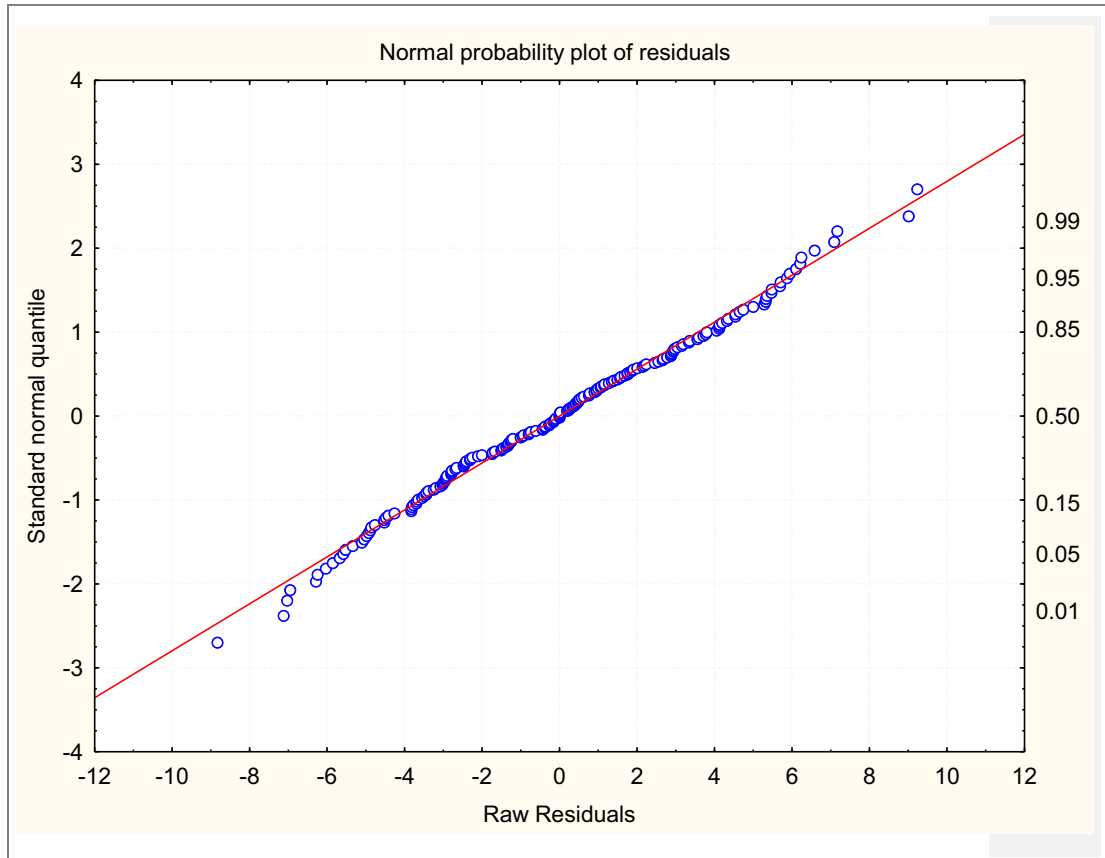


**Figure 72** Plot of standard normal quantile vs residuals for all the inspection data contained in Appendix 3, showing a close adherence to a normal distribution

#### 4.2 Findings of the analysis

The two continuous predictors (flaw width and flaw depth) have significant effects on detection probability – the size and direction of these effects are shown in the data for width and depth contained in Table 14. The estimate of the effect of width is -0.03 which means the probability of detecting a flaw decreases as the width increases. The estimate for depth is 10.91 which means the probability of detection increases as depth increases. It is difficult to interpret the size of the effect of these two variables as it will depend on values of the other variables and the range of values over which depth and width were measured. Because the Wald statistic is bigger for depth than for width, then depth has a larger effect on the probability of detection than width. Table 15 shows the mean values for the width and depth predictors.

**Table 14** Summary of data for inspection reliability analysis

Effect	<b>Response - Parameter estimates (responedata.sta)</b> <b>Distribution: BINOMIAL, Link function: LOGIT</b> <b>Modelled probability that Response = 1</b>					
	Level of Effect	Column	Estimate	Standard Error	Wald Stat.	p
Intercept		1	-1.62606	0.112995	207.0878	0.000000
Width		2	-0.02973	0.009164	10.5207	0.001180
Depth		3	10.90811	0.820952	176.5483	0.000000
Colour	grey	4	0.46089	0.058146	62.8276	0.000000
Colour	white	5	0.08545	0.057162	2.2345	0.134964
Finish	gloss	6	0.22982	0.040925	31.5355	0.000000
mm	20 mm	7	-0.04992	0.059511	0.7036	0.401564
Ply	17 ply	8	0.21291	0.041625	26.1627	0.000000
Colour*Finish	1	9	-0.22759	0.058056	15.3683	0.000088
Colour*Finish	2	10	-0.10780	0.057115	3.5622	0.059111
Colour*mm	1	11	-0.10501	0.058012	3.2769	0.070262
Colour*mm	2	12	0.13301	0.057134	5.4197	0.019911
Finish*mm	1	13	-0.04591	0.040865	1.2622	0.261239
Colour*ply	1	14	-0.08941	0.057934	2.3820	0.122743
Colour*ply	2	15	0.06293	0.057083	1.2154	0.270256
Finish*ply	1	16	0.00448	0.040832	0.0120	0.912726
mm*ply	1	17	-0.03938	0.041029	0.9211	0.337184
Colour*Finish*mm	1	18	-0.08098	0.058003	1.9494	0.162651
Colour*Finish*mm	2	19	-0.00935	0.057110	0.0268	0.869959
Colour*Finish*ply	1	20	-0.02241	0.057939	0.1496	0.698946
Colour*Finish*ply	2	21	0.02319	0.057086	0.1651	0.684512
Colour*mm*ply	1	22	0.00886	0.057971	0.0233	0.878579
Colour*mm*ply	2	23	-0.04449	0.057084	0.6075	0.435715
Finish*mm*ply	1	24	0.05783	0.040819	2.0073	0.156545
Colour*Finish*mm*ply	1	25	-0.01400	0.057936	0.0584	0.809108
Colour*Finish*mm*ply	2	26	-0.08312	0.057083	2.1204	0.145348
Scale			1.00000	0.000000		

**Table 15** Mean values for the width and depth predictors

Variable	Mean
Width	20.65908
Depth	0.24784

The effects of the categorical predictors are shown in Figures 73-78 with associated tables of means (Tables 16-20). In all cases the predicted means are computed at the mean values of the width and depth – so they have been standardised to remove the effect of different widths and depths. These graphs are indications only of the significant differences.

Graphs are shown only for those effects that were significant in Table 13. They are easy to interpret except perhaps for the two interaction effects. Colour\*finish is looking at how the differences in probability of detection between the two surface finishes varies across the 3 colours – so Figure 76 shows that there is a significant difference in the detection probability of the two finishes only in the blue colour. This difference (in the blue) is enough to give a significant difference in finish for the all colours plot (Figure 73). This shows how important it is to include interaction effects in statistical analysis. The other interaction that was significant was colour\* impactor diameter mm – in this case the effect of impactor diameter was not significant on its own. This interaction has been plotted in two ways (Figures 77 and 78) to help interpretation – it can be seen that there is no significant difference in the probability of detection between grey and white when surface flaws are formed by 20 mm impactors but there is a difference for 87 mm diameter impactors.

4.2.1 **Effect of colour on detection probability- gloss and grey samples combined**

Figure 73 shows that detection probability is greatest in grey samples and is reduced almost by half in the blue ones. White samples have intermediate values.

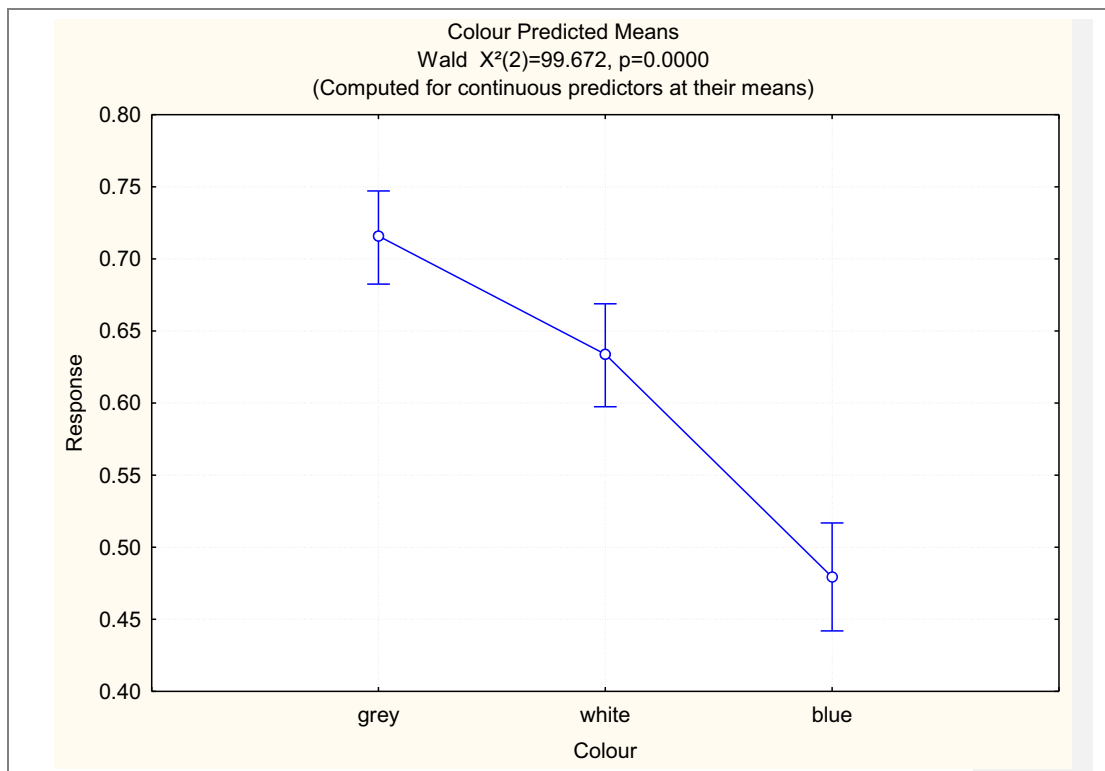


**Figure 73** Effect of sample colour on probability of defect detection; both surface finishes combined; mean width and depth defect sizes.

**Table 16** Values of standard error and response means for colour analysis

Cell No.	Colour Predicted Means (responedata.sta) Wald $X^2(2)=99.672$ , $p=0.0000$ (Computed for continuous predictors at their means)					
	Colour	Response Mean	Response Std.Err.	Response -95.00	Response +95.00	N
1	grey	0.715895	0.081004	0.682489	0.747090	1024
2	white	0.633846	0.078494	0.597418	0.668804	1087
3	blue	0.479254	0.076582	0.441936	0.516806	1152

4.2.2 **Effects of surface finish**

The effects of surface finish on probability of defect detection for all colours combined are shown in Figure 74. It can be seen that matt surface finish reduces the probability of detection from 0.66 to 0.56

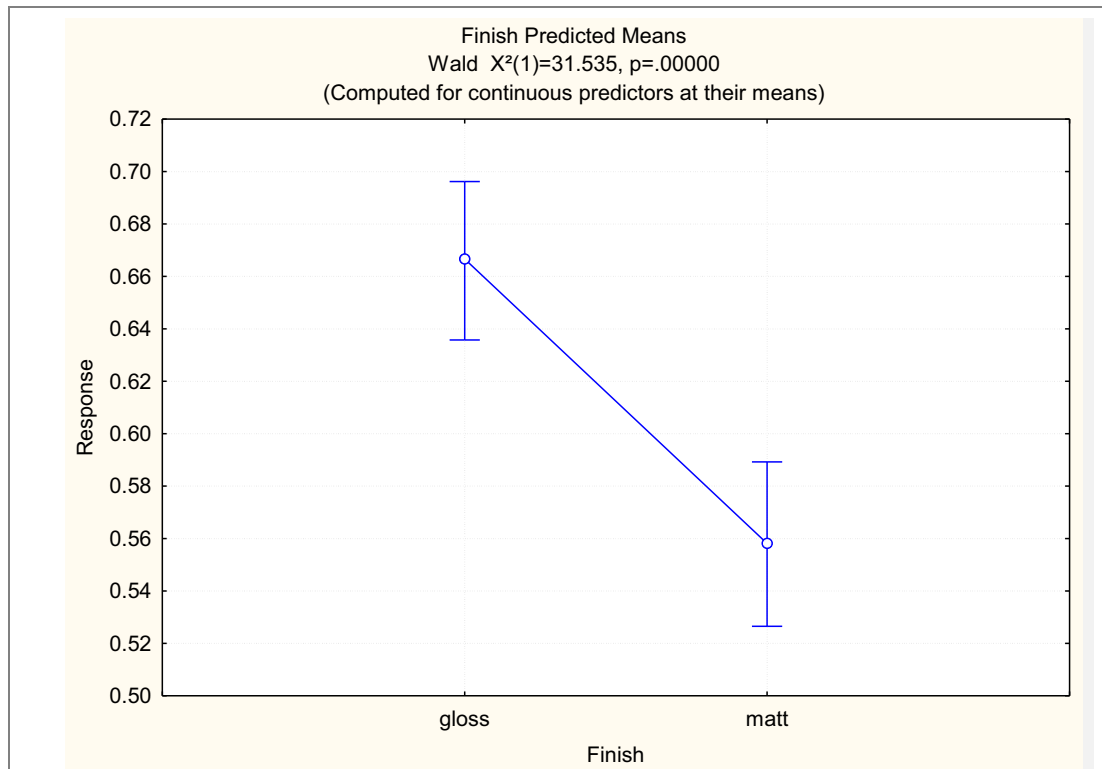


**Figure 74** Effect of sample surface finish, all colours combined on detection probability; mean width and depth defect sizes

**Table 17** Values of standard error and response means for surface finish analysis

Cell No.	Finish Predicted Means (responedata.sta) Wald $X^2(1)=31.535$ , $p=.00000$ (Computed for continuous predictors at their means)					
	Finish	Response Mean	Response Std.Err.	Response -95.00	Response +95.00	N
1	gloss	0.666662	0.069362	0.635762	0.696194	1504
2	matt	0.558106	0.064832	0.526540	0.589211	1759

### 4.2.3 Effects of sample surface finish and colour separated

Figure 75 shows the effects of colour and surface finish with their effects considered separately. In this more detailed representation it can be seen that for grey samples there is no significant effect of surface finish, a slight effect for the white- still not statistically significant, and a major effect of surface finish for the blue samples. In the blue samples a matt surface finish reduces the detection probability by a factor of 2. there is still some small effect of colour on detection probability in the gloss surfaces, with blue once again having the lowest probability of detection. All these effects are considered at the mean values of defect depth and width.

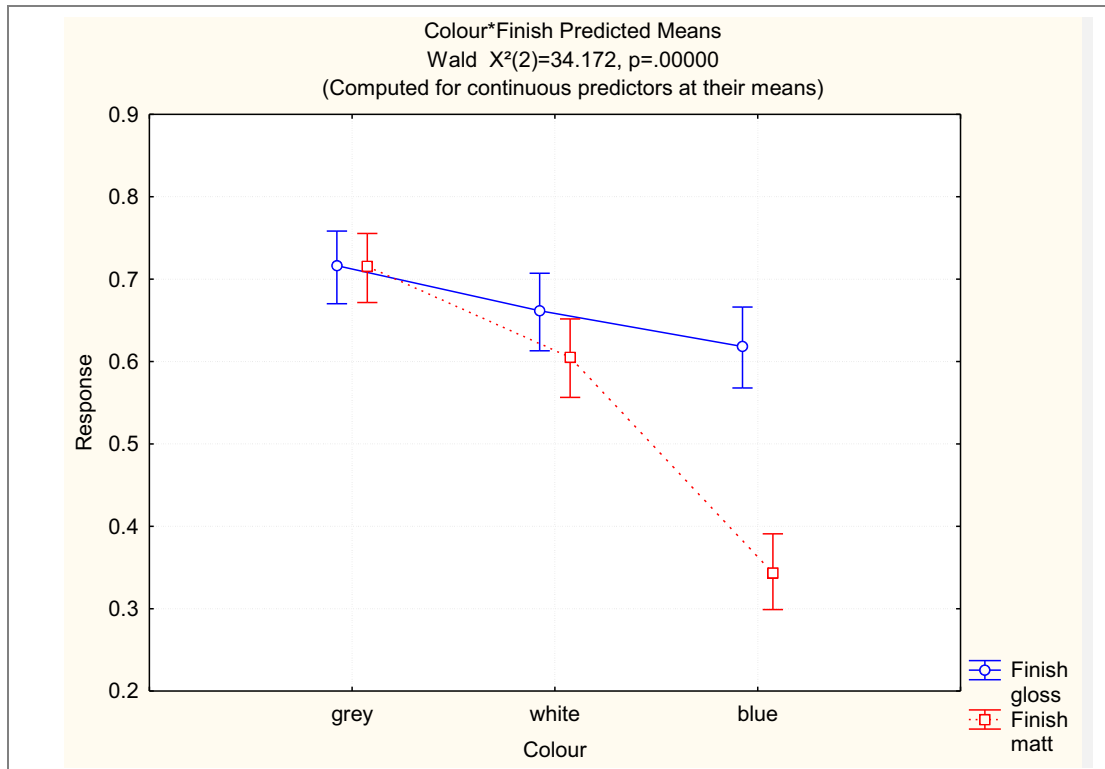


**Figure 75** Effects of sample colour and surface finish on probability of defect detection; colour and surface finish separated; flaw width and depth at mean values

**Table 18** Values of standard error and response means for separated colour and surface finish analysis

Cell No.	Colour*Finish Predicted Means (responsedata.sta) Wald $X^2(2)=34.172$ , $p=.00000$ (Computed for continuous predictors at their means)						
	Colour	Finish	Response Mean	Response Std.Err.	Response -95.00	Response +95.00	N
1	grey	gloss	0.716348	0.110633	0.670251	0.758325	480
2	grey	matt	0.715442	0.105006	0.671705	0.755474	544
3	white	gloss	0.661677	0.107335	0.613050	0.707113	512
4	white	matt	0.605091	0.101792	0.556501	0.651690	575
5	blue	gloss	0.618263	0.106324	0.567962	0.666151	512
6	blue	matt	0.343385	0.104221	0.298854	0.390853	640



#### 4.2.4 Effects of sample ply thickness on detection probability

There is a significant effect of ply thickness as Figure 76 shows. However ply thickness will influence defect shape particularly defect width as Figure 41 demonstrates. Hence this effect is a manifestation of the effect of defect width on detection probability.

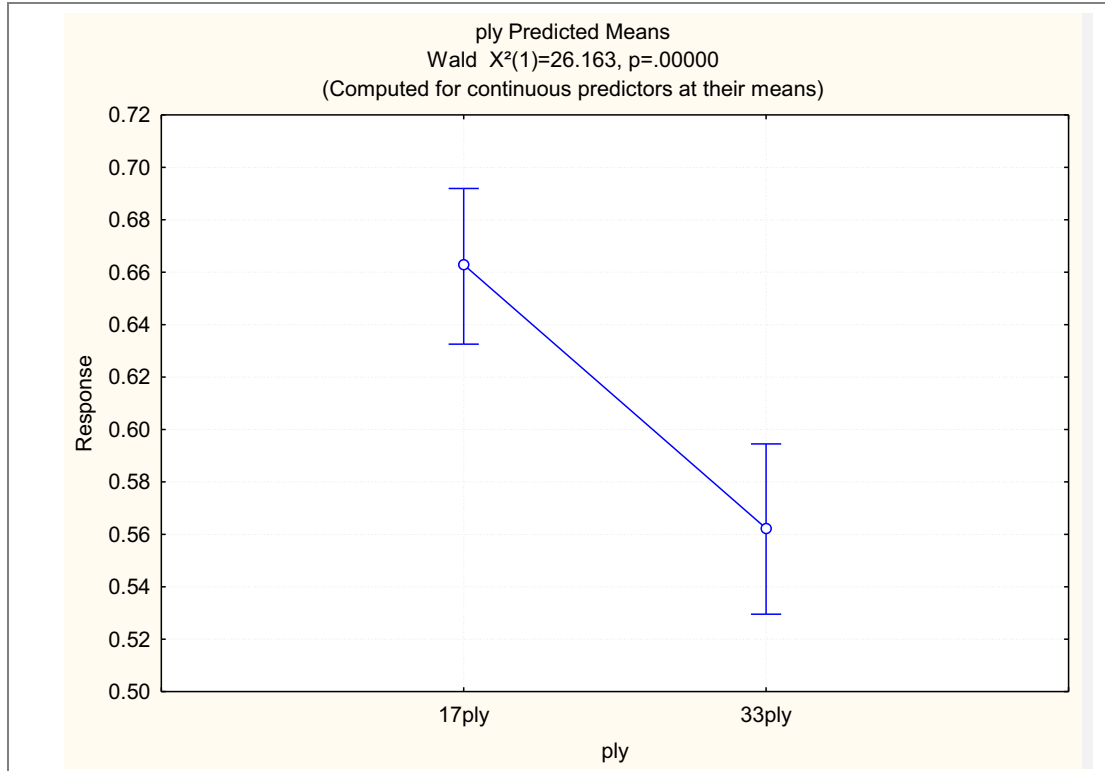


**Figure 76** Effect of impact sample thickness on detection probability; all colours and surface finishes combined; mean values of defect depth and width

**Table 19** Values of standard error and response means for ply thickness analysis

Cell No.	ply Predicted Means (responedata.sta) Wald X <sup>2</sup> (1)=26.163, p=.00000 (Computed for continuous predictors at their means)					
	ply	Response Mean	Response Std.Err.	Response -95.00	Response +95.00	N
1	17 ply	0.662893	0.067805	0.632547	0.691954	1632
2	33 ply	0.562273	0.067322	0.529537	0.594476	1631

#### 4.2.5 Effects of colour and impactor diameter on probability of detection

Figures 77 and 78 show the combined and separate effects of colour and impactor diameter on probability of detection. As for the ply thickness, impactor diameter will affect the defect profile, 87 mm diameter impactors producing wider defects for a given depth as Figure 41 indicates. Figure 77 and 78 show that colour is more dominant than impactor diameter, and that sometimes probabilities of detection are increased with increasing diameter, and on other occasions they are decreased.

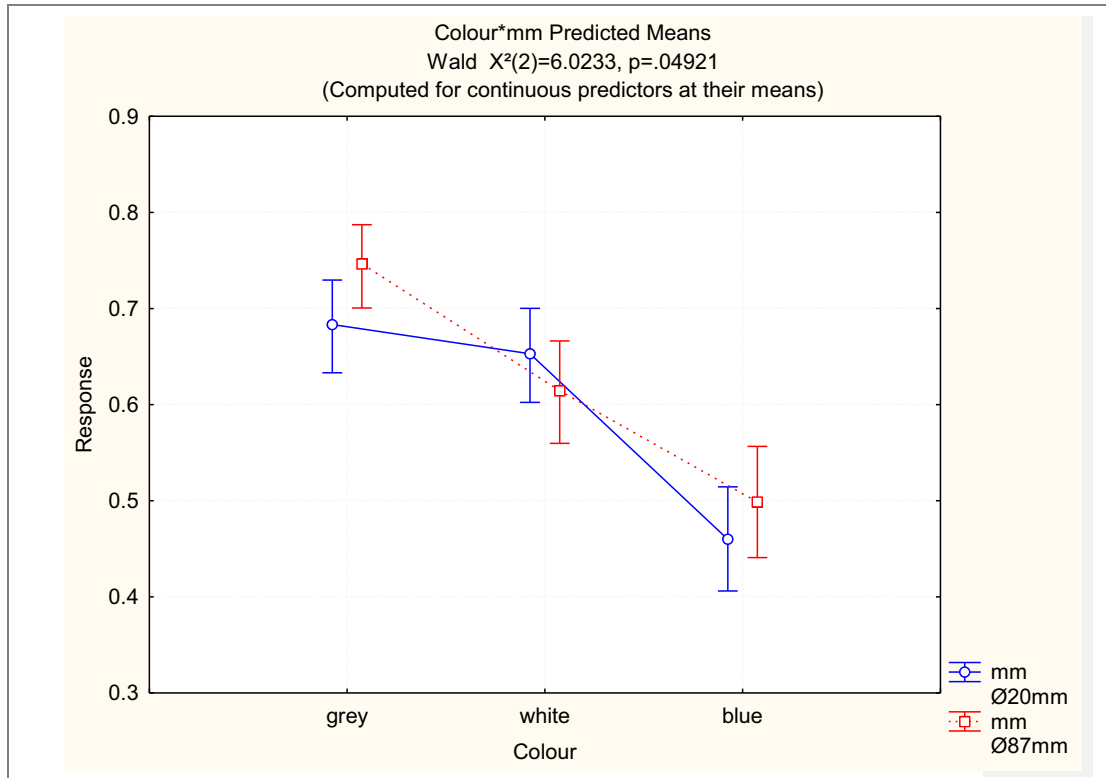


**Figure 77** Effect of colour and impactor diameter on inspection reliability

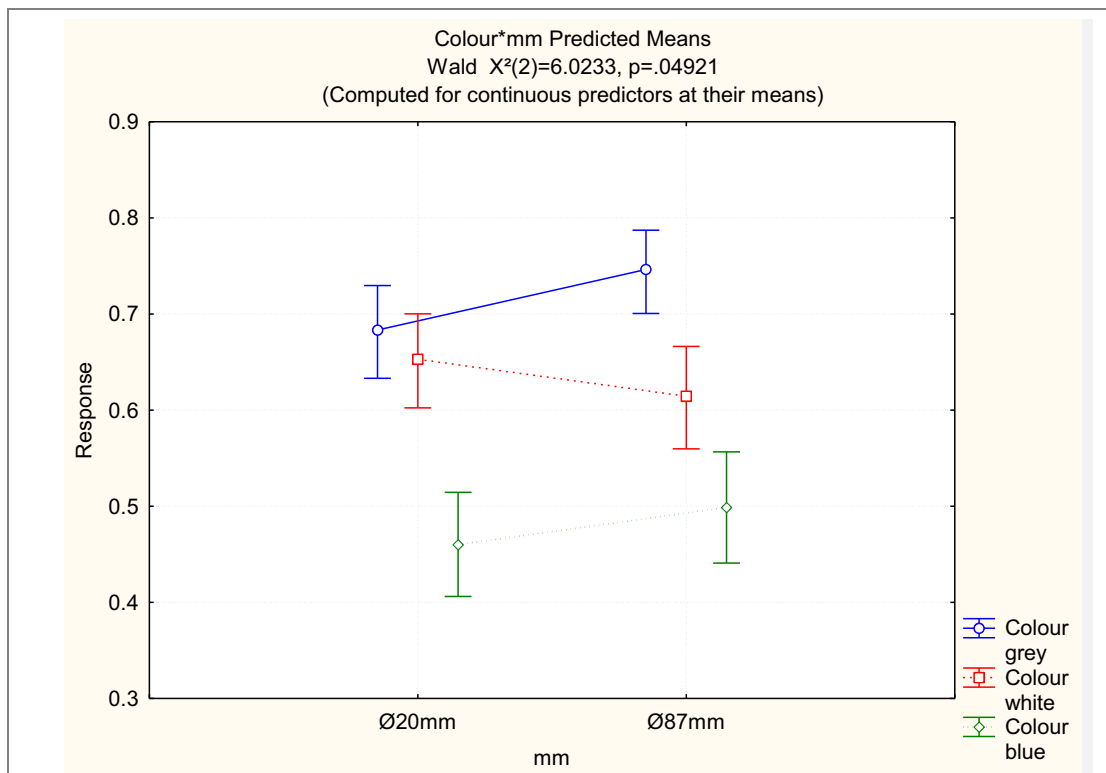


**Figure 78** Effect of impactor diameter on inspection reliability in different colour samples

**Table 20** Values of standard error and response means for separated colour and impactor diameter analysis

Cell No.	Colour*mm Predicted Means (responedata.sta) Wald $X^2(2)=6.0233$ , $p=.04921$ (Computed for continuous predictors at their means)						
	Colour	mm	Response Mean	Response Std.Err.	Response -95.00	Response +95.00	N
1	grey	20 mm	0.683360	0.113883	0.633156	0.729628	512
2	grey	87 mm	0.746328	0.116721	0.700584	0.787207	512
3	white	20 mm	0.652906	0.110348	0.602358	0.700227	543
4	white	87 mm	0.614356	0.115048	0.559689	0.666284	544
5	blue	20 mm	0.459851	0.111644	0.406120	0.514531	576
6	blue	87 mm	0.498720	0.118453	0.440887	0.556588	576

## 5 Conclusions

### 5.1 Surface Flaw Geometry Effects

The results of the visual inspection trials show that different surface flaw geometries had different visual inspection detection rates. The following detailed conclusions can be drawn:

- 1 Increased detection rates were observed with larger depths and widths, but the positive effect of depth on detection rate is mitigated by a negative effect of width on detection rate for relatively large widths.
- 2 A region of 90-100% detection occurred in all samples at the largest depths and widths. The size and location of this region changed with surface finish and colour being smallest in matt blue and largest in the white and grey samples.
- 3 Detection rates below 50% were observed for flaws <10 mm wide
- 4 Detection rates of 30%~50% were observed for surface flaws of widths between 10 mm and 15 mm
- 5 Detection rates for a 40.4 mm wide, 0.25 mm deep flaw varied between 0% - 67%
- 6 Detection rates for flaws of the same depth varied with flaw width.

### 5.2 Surface Colour Effects

Variations in the detection rates were observed when different coloured specimen panels were used, and the following conclusions can be drawn:

- 1 The results from the blue colour specimens were different to the results from the grey and white specimens; the most instances of 0% detection were observed on gloss blue specimens.
- 2 Flaw depths >0.7 mm and width >22.5 mm - 30 mm are required for >90% detection with gloss blue specimens. The region of >90% detection was smallest in the matt blue samples, and the region of <20% detections the greatest.

- 3 Flaw depth of  $>0.25$  mm and width between 20 mm and 35 mm are required for  $>90\%$  detection on all other gloss specimens.
- 4 There was greater variation in detection rates for flaws between 0.2 mm and 0.3 mm deep and 25 mm and 40 mm wide on white specimens compared to grey specimens.

### 5.3 Surface Finish Effects

The reliability of visual inspection of surface flaws is also affected by surface finish. Different detection rates were observed on specimens with different surface finish; the extent of the changes depended on the colour. The following conclusions regarding the effect of surface finish can be made:

- 1 Surface finish had little effect on detection rates when the surface colour was grey.
- 2 The application of a matt finish to white specimens reduced detection rates for  $>35$  mm wide/  $>0.3$  mm deep flaws compared to gloss white specimens.
- 3 The variation on detection with width spread across a greater flaw width range on matt white, compared to gloss white for flaws between 0.2 mm and 0.3 mm deep and  $>20$  mm wide.
- 4 The application of a matt finish to blue specimens reduced detection rates for flaws below 0.3 mm deep compared to gloss blue specimens.

### 5.4 Statistical Analysis

- 1 The statistical analysis confirms the qualitative conclusions of 3.1 and 3.2 above and shows that the effects of defect depth, width colour and surface finish are all statistically significant.
- 2 The effects of increasing defect depth on probability of detection is powerful and positive- increasing depth increasing the probability of detection.
- 3 The effects of increasing defect width is less powerful and negative i.e. increasing defect width decreases the probability of detection.
- 4 There is a significant effect of colour on probability of detection, grey being the best and blue the worst.
- 5 Effects of surface finish depend strongly on the colour. There is little effect of surface finish for grey and white samples; however there is a major effect in blue, with a matt surface finish reducing the probability of detection by a factor of 2.

## 6 Implications for Safety

- 1 Wide, shallow surface flaws can be difficult to detect although they could be associated with significant hidden delamination. It must not be assumed that impact damage dents associated with large sub-surface delamination will be more reliably detected than dents with smaller sub-surface damage. The idea of "bigger is more detectable" does not necessarily apply to visual inspection reliability for surface dents. SRM manuals should specify surface flaws requiring repair in terms of both depth and width.
- 2 Detection rates of 3D surface flaws produced by impact damage were affected by flaw depth and flaw width, surface colour and finish. The lighting conditions available during inspection could also affect the reliability of visual inspection of 3D surface flaws [27]. When assessing the reliability of visual inspection of

composite structures, attention must be paid to colours and finish of the inspection area, what the available lighting conditions will be, and the size and shape of the damage that is actually likely to occur. For example, inspection reliability data for relatively deep, flaws of small width on gloss grey structures that are brightly lit by grid lights could be used for calculation of damage tolerance sizes. If the structure when in service is actually painted gloss blue, is located on a poorly lit fuselage underside, and suffers impact damage causing significant subsurface damage and a wide, shallow flaw, the flaw will have much reduced probability of detection than originally. If the flaw is not detected, the repair will not be made, and the structure may continue to fly with an airworthiness hazard.

- 3 Consideration must be paid to the likely interpretation of flaw significance by personnel whose experience has been with metallic structures. Such personnel may be accustomed to the presence of shallow, insignificant surface dents on a metallic structure, which pose no airworthiness issues. However, the same personnel may be unaware that similarly shaped dents on a composite structure could be an indication of significant sub-surface damage, and failure to instigate further investigation or repair could have severe airworthiness implications.

- 4 **State of knowledge of pilots, maintenance and ground crew personnel**

Whilst this study assessed the reliability of visual inspection of surface flaws due to impact damage on a composite aircraft structure, the participants in the experiments were all given examples of surface flaws prior to inspecting, i.e. they all knew what to look for. There is some concern that not all aviation personnel are aware of what a surface flaw due to impact actually looks like on a composite aircraft structure. In fact, the early stages of this study required work to address this lack of information. Therefore, in order to assess whether there is an industry wide knowledge deficit, and what future training may be required, it would be beneficial to study the current state of knowledge regarding impact damage to composite aircraft within aviation personnel groups i.e. pilots, maintenance personnel and ground crew.

INTENTIONALLY LEFT BLANK

## References

- 1 Kanki BG, Brasil CL "Analysis of ramp damage incidents and implications for future composite aircraft structure " NASA Technical report 2009.
- 2 Airbus Industrie, Airbus A340 (SRM) Structural Repair Manual Rev Jan 01/03, Blagnac Cedex, France, 2003
- 3 Welch, J. M. Repair Design, Test, and Process Considerations for Lightning Strikes, presented at CACRC/MIL-HDBK-17 Conference, May 7-11 2007, Amsterdam, Netherlands
- 4 Gardiner, G. "Lightning Strike Protection for Composite Structures", High Performance Composites, July 2006, Available at <http://www.compositesworld.com/articles/lightning-strike-protection-for-composite-structures.aspx>
- 5 Civil Aviation Authority Safety Regulation Group, CAP562 Civil Aircraft Airworthiness Information and Procedures, Issue 2, Amendment 1, 2005
- 6 Cartié, D.D.R. Effect Of Resin & Fibre Properties On Impact And Compression After Impact Performance Of CFRP, Composites: Part A 33 (2002) 483-4937. Brookes, R.E.
- 7 Surface And Subsurface Damage In Plain Weave Carbon Epoxy Laminates Due To Low Velocity Impacts, MSc Thesis, Cranfield University, 2004.
- 8 Sohn, M.S., Hua, X.Z., Kimb, J.K. and Walker, L. Impact Damage Characterisation of Carbon Fibre/Epoxy Composites with Multi-Layer Reinforcement, Composites: Part B 31 (2000) 681-691.
- 9 Boulic, A. Quantitative Morphology of Impact Damage to Composite Aircraft Structures, Unpublished Report, Polytech'Orléans, France, 2007
- 10 Transportation Safety Board of Canada, Assessment of the Response from Transport Canada to Aviation Safety Recommendation A06-05 Inspection Program of Rudder Assembly, 2007.
- 11 European Aviation Safety Agency, Certification Specifications for Large Aeroplanes CS-25, Amendment 5, 2008.
- 12 Psymouli, A., Harris, D. and Irving, P. The Inspection of Composite Aircraft Structures: A Signal Detection Approach, Human Factors and Aerospace Safety, 2005, Vol 5; No. 2, 91-108
- 13 Lock, M.W.B. "The Effect of Aircraft Maintenance on Human Factors", in RTO-MP-10: Airframe Inspection Reliability under Field/Depot Conditions (Paper 14), RTO/NATO, 1998
- 14 Tsutsui, K., Taira, M. and Sakata, H. Neural Mechanisms of Three-Dimensional Vision, Neuroscience Research 51 (2005), 221-229
- 15 Todd, J.T. The Visual Perception of 3D Shape, TRENDS in Cognitive Sciences, Vol. 8 No.3 March 2004, 115-121.
- 16 Wexler, M. and van Boxtel, J.J.A. Depth Perception by the Active Observer, TRENDS in Cognitive Sciences, Vol 9 No 9 September 2005, 431-438.

- 17 Daykin, E. A Review of Inspection Procedures Associated With the Flight Scheduling Of Large Passenger Carrying Aircraft, MSc Thesis, Cranfield Institute of Technology, 1986
- 18 Murgatroyd, R.A., Worrall, G.M. and Waites, C. A Study of the Human Factors Influencing the Reliability of Aircraft Inspection, CAA Paper 95005, Civil Aviation Authority, 1995
- 19 Rummel, W. "Human Factors Considerations In The Assessment Of Non-Destructive Evaluation (NDE) Review," Review Of Progress In Quantitative Non-Destructive Evaluation, Vol. 3A, ed., D.O. Thompson and D.E. Chiment, 1984, Plenum Press, New York and London.
- 20 Dupont, G. "The Dirty Dozen Errors in Maintenance" in Meeting Proceedings of the Eleventh FAA Meeting on Human Factors Issues in Aircraft Maintenance and Inspection, FAA Office of Aviation Medicine, Washington, D.C. 1997
- 21 Spencer, F. and Schurman, D. Reliability Assessment at Airline Inspection Facilities Volume 3: Results of an Eddy Current Inspection Reliability Experiment, DOT/FAA/CT-92, 12, III, Sandia National Laboratories, Albuquerque, New Mexico, 1995
- 22 Asada, H., Sotozaki, T., Endoh, S. and Tomita, T. "Practical Evaluation of Crack Detection Capability for Visual Inspection in Japan" in RTO-MP-10: Airframe Inspection Reliability under Field/Depot Conditions (Paper 15), RTO/NATO, 1998
- 23 Erhart, D., Ostrom, L.T. and Wilhelmsen, C.A. Visual Detectability of Dents on a Composite Aircraft Inspection Specimen: an initial study, International Journal of Applied Aviation Studies, 4, Number 2, FAA Academy, 2004
- 24 Gant, S. K. "Visual Assessment of Impact Damage on Painted Composite Aircraft Structures," Proceedings of the International SAMPE Symposium & Exhibition 52, 2007
- 25 Drury, C.G. and Prabhu, P.V. Information Requirements of Aircraft Inspection: Framework and Analysis, Int. J. Human – Computer Studies (1996) 45 , 679-695
- 26 Megaw, E.D. and Richardson, J. Eye Movements and Industrial Inspection, Applied Ergonomics September 1979, 10.3, 145-154
- 27 Gramopadhye, A. K., Drury, C. G. and Prabhu, P. V. Training Strategies for Visual Inspection, Human Factors and Ergonomics in Manufacturing, (1997) Vol. 7 (3) 171–196
- 28 Brombach, J., Hütte, T. and Strasser, H. Surface-Specific Lighting Scenarios Enhancing the Perceptibility of 3-Dimensional Flaws, Occupational Ergonomics 6 (2006) 75–83
- 29 Dalton, J. and Drury, C. G. Inspectors' Performance and Understanding in Sheet Steel Inspection, Occupational Ergonomics 4 (2004) 51–65
- 30 Drury, C. G., Maheswar, G., Das, A. and Helander, M. G. Improving Visual Inspection using Binocular Rivalry, International Journal of Production Research, 39:10, 2143-2153, July 2001
- 31 Vukelich, S. I., Petrin, C.L. and Annis, C. AGARD Lecture Series 190 – A Recommended Methodology for Quantifying NDE/NDI Based on Aircraft Engine Experience, AGARD-LS-190, AGARD/ NATO, Neuilly sur Seine, France, 1993



- 32 Spencer, F., Borgonovi, G., Roach, D., Schurman, D. and Smith, R. Reliability Assessment at Airline Inspection Facilities, Volume 1: A Generic Protocol for Inspection Reliability Experiments, DOT/FAA/CT-92/12-V-1, May 1993
- 33 US Department of Defence, MIL-HDBK-1823: Non-destructive Evaluation System Reliability Assessment, Draft Copy, 28 February 2007, available at <http://www.statisticalengineering.com/mh1823/MIL-HBK-1823.pdf>
- 34 Bruce, D. "NDT Reliability Estimation From Small Samples And In-Service Experience", in RTO-MP-10: Airframe Inspection Reliability under Field/Depot Conditions (Paper 3), RTO/NATO, 1998
- 35 Berens, A.P. and Hovey, P.W. "Characterization of NDE Reliability" in Review of progress in quantitative nondestructive evaluation Volume 1 - Proceedings of the Eighth U.S. Air Force/Defense Advanced Research Projects Agency Symposium on Quantitative Nondestructive Evaluation, Boulder, CO, United States, 2-7 Aug. 1981. 586 pp. 1982, New York, Plenum Press
- 36 Bullock, M. and Fahr, A. Statistical Functions and Computational Procedures for the POD Analysis of Hit/Miss NDI Data, LTR-ST-1964, NRC, Institute for Aerospace Research, Structures Materials and Propulsion Laboratory, Canada, March 1994
- 37 Hexcel Composites, Hexply 8552, Product Specification, Publication FTA 072a, May 2003
- 38 Airbus UK Limited, Airbus UK Process Specification – ABP 4-1123, March 2006  
Airbus UK Limited, Airbus UK Process Specification – ABP 4-2127, December 2005  
Airbus UK Limited, Airbus UK Process Specification – ABP 5-1351, October 2005
- 39 Boeing Company, Boeing Specification Support Standard BSS7260, Revision C, Seattle, WA, USA, 1988
- 40 L Cook "Visual Inspection Reliability for composite aircraft structures" Ph D Thesis Cranfield University 2011.
- 41 Degussa Methacrylates, Plexiglas GS Product Specification, Ref. No. 211-1, Röhm GmbH, Germany, November 2006
- 42 PPG Aerospace/ DeSoto Aerospace Coatings, Technical Data for Desothane HS topcoat CA 8000 series, PRC-DeSoto Europe, June 2000 revision
- 43 Akzo Nobel Aerospace Coatings Inc, Technical Data for Aerodur Finish C 21/100, June 2005 revision
- 44 Guseva, O., Brunner, S., and Richner, P. Service Life Prediction for Aircraft Coatings, Polymer Degradation and Stability 82 (2003) 1-13
- 45 Gallwey, T.J. Task Complexity in Visual Inspection, Human Factors, 1986, 28(5), 595-606
- 46 StatSoft, Inc. STATISTICA (data analysis software system), version 8.0. [www.statsoft.com](http://www.statsoft.com). (2008).

INTENTIONALLY LEFT BLANK

## Acknowledgements

The authors would like to thank the CAA for supporting this project.

The authors would like to thank the following individuals and organisations for their help and assistance with the work of this project:

Mr Giovanni Marengo and Mr Paul Saunders, GKN Aerospace, East Cowes, UK for supply of materials and laminate painting.

Mr Trevor Mead and Mr Russell Martin, M& M patterns, Milton Keynes, UK, for machining of specimens.

Mr. Roy Harris, Automotive Engineers, Milton Keynes, UK, for painting of specimens.

Mr. Gavin Creech, Scott Bader Company Limited, Wollaston, UK for gloss measurements.

The authors would like to thank Mr Denis Cartié, Mr Jim Hurley, Mr Tony Scott and Mr Barry Walker for their invaluable technical support at Cranfield University.

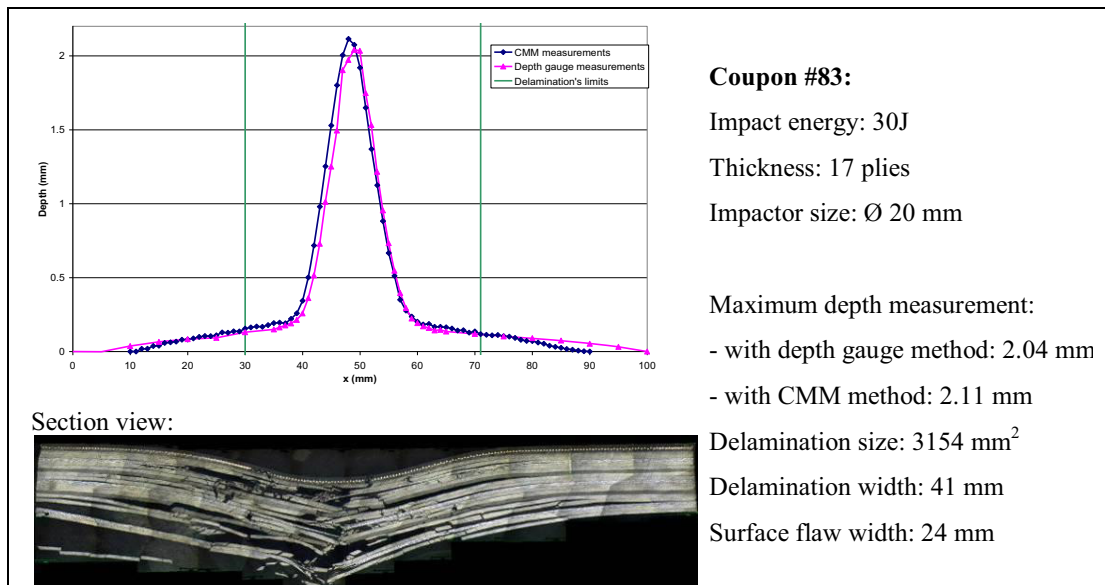
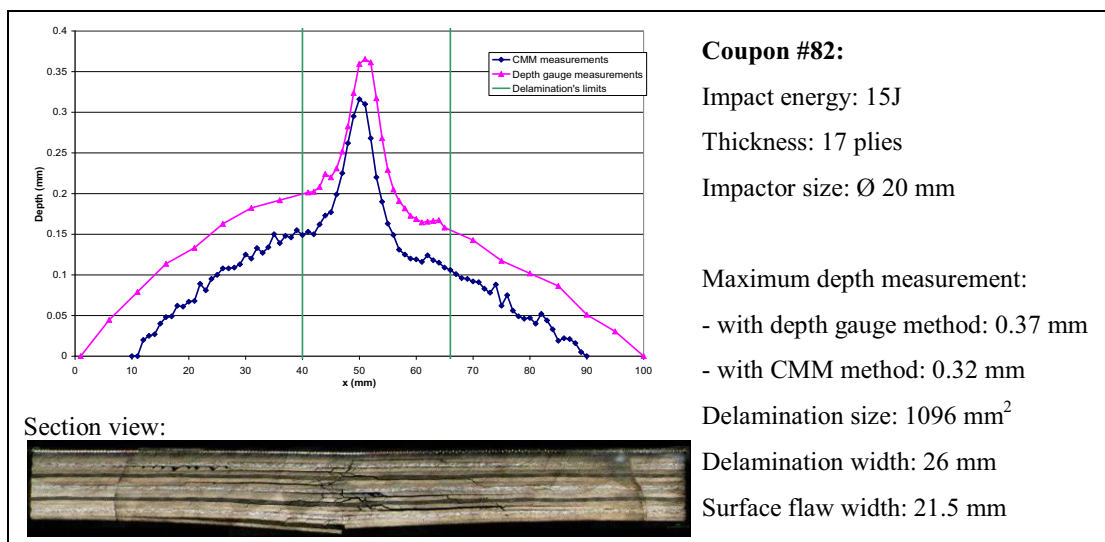
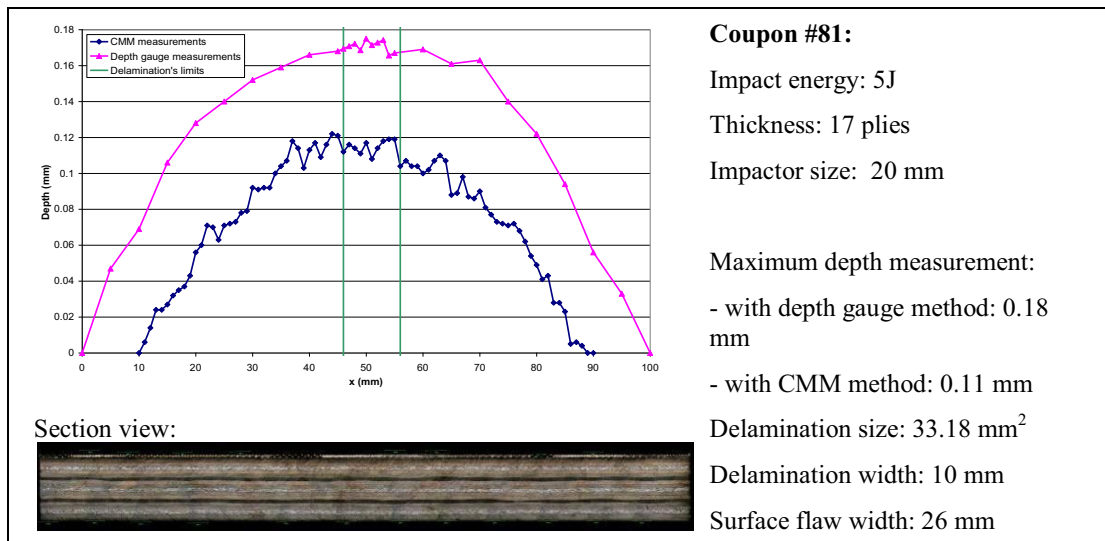
The authors would like to thank Miss Anne Boulic, of Polytech Orléans for her valuable contribution to the work of this project.

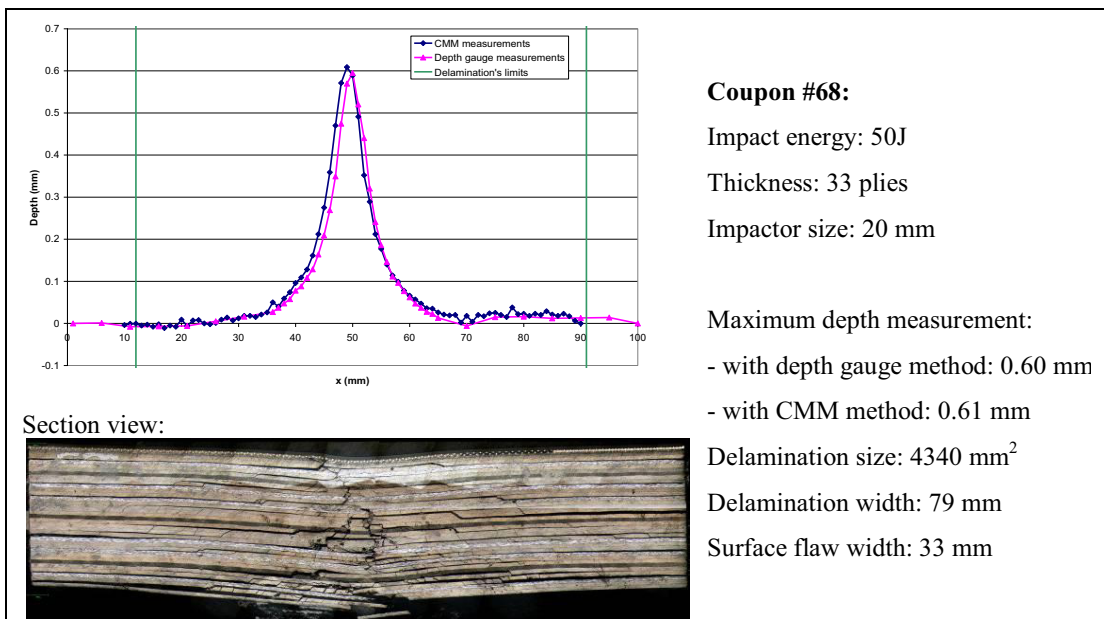
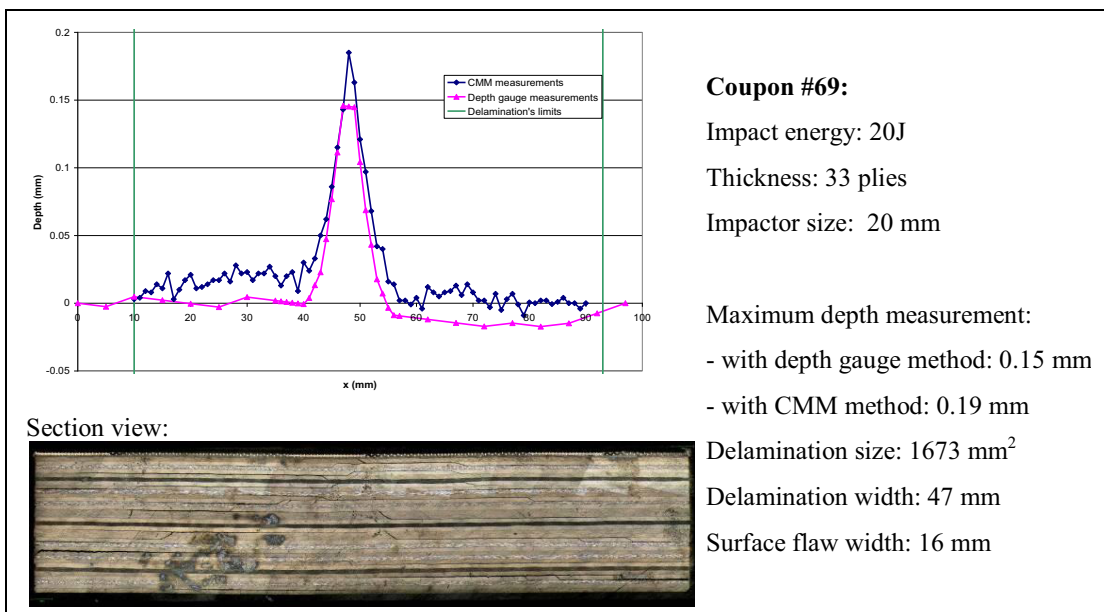
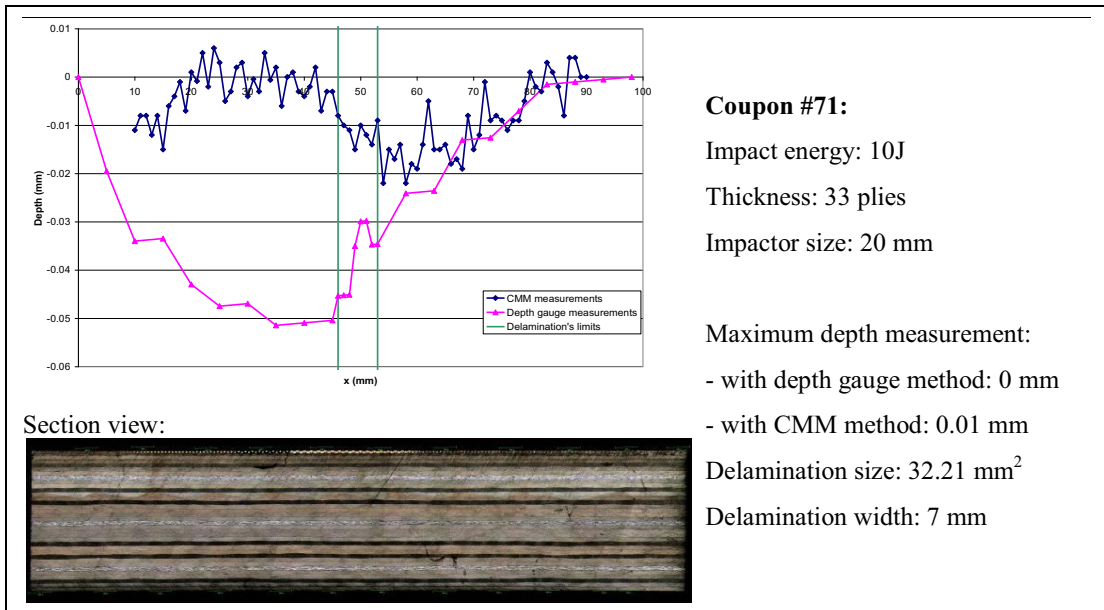
The authors would finally like to thank Mr Ben Hopper of Cranfield University for continued and invaluable help with visual inspection trials.

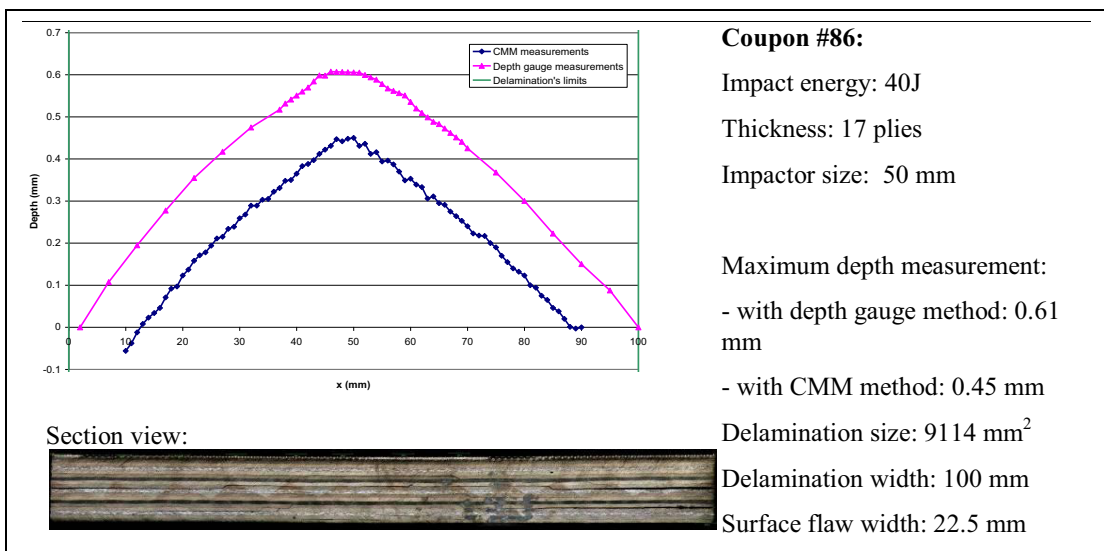
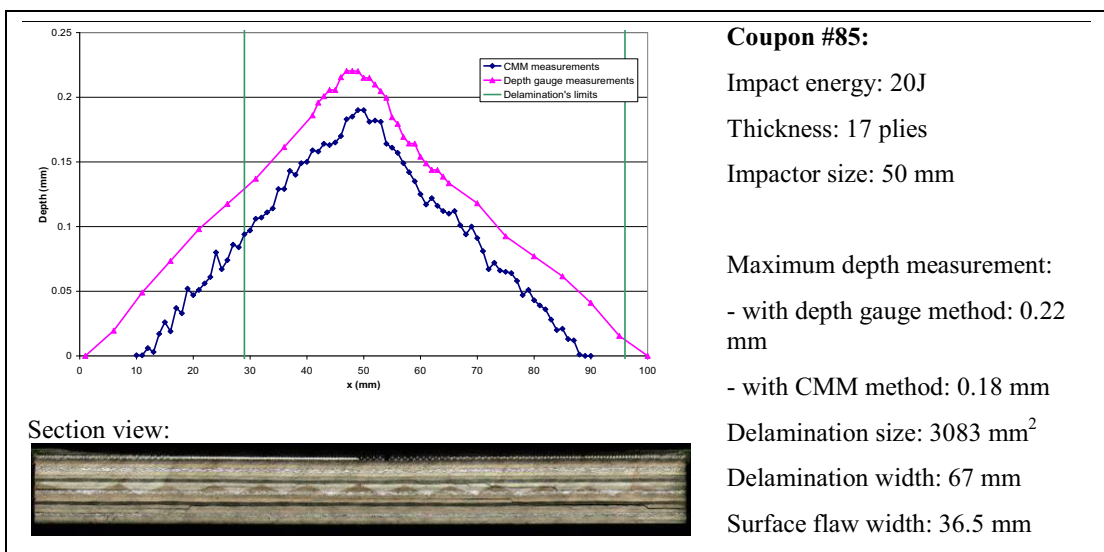
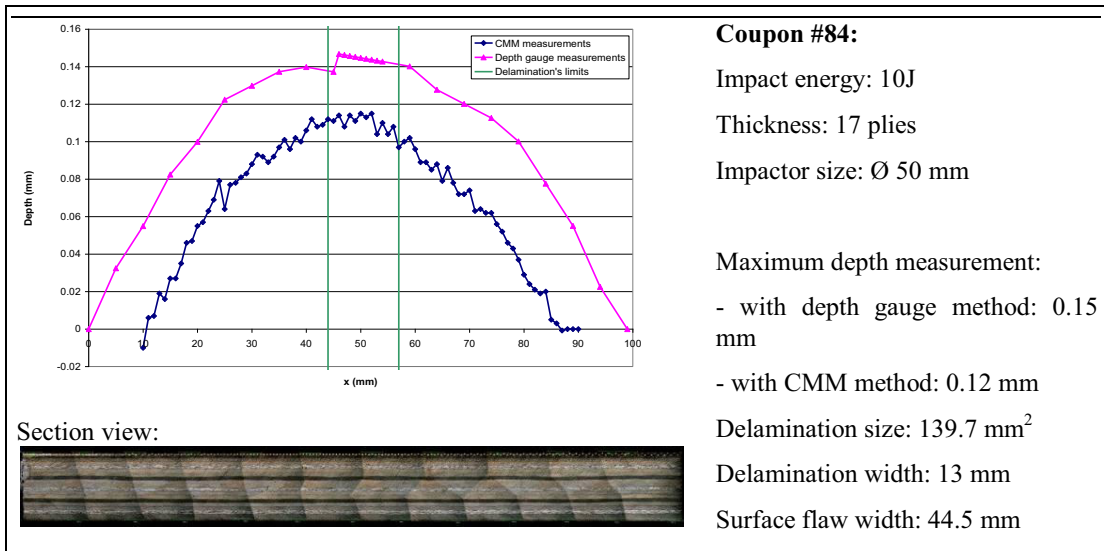
INTENTIONALLY LEFT BLANK

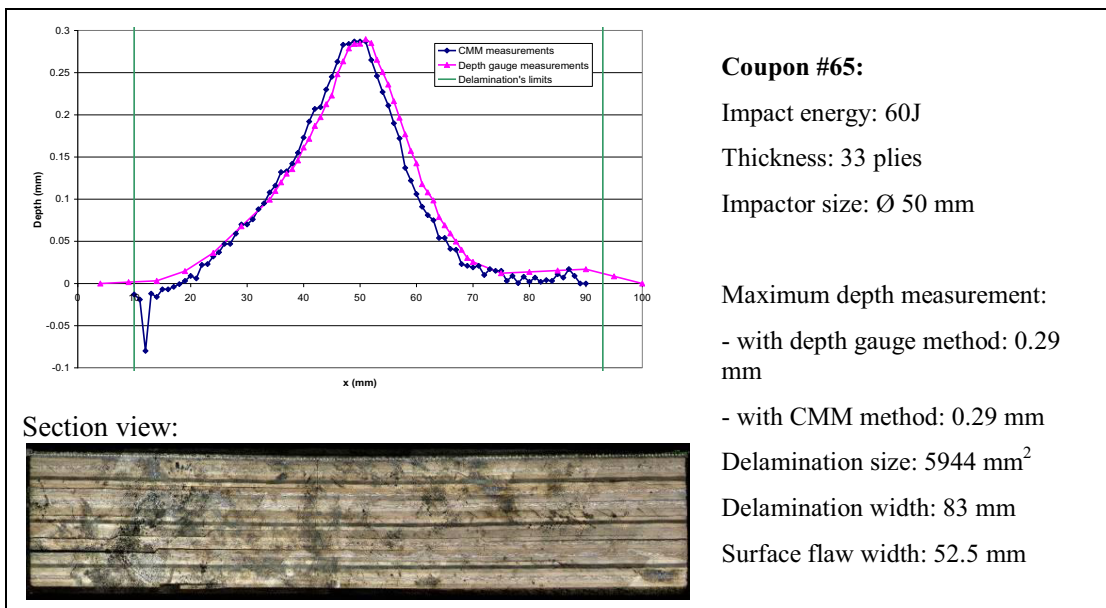
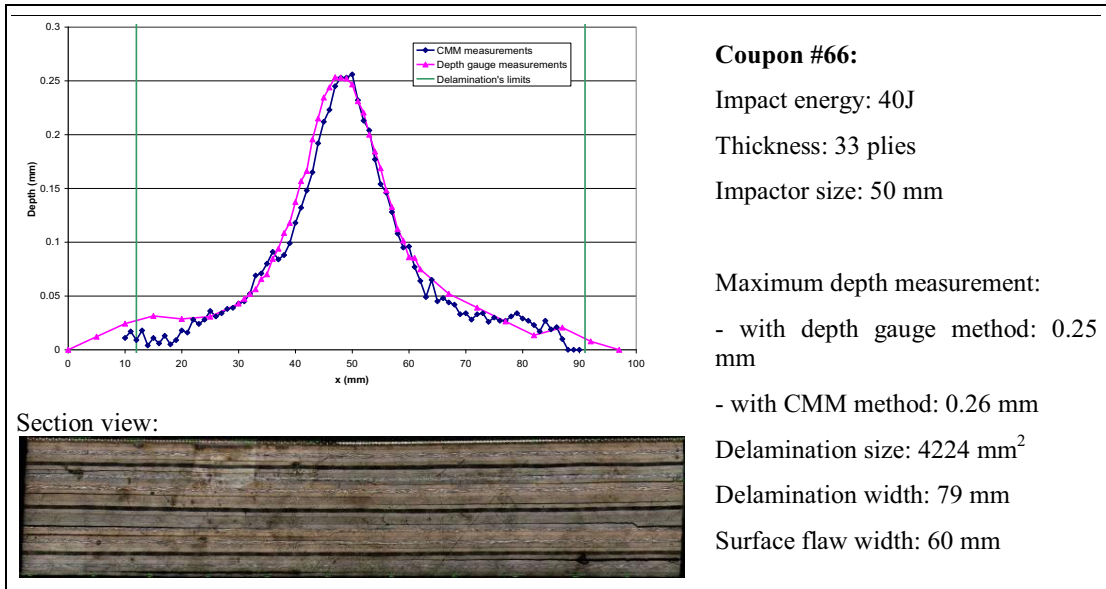
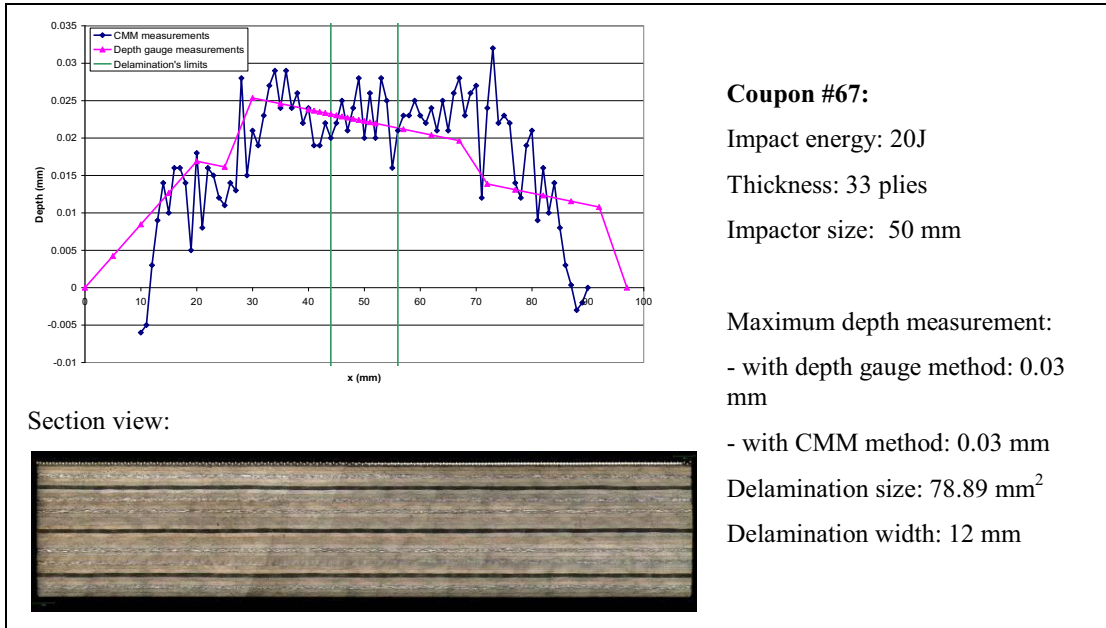
## Appendix A1

### Characterisation of impact damage surface flaws





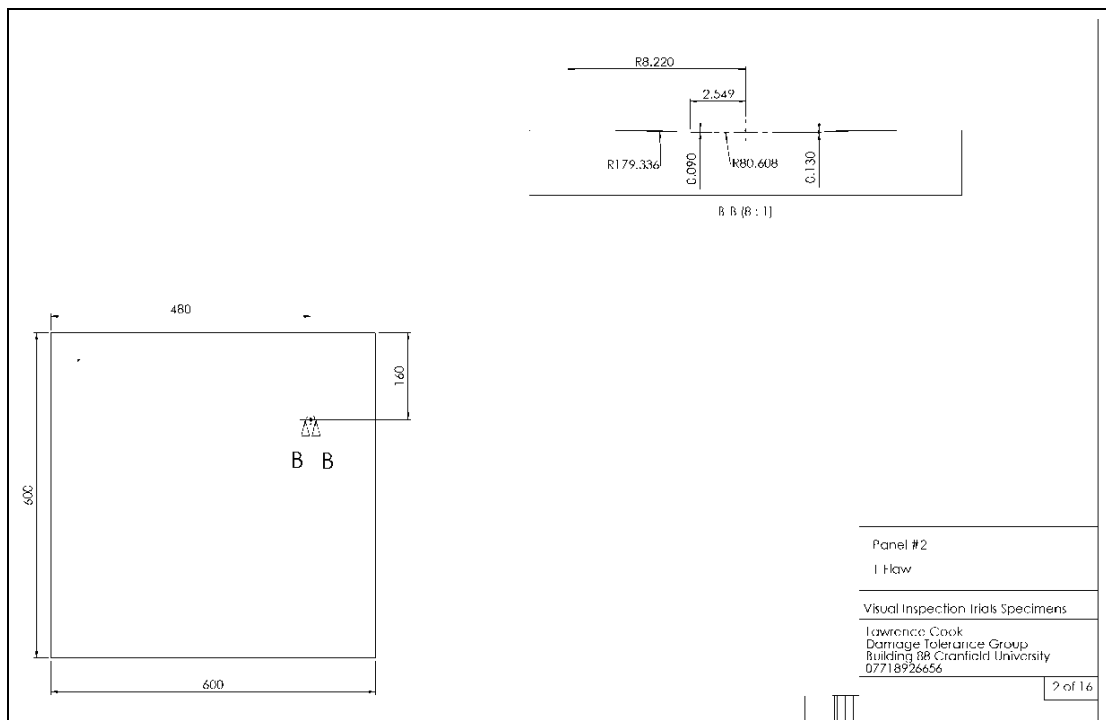
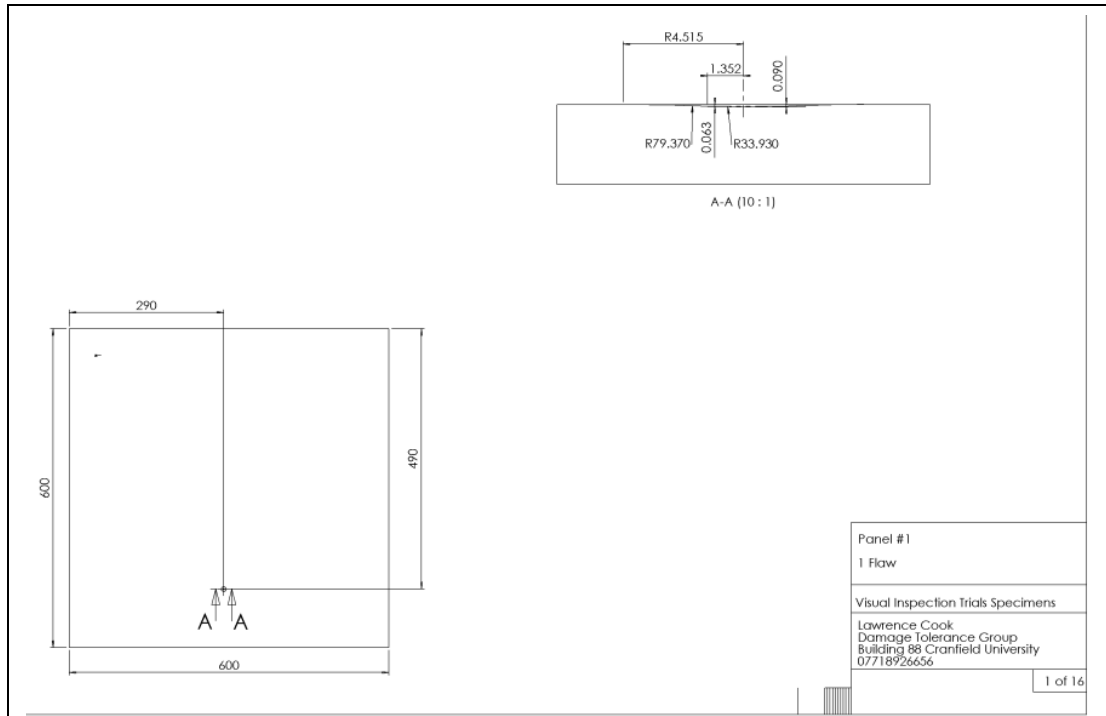


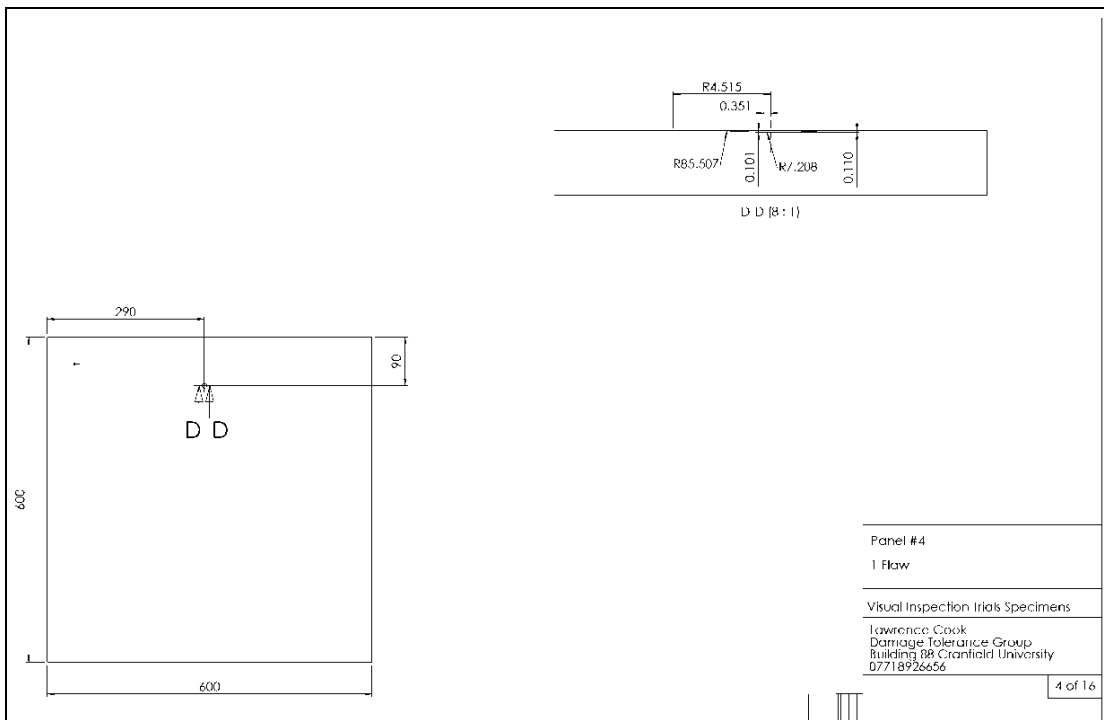
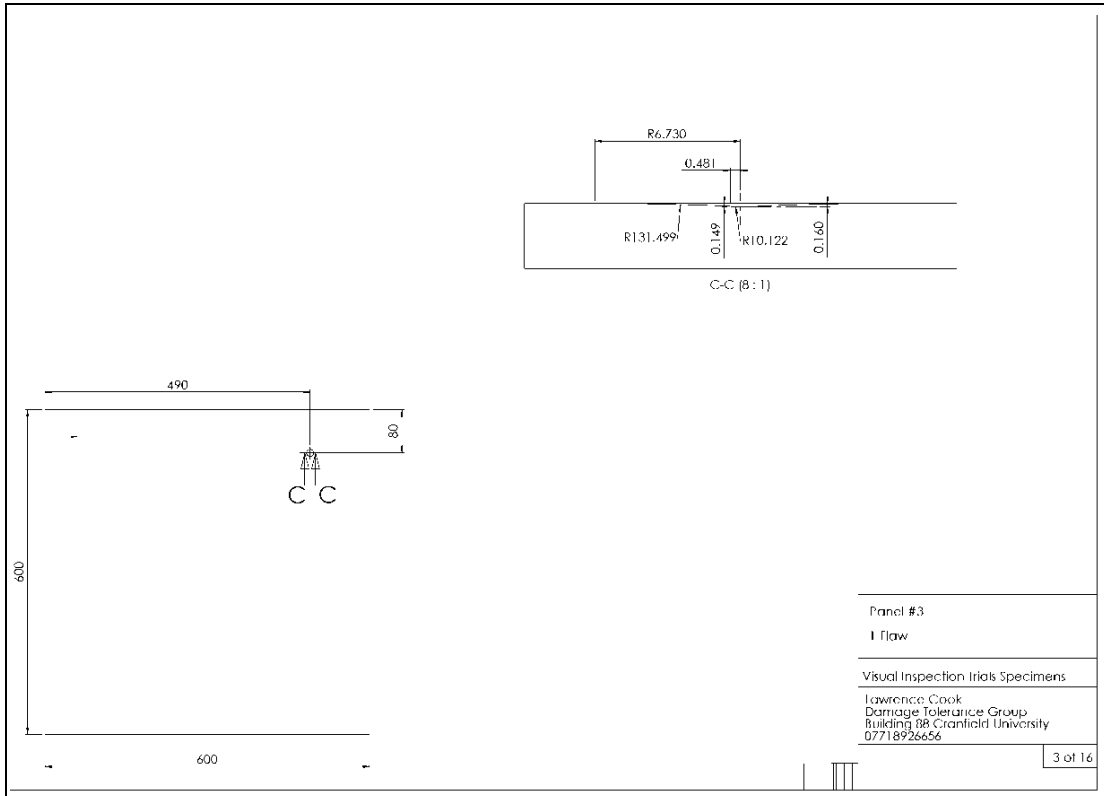


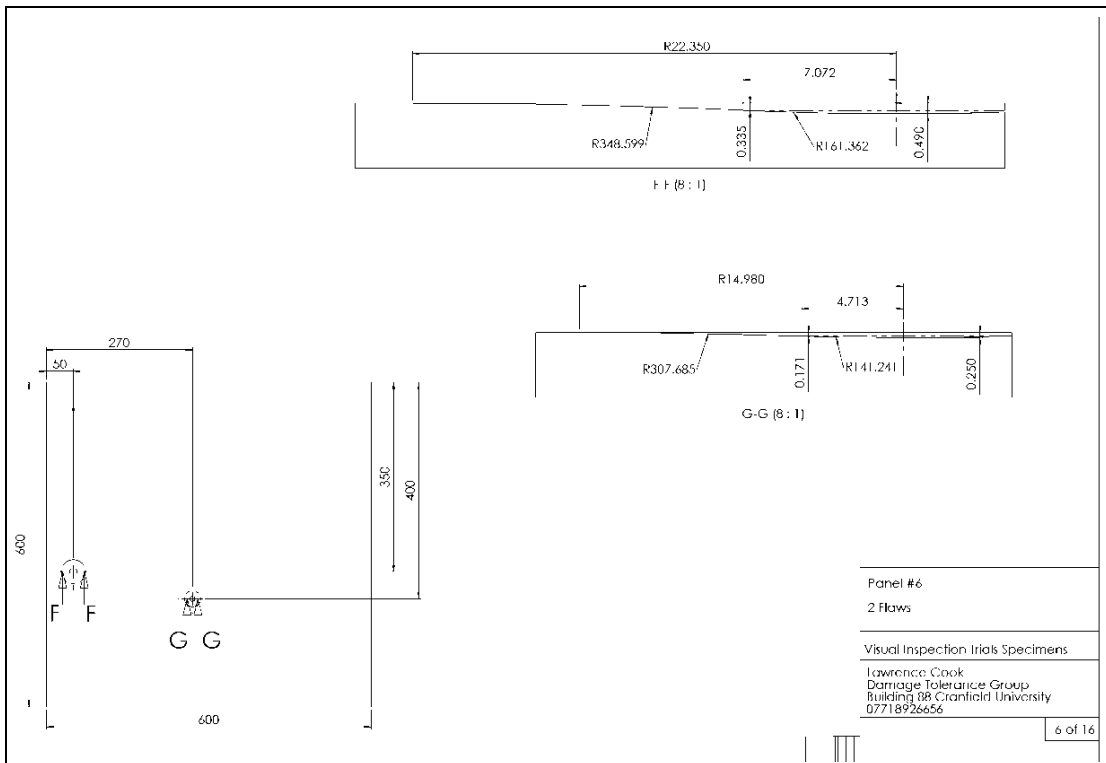
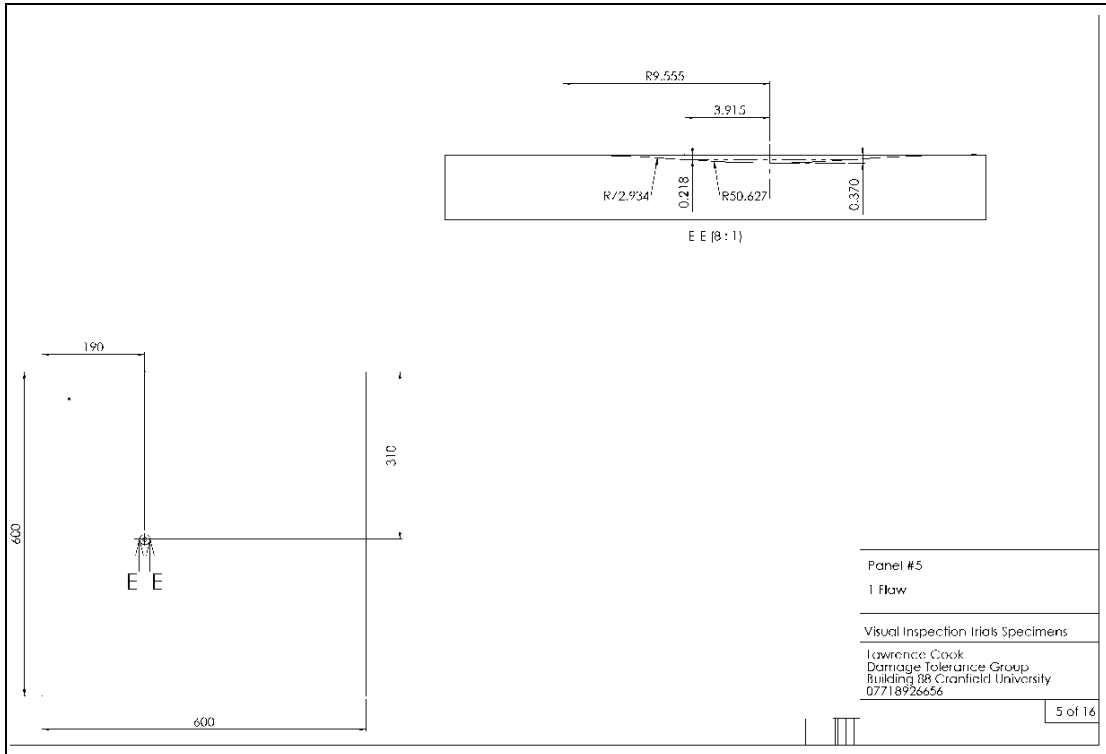


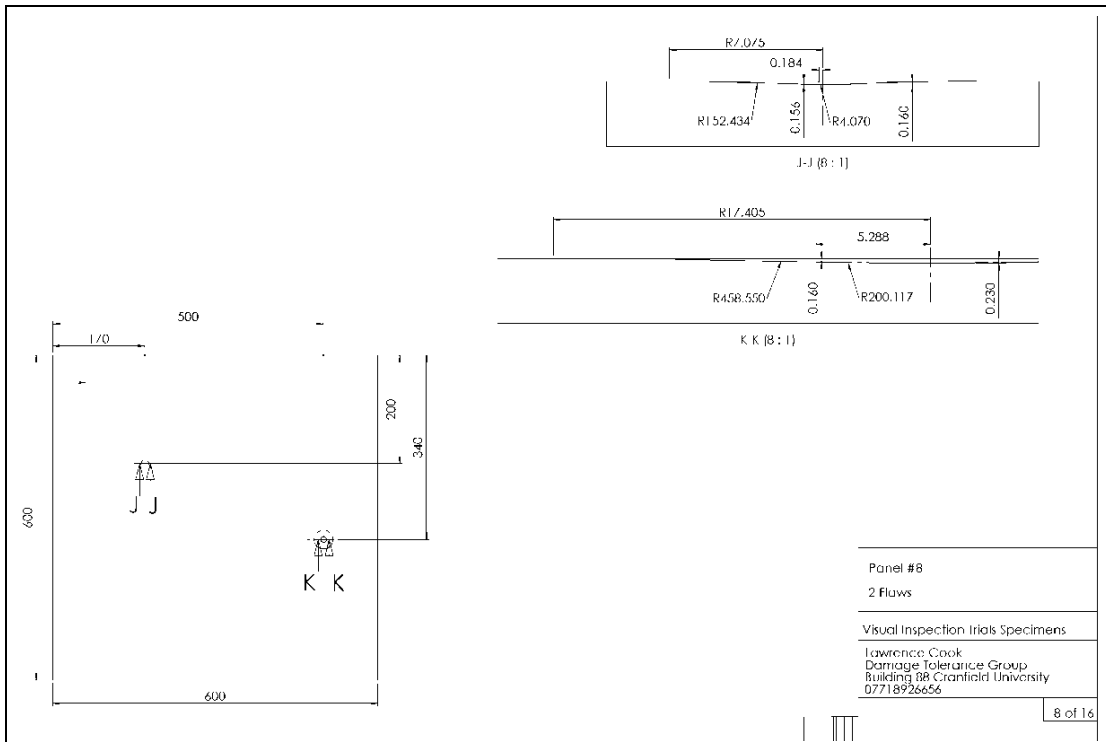
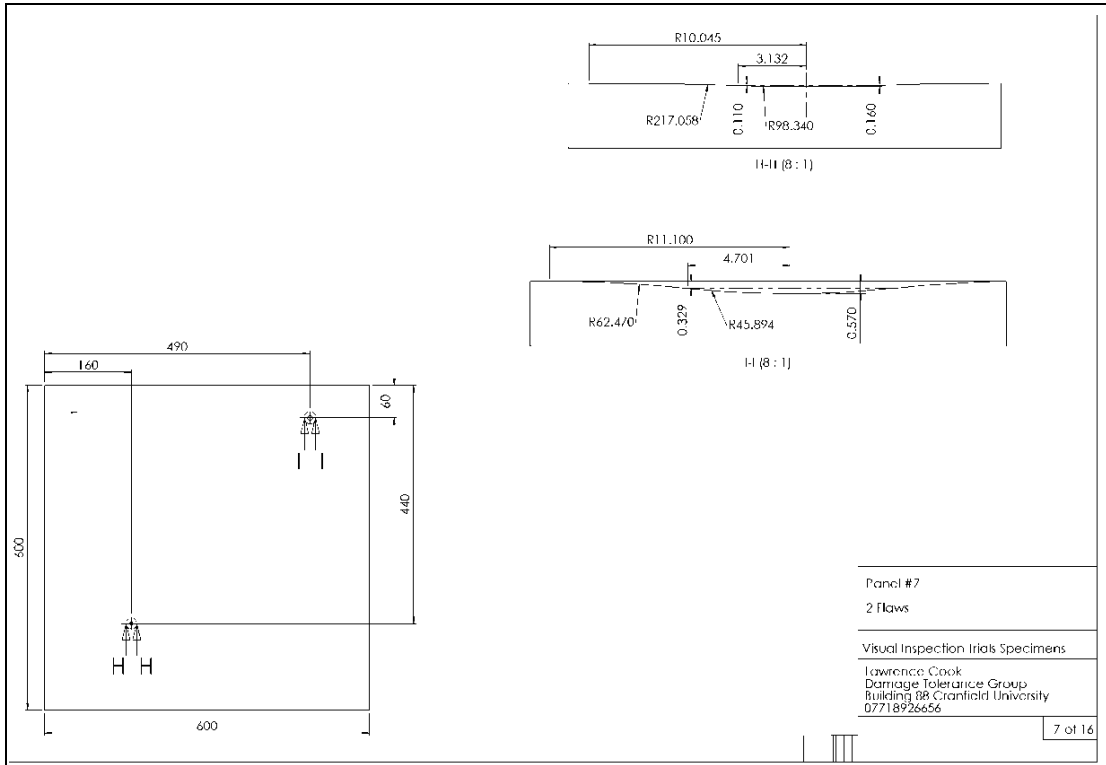
## Appendix A2

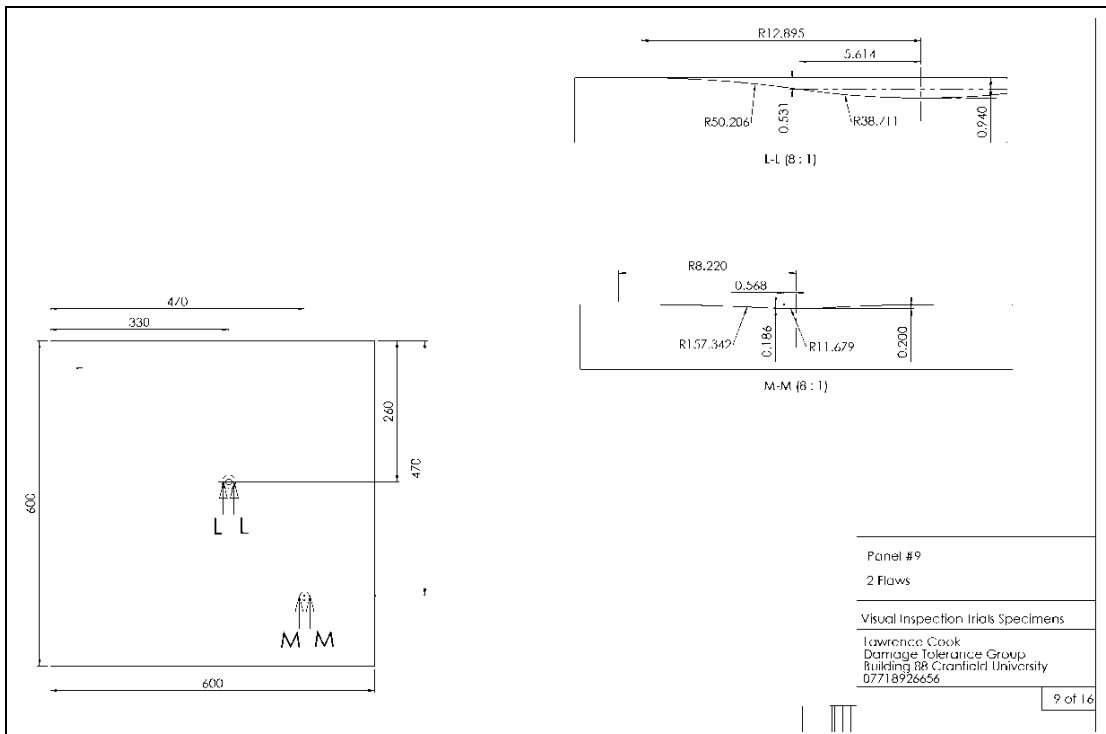
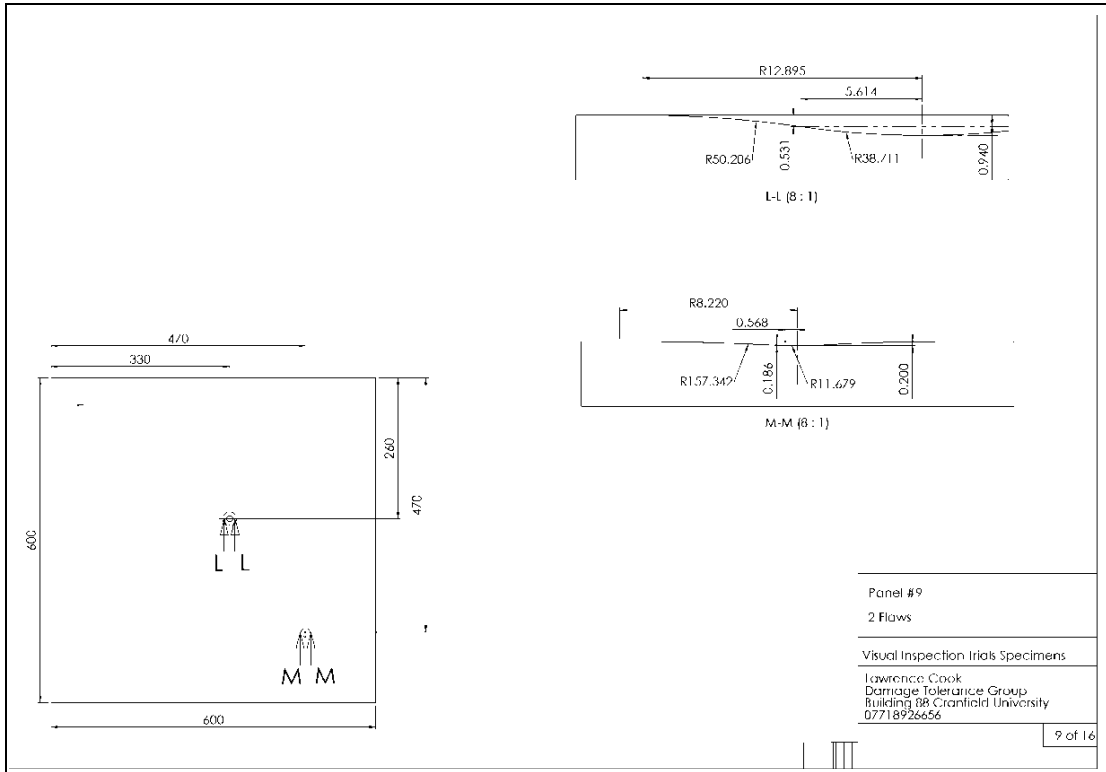
### Drawings of specimen panels

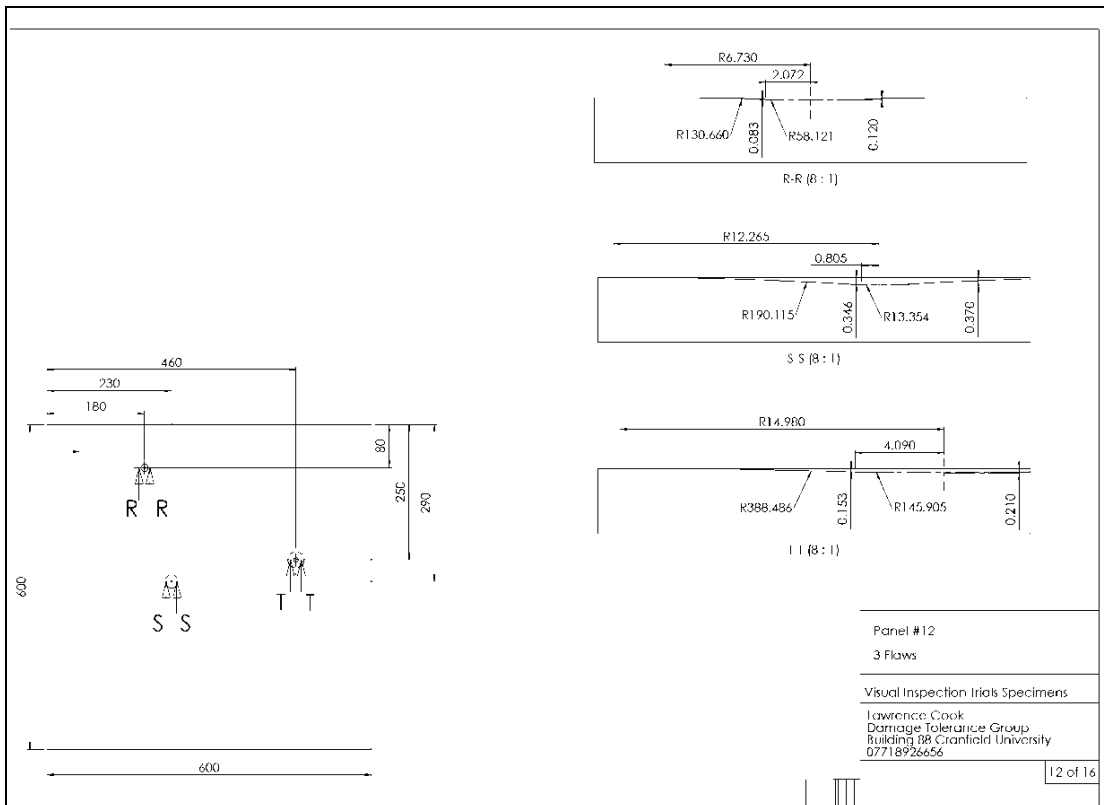
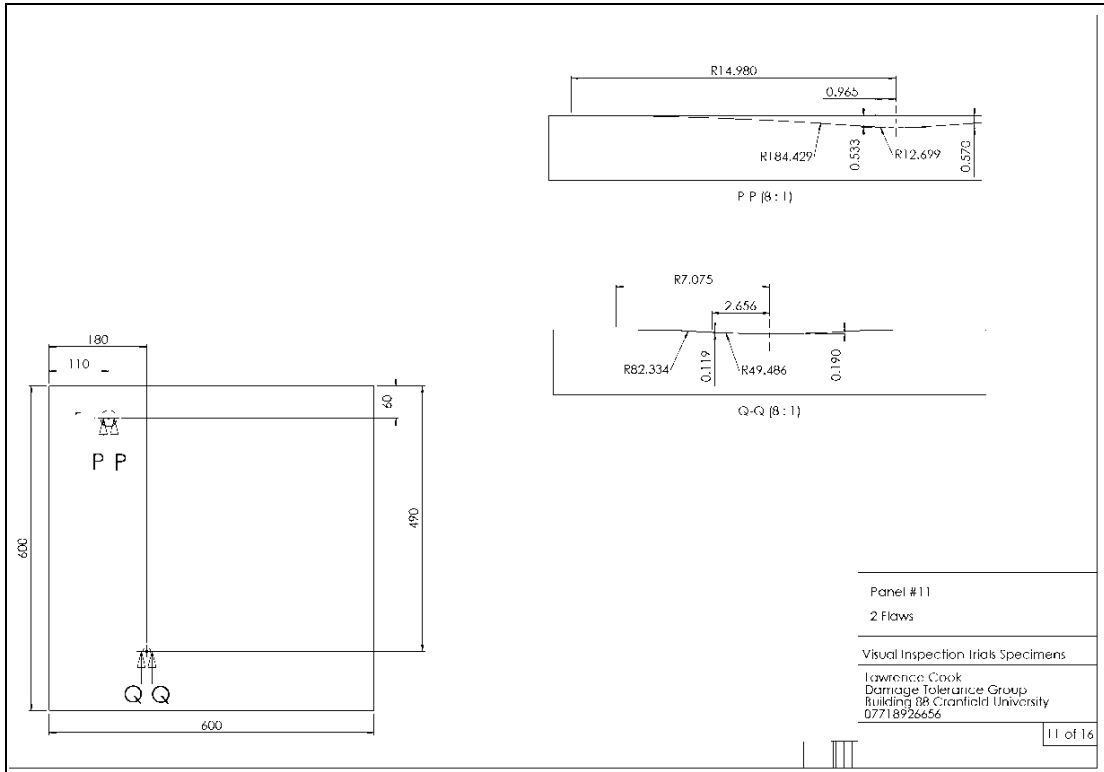


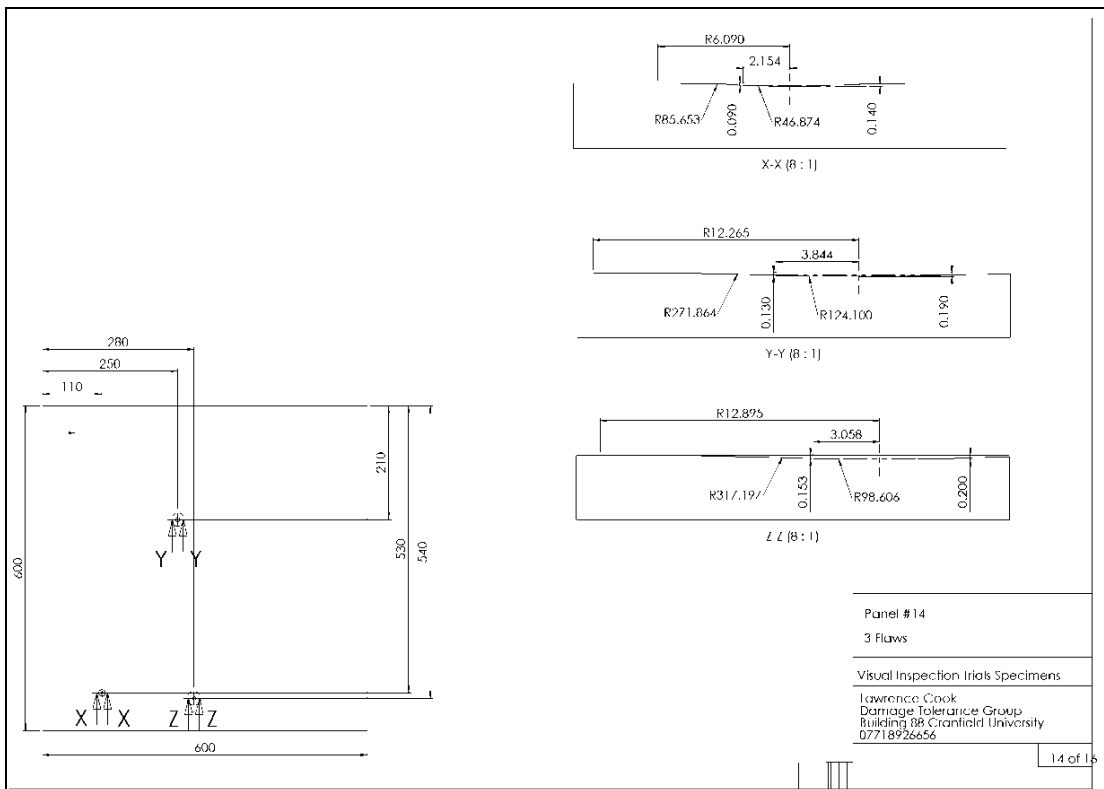
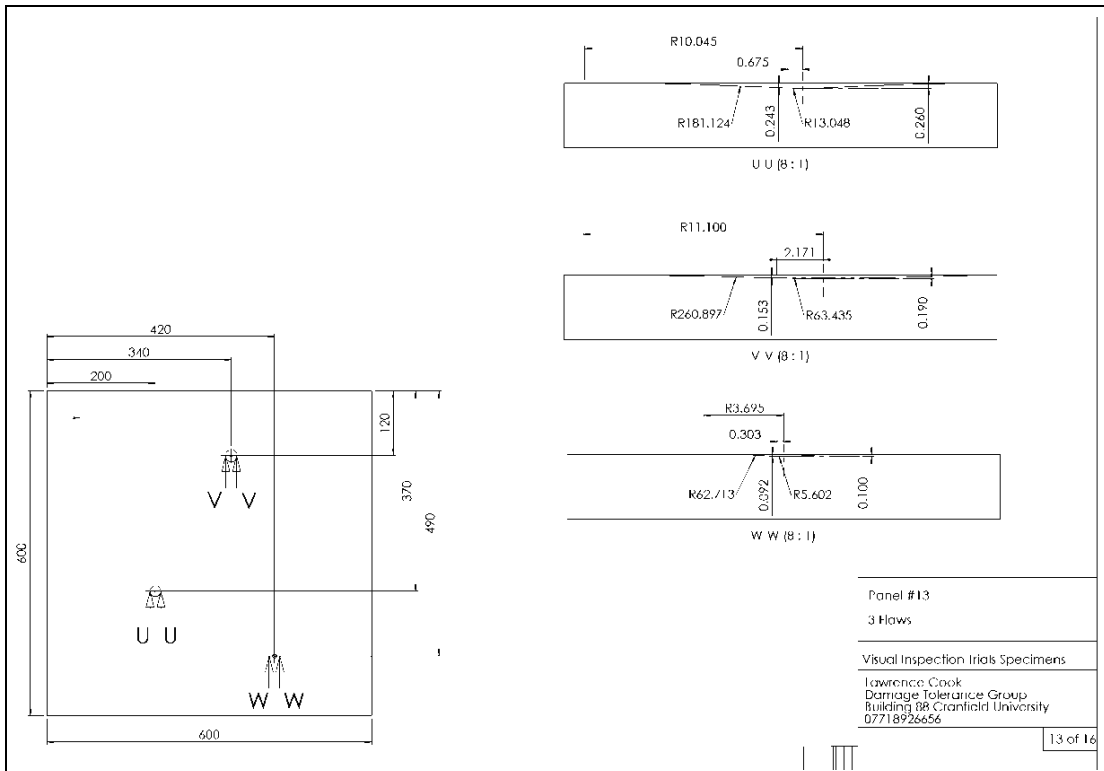


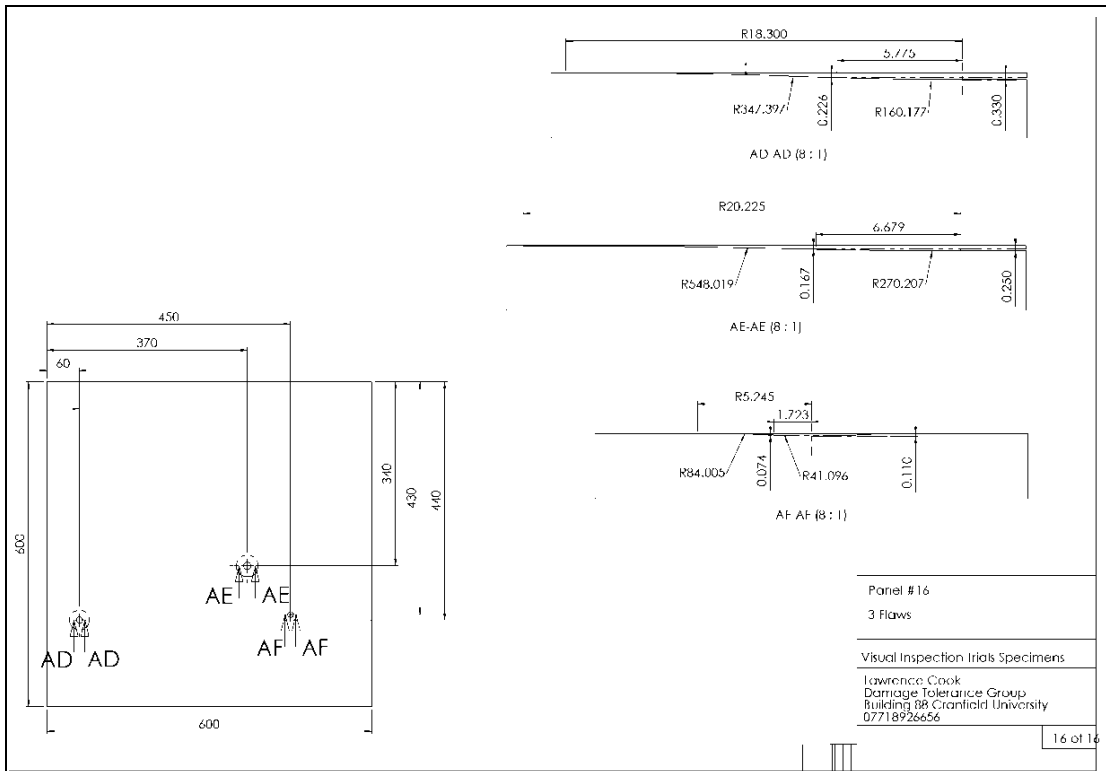
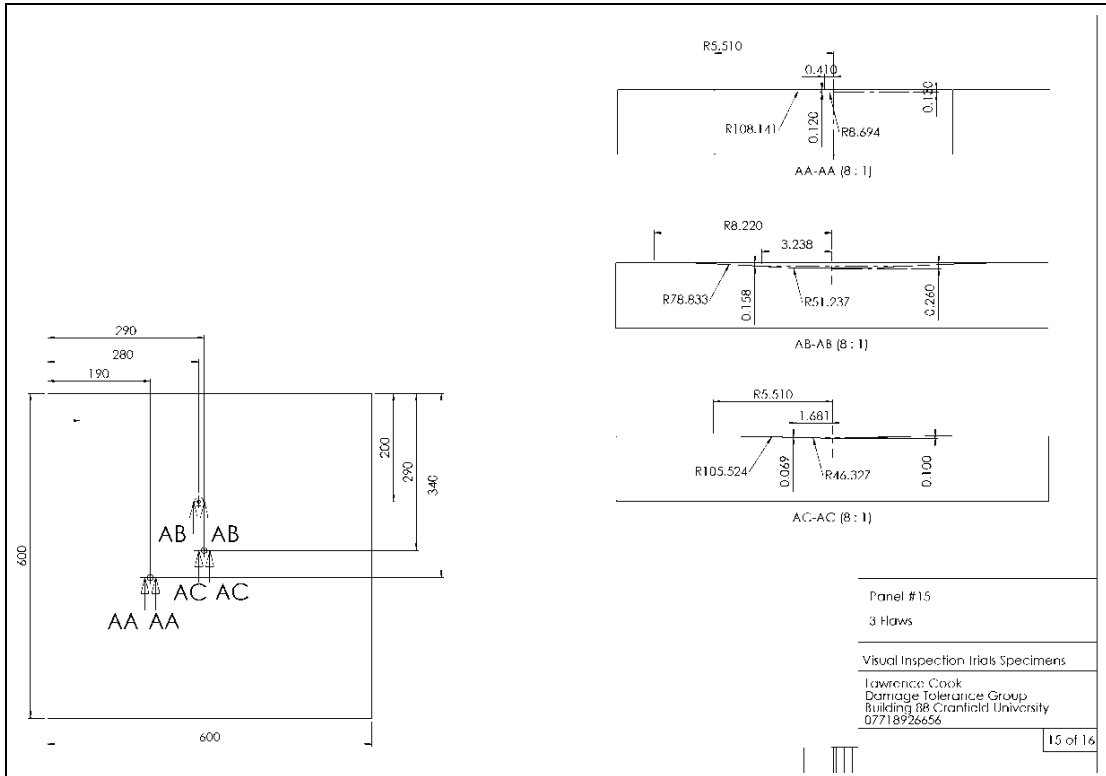














# Appendix A3

## Hit / Miss data collected from visual inspection trials

Flaw Number	Type	Width	Depth	Participant Number													Total Detections	Percentage								
				1	2	3	4	5	6	7	8	9	10	11	12	13			14	15	16	17				
1	Ø20mm/17ply	9.03	0.09	-	0	1	-	1	0	0	0	1	0	0	1	0	0	1	0	0	1	0	0	5	33%	
2	Ø20mm/17ply	10.49	0.11	-	0	0	-	1	0	0	0	0	0	0	0	0	0	0	0	0	0	0	0	1	7%	
3	Ø20mm/17ply	12.18	0.14	-	1	1	-	1	0	1	1	1	1	1	1	1	1	1	1	1	1	1	1	13	87%	
4	Ø20mm/17ply	14.15	0.19	-	1	1	-	1	1	1	1	1	1	1	1	1	1	1	1	1	1	1	1	14	93%	
5	Ø20mm/17ply	16.44	0.26	-	1	1	-	1	0	0	0	0	0	0	0	0	0	0	0	0	0	0	0	4	27%	
6	Ø20mm/17ply	19.11	0.37	-	1	1	-	1	1	1	1	1	1	1	1	1	1	1	1	1	1	1	1	15	100%	
7	Ø20mm/17ply	22.2	0.57	-	1	1	-	1	1	1	1	1	1	1	1	1	1	1	1	1	1	1	1	14	93%	
8	Ø20mm/17ply	25.79	0.94	-	1	1	-	1	1	1	1	1	1	1	1	1	1	1	1	1	1	1	1	15	100%	
9	Ø20mm/33ply	7.39	0.1	-	1	0	-	0	0	0	0	0	0	0	0	0	0	0	0	0	0	0	0	2	13%	
10	Ø20mm/33ply	9.03	0.11	-	0	1	-	0	0	1	1	0	1	0	0	0	0	0	0	0	0	0	0	4	27%	
11	Ø20mm/33ply	11.02	0.13	-	1	0	-	1	1	1	1	1	0	1	0	1	1	1	1	1	1	1	1	12	80%	
12	Ø20mm/33ply	13.46	0.16	-	1	0	-	0	1	0	0	1	0	0	0	0	0	0	0	0	0	0	0	3	20%	
13	Ø20mm/33ply	16.44	0.2	-	0	0	-	0	0	1	0	1	0	0	0	0	0	0	0	0	0	0	0	3	20%	
14	Ø20mm/33ply	20.09	0.26	-	1	1	-	1	1	1	0	1	1	1	1	1	1	1	1	1	1	1	1	14	93%	
15	Ø20mm/33ply	24.53	0.37	-	1	1	-	1	1	1	1	1	1	1	1	1	1	1	1	1	1	1	1	15	100%	
16	Ø20mm/33ply	29.96	0.57	-	1	1	-	1	1	1	1	1	1	1	1	1	1	1	1	1	1	1	1	15	100%	
17	Ø87mm/17ply	11.02	0.1	-	0	1	-	1	0	0	0	0	1	1	0	0	1	0	0	1	0	0	0	5	33%	
18	Ø87mm/17ply	13.46	0.12	-	0	0	-	1	1	0	0	0	0	0	0	0	1	0	0	1	0	0	1	5	33%	
19	Ø87mm/17ply	16.44	0.13	-	0	0	-	0	0	0	0	0	0	0	0	1	1	0	0	0	0	0	2	13%		
20	Ø87mm/17ply	20.09	0.16	-	1	1	-	0	1	1	0	1	1	1	1	0	1	0	1	0	1	0	1	10	67%	
21	Ø87mm/17ply	24.53	0.19	-	1	1	-	1	1	1	1	1	1	1	1	1	1	1	1	1	1	1	1	15	100%	
22	Ø87mm/17ply	29.96	0.25	-	1	1	-	1	1	1	1	1	1	1	0	1	1	1	1	1	1	1	1	14	93%	
23	Ø87mm/17ply	36.6	0.33	-	1	1	-	1	1	1	1	1	1	1	1	1	1	1	1	1	1	1	1	14	93%	
24	Ø87mm/17ply	44.7	0.49	-	1	1	-	1	1	1	1	1	1	1	1	1	1	1	1	1	1	1	1	15	100%	
25	Ø87mm/33ply	14.15	0.16	-	0	1	-	1	1	1	0	1	1	1	1	1	1	1	1	1	1	1	1	13	87%	
26	Ø87mm/33ply	16.44	0.17	-	0	1	-	0	0	1	1	1	1	0	0	1	1	0	1	0	1	0	1	8	53%	
27	Ø87mm/33ply	19.11	0.18	-	1	1	-	1	0	1	1	1	1	0	1	1	1	1	1	1	0	1	1	12	80%	
28	Ø87mm/33ply	22.2	0.19	-	0	1	-	1	0	1	0	1	1	0	1	1	1	1	1	0	0	1	1	9	60%	
29	Ø87mm/33ply	25.79	0.2	-	1	1	-	1	0	1	1	1	1	1	0	0	1	1	0	1	1	0	1	11	73%	
30	Ø87mm/33ply	29.96	0.21	-	0	0	-	0	0	0	0	1	1	0	0	1	1	1	1	1	0	1	1	6	40%	
31	Ø87mm/33ply	34.81	0.23	-	0	1	-	0	0	1	0	1	0	0	1	0	0	0	0	0	0	0	0	4	27%	
32	Ø87mm/33ply	40.45	0.25	-	0	1	-	1	1	1	1	1	1	1	1	1	1	1	1	1	1	1	1	10	67%	
				False Calls:																						
				-	13	1	-	21	9	0	31	14	20	23	19	16	29	6	6	8						

Flaw Number		Type	Width	Depth	Participant Number																	Total Detections	Percentage
					1	2	3	4	5	6	7	8	9	10	11	12	13	14	15	16	17		
1	Ø20mm/17ply	9.03	0.09	0	1	0	1	0	0	0	1	0	0	0	0	1	1	0	1	7	41%		
2	Ø20mm/17ply	10.49	0.11	1	0	0	1	0	1	1	0	0	1	0	0	0	1	0	0	6	35%		
3	Ø20mm/17ply	12.18	0.14	1	1	1	1	0	1	0	0	0	1	0	1	1	1	1	12	71%			
4	Ø20mm/17ply	14.15	0.19	1	1	1	1	1	1	1	1	1	1	1	1	1	1	1	16	94%			
5	Ø20mm/17ply	16.44	0.26	1	1	0	0	0	0	1	0	0	0	0	0	1	1	0	6	35%			
6	Ø20mm/17ply	19.11	0.37	1	0	1	1	1	1	1	1	1	1	1	1	1	1	1	16	94%			
7	Ø20mm/17ply	22.2	0.57	1	1	1	1	1	1	1	1	1	1	1	1	1	1	0	16	94%			
8	Ø20mm/17ply	25.79	0.94	1	1	1	1	1	1	1	1	1	1	1	1	1	1	1	17	100%			
9	Ø20mm/33ply	7.39	0.1	0	0	0	0	0	1	0	0	0	0	0	0	1	0	0	2	12%			
10	Ø20mm/33ply	9.03	0.11	0	1	0	0	1	0	0	0	1	0	0	0	1	1	0	5	29%			
11	Ø20mm/33ply	11.02	0.13	1	1	1	1	1	1	1	1	1	1	1	1	1	1	1	17	100%			
12	Ø20mm/33ply	13.46	0.16	0	1	1	0	1	0	0	0	0	0	0	0	0	0	0	3	18%			
13	Ø20mm/33ply	16.44	0.2	0	1	0	1	1	0	1	0	1	0	0	0	1	1	0	8	47%			
14	Ø20mm/33ply	20.09	0.26	1	1	1	1	1	1	1	1	1	1	1	1	1	1	1	17	100%			
15	Ø20mm/33ply	24.53	0.37	1	0	1	1	1	1	1	1	1	1	1	1	1	1	1	16	94%			
16	Ø20mm/33ply	29.96	0.57	1	1	1	1	1	1	1	1	1	1	1	1	1	1	1	17	100%			
17	Ø67mm/17ply	11.02	0.1	0	0	0	0	1	0	1	0	0	1	0	0	0	1	0	4	24%			
18	Ø67mm/17ply	13.46	0.12	0	1	0	0	0	1	1	0	0	1	0	0	0	1	0	5	29%			
19	Ø67mm/17ply	16.44	0.13	0	1	0	0	1	0	0	1	0	0	0	0	1	0	0	4	24%			
20	Ø67mm/17ply	20.09	0.16	1	1	0	0	1	1	1	1	1	1	1	1	1	1	1	12	71%			
21	Ø67mm/17ply	24.53	0.19	1	0	1	0	1	1	1	1	1	1	1	1	1	1	1	15	88%			
22	Ø67mm/17ply	29.96	0.25	1	1	1	1	1	1	1	1	1	1	1	1	1	1	1	15	88%			
23	Ø67mm/17ply	36.6	0.33	1	1	1	1	1	1	1	1	1	1	1	1	1	1	1	17	100%			
24	Ø67mm/17ply	44.7	0.49	1	0	1	1	1	1	1	1	1	1	1	1	1	1	1	15	88%			
25	Ø67mm/33ply	14.15	0.16	1	0	1	0	1	0	1	0	0	1	0	1	0	1	1	9	53%			
26	Ø67mm/33ply	16.44	0.17	1	0	1	1	1	1	1	1	1	1	1	1	1	1	1	11	65%			
27	Ø67mm/33ply	19.11	0.18	1	1	0	0	1	0	0	1	0	1	0	1	0	1	0	7	41%			
28	Ø67mm/33ply	22.2	0.19	0	1	0	0	1	0	1	0	1	1	0	1	1	1	0	8	47%			
29	Ø67mm/33ply	25.79	0.2	1	1	1	1	0	0	1	0	0	0	1	1	1	0	1	9	53%			
30	Ø67mm/33ply	29.96	0.21	0	1	0	0	1	0	1	1	0	0	0	1	1	0	0	6	35%			
31	Ø67mm/33ply	34.81	0.23	1	1	0	1	1	0	1	1	1	0	0	1	1	0	1	10	59%			
32	Ø67mm/33ply	40.45	0.25	1	1	1	1	1	1	0	1	0	0	0	1	1	1	0	10	59%			
				False Calls:	45	3	1	12	19	5	1	0	29	0	0	4	1	26	39	6	0	191	11.23529412







